STUDY ON SPIN ABSORPTION EFFECT IN FERROMAGNETIC/NONMAGNETIC HYBRID NANOSTRUCTURES

野村, 竜也

https://doi.org/10.15017/1931699

出版情報：Kyushu University, 2017, 博士（理学）, 課程博士
バージョン：
権利関係：

Study on spin absorption effect in ferromagnetic/nonmagnetic hybrid nanostructures

A thesis submitted for the degree of
Doctor of Science

at

Kyushu University

by

Tatsuya Nomura

March, 2018

Abstract

Spin current, which is a flow of the spin angular momentum, exists in a ferromagnetic metal because the spin of the conduction electrons are polarized. In general, there is no spin current in a nonmagnetic metal because of no spin polarization. However, by using a ferromagnetic/nonmagnetic hybrid structures, the spin current can be injected into the nonmagnetic metal. This spin injection can be performed by electrically, thermally and optically. However, because of the extremely short life time with a tiny quantity, the detection of the spin current is not so simple. Lateral spin valve consisting of two ferromagnetic electrodes bridged by a nonmagnetic strip enables to perform the nonlocal spin injection measurement, which can detect the spin current sensitively and precisely. Therefore, the spin transport in a lateral spin valve has been investigated intensively.

It is well known that the additional structure in contact with the materials having non-equilibrium spins significantly affects its spin distribution when the spin relaxation of the contact is very strong. By extending this phenomenon intentionally, we can extract the spin current from the nonmagnetic metal effectively. This is known as the spin absorption effect. Especially, when the ferromagnetic electrode is connected to the nonmagnetic metal, the absorbed spin current exerts the spin transfer torque in the

magnetization. It is an important milestone to deepen understanding the spin absorption effect because this phenomenon is attractive both from the fundamental and application viewpoints. Here, we intensively investigate the spin absorption effect in the laterally configured ferromagnetic/nonmagnetic hybrid structure.

First, we investigate the influence of the geometry on the spin absorption effect. Since, in most cases, the additional contact brings the geometrical disorder, which produces the spin scattering. To exclude the influence of the geometrical scattering, we have developed a specially designed lateral spin valve. In this device, we were able to estimate the spin absorption effect not only from the top surface but also from the side surface.

During the above geometrical study, we observed a small unexpected change of the nonlocal spin signal. To explain this, we focused on the anisotropy of the spin absorption effect. Since it is expected that the transverse spin diffusion length is much shorter than the longitudinal spin diffusion length, the observed additional change may be related to the anisotropy. To confirm our expectation, we have developed a lateral spin valve with the V-shape electrodes. We confirmed that the quantized axis of the spin is well controlled by the magnetic field. By using this device, we clarified the difference between the longitudinal and transverse spin current absorption.

Although we have obtained the expected property of the spin absorption effect, the quantitative evaluation of the spin absorption effect is difficult because of the significant reduction of the spin accumulation. To overcome this difficulty, we have recently developed a high performance lateral spin valve based on highly spin-polarized ferromagnetic CoFeAl electrodes. This allows us to estimate the spin absorption effect more precisely.

In the last chapter, we investigate the spin absorption effect more quantitatively and precisely by using the spin absorber with the large junction. Finally, we obtained the quantitative information of the spin absorption effect. Also, we found that the spin absorption with the large junction size induces un-conventional temperature dependence of the spin accumulation signal.

Thus, the systematic experimental studies on the spin absorption effect provides not only the validity of the spin diffusion model but also the unique characteristics, which are useful for manipulating spin currents.

Contents

List of Figures

Chapter 1

Introduction

1.1 Background

The development of physics of magnetism in recent years is a result of microfabrication technologies. Although magnetism has been studied in macroscopic systems so far, quantization of angular momentum was discovered by Stern and Gerlach experiments [1]. Recognizing the existence of spin, research on the magnetization process of the artificial micro magnetic material has started to draw attention. In order to clarify the properties of magnetic materials smaller than the magnetic domain size, the micro-fabrication technology which is cultivated in the semiconductor field was applied. However, as the sample became submicron size, it was difficult to observe the magnetization process of the ferromagnet. Under such circumstances, research on high sensitivity magnetization measurement using the galvanomagnetic effect has started. In the ferromagnet, the band structure is different between up and down spin band because of the exchange splitting. Therefore, it causes the spin dependent conductivity of electrons [2]. As a representative

effect, the anisotropic magnetoresistive effect is known. The anisotropic magnetoresistive effect is a phenomenon in which the conductivity of electrons in a ferromagnetic material varies depending on the relative angle to the magnetization direction. By this phenomenon, when the magnetization in the ferromagnetic material is rotated, the electric resistance is modulated. This enables us to detect the magnetization characteristics of the ferromagnetic material electrically. However, since the magnetoresistance ratio changes only by a few %, it is insufficient as a detection method of the magnetization. Therefore, research using laminated artificial lattice was attracted attention as a next step. In 1986, P. Grunberg et al. discovered that Fe are antiferromagnetically coupled via Cr in a Fe/Cr/Fe hybrid structure [3]. In response to this result, A. Fert et al. discovered the 50 % magnetoresistance ratio by sweeping the external magnetic field while applying an in-plane current to the Fe/Cr artificial lattice in 1988 [4]. This is called giant magnetoresistance (GMR) effect, and research based on a composite structure including a magnetic material came to attract attention as a result of this. The origin of GMR effect was thought to be the spin dependent scattering at the interface. Therefore, it was expected that a larger magnetoresistance effect can be obtained when the same experiment is performed by directly applying a current normal to the surface in the Fe/Cr/Fe hybrid structure. However, since the cross-sectional area of the sample is large, it was difficult to detect the magnetoresistance ratio electrically when a current is applied directly normal to the surface. Hence, research on CPP-GMR (current perpendicular to the plane giant magnetoresistance) was conducted using various microfabrication techniques [5–9]. From this series of research, unique microfabrication technologies have been proposed, and CPP-GMR measurements in nano-meter-scale samples have been

realized. As described above, in order to realize a large magnetoresisance, the development of microfabrication technology had been drawing more and more attention, because the magnetoresistance ratio depends on the resistance-area product of the channel.

While research on the galvanomagnetic effect was in progress, research on multiple-degrees of freedom of electrons in a composite structure including a magnetic material was reported in 1985 [10]. Although spin current was observed in this report, the signal at this time was small and not much attention was paid. As the development of microfabrication technology enabled the fabrication of samples shorter than the spin diffusion length of electrons, spin current became a focus of attention. Research on spin current has been developed using a nonlocal method in a lateral spin valve [12–16]. The lateral spin valve eliminates the charge of electron, and can create only spin conduction which is called pure spin current. And, the lateral spin valve enables to control the pure spin current, and various methods for controlling it have been reported [17,18]. Furthermore, the amount of spin current in the channel can be estimated as a spin signal, and it is also theoretically well agreed upon [19, 21, 88]. However, the experimental systems so far have been limited to ideal one-dimensional spin conduction. One-dimensional spin conduction is a phenomenon in which the spin channel width is sufficiently shorter than the spin diffusion length, and the spin diffuses one-dimensionally and spin quantization axis is limited to collinear arrangement described as parallel or anti-parallel states.

Here we propose the necessity for studies of spin diffusion with three-dimensional geometry. Because the pure spin current has no big Joule loss, it is gaining attention as one of the candidates for next generation energy saving devices replacing conventional electronics [22–25]. In recent years, spin injection into various substances has been

observed, and various types of spin devices have been also proposed [17, 18, 27–30, 53]. For example, in case of the spin injection into the semiconductor spin channel, the cross sectional areas of the device are designed to be larger than that of the metal because of its high electric resistance. Additionally, spin devices utilizing the spin quantization axis control techniques have also been developed. Therefore, a study on spin diffusion in a ferromagnetic/nonmagnetic hybrid system considering three-dimensional geometry is required. Spin diffuses so as to be absorbed into a material with strong spin relaxation. This is called the spin absorption effect which is also in good agreement with theory. However, it is not clear the behavior of the spin absorption effect in the spin absorber with the three-dimensional freedom is. Therefore, in this research, we investigated the spin absorption effect in this system.

1.2 Outline

This study investigated the spin absorption effect in a system with three-dimensional freedom. The three-dimensional degree of freedom is defined here as the following three cases. I: The system has geometrical differences comparing to the conventional structures. II: The spin absorber has a non-colinear magnetization orientation with respect to the polarization of the spin current. III: Length of the spin absorber is longer than the spin diffusion length in the spin channel. A flow chart of this series of research conducted in this research is shown in Figure 1.1, and a concrete outline is described below.

- Chapter 1: Description of research background and motivation.

- Chapter 2: Outline of theory on spin-dependent conduction.

- Chapter 3: Experimental method; Explanation of the microfabrication technology and measurement technique used in the experiments.

- Chapter 4: Experiments on the geometric dependence of the spin absorption effect. We investigate the spin absorption effect in a nano-pillar-based lateral spin valve consisting of five ferromagnetic nanodots fabricated on a uniform nonmagnetic film, and show that the spin absorption efficiency is smaller than that of a conventional lateral spin valve based on nanowire junctions. We also found that the absorption efficiency of the spin current is significantly enhanced by using a thicker ferromagnetic nanodot. This can be understood by taking into account quantitatively the spin absorption through the side surface of the ferromagnetic dot. Additionally, the existence of the spin scattering effect is demonstrated by using a T-shaped lateral spin valve in which the spin absorber is located at a position branched from the spin diffusion path. From a series of the spin signals, spin absorption effect by transverse spin relaxation was implied in this sample structure. By observing the inverse spin Hall effect by replacing the absorber of T-shaped lateral spin valve with heavy metal, we confirmed transverse spin current was generated.

- Chapter 5: Experiments on the relative angle dependence between the spin vector of the absorber and the spin current polarization direction in the spin absorption effect. In order to investigate longitudinal/transverse spin absorption efficiency and spin relaxation length in the same sample, we proposed a V-shaped lateral spin valve structure. We confirmed that the V-shaped lateral spin valve can generate

the longitudinal and transverse components of spin current by detecting the inverse spin Hall voltage. Finally, we compared longitudinal and transverse spin relaxation lengths using this sample.

- Chapter 6: Experiments on the spin absorption effect in a system where the spin absorber is extremely large compared to the spin diffusion length of the nonmagnetic material. We proposed a lateral spin valve device with a nonmagnetic/ferromagnetic bilayer spin channel. This structure showed that the magnetization direction of the large spin absorber rotates by the sweep of the external magnetic field. Here, we estimated the longitudinal and transverse spin modulation ratio and its spin relaxation lengths in this device. Then, we measured the temperature dependence of the spin signal and interestingly, the room temperature spin signal was larger than that at low temperature. In order to investigate this anomalous behavior, we extended the conventional one-dimensional spin diffusion model to a bi-layer channel structure, and found that the spin signal depends on the relative strength of flow among the two-dimensional spin absorber, the spin detector and other regions. By applying this conclusion to the conventional type of lateral spin valve, we have conceived that the temperature dependence of the spin signal depends on the junction area at the injector and detector. Here, we confirmed it by measuring the line width dependence of the temperature dependence of the spin signal.

- Chapter 7: Conclusion.

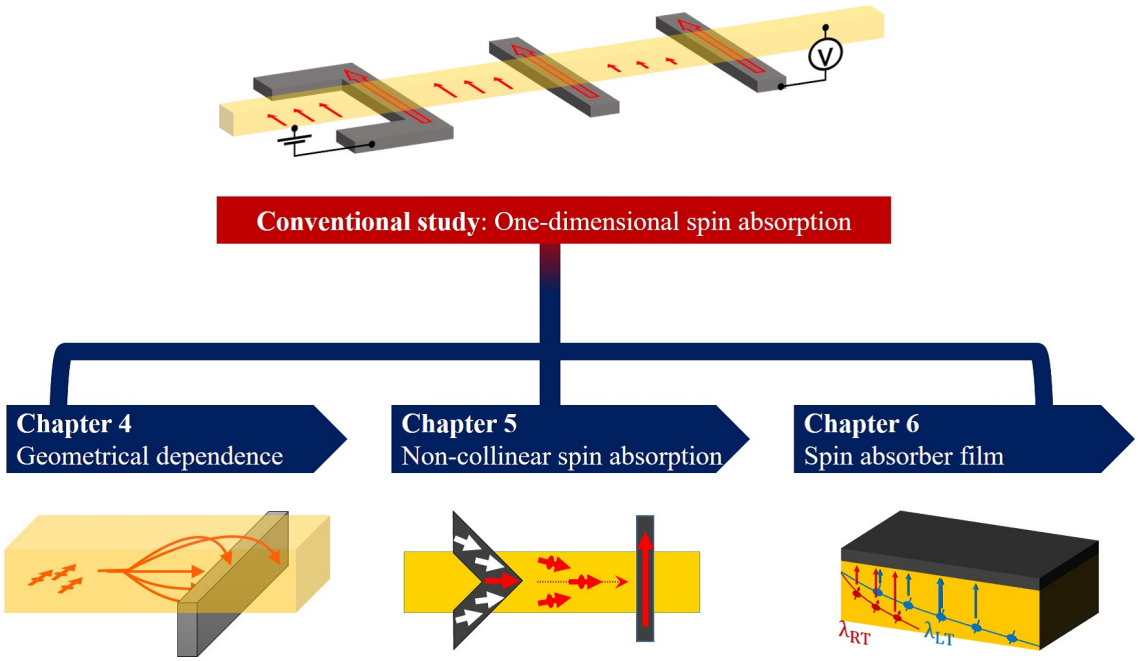

Figure 1.1: Structure of this thesis.

Chapter 2

Basic theory of electrically driven charge and spin transport

2.1 Introduction

In this chapter, the basic theory for multiple degrees of freedom of conduction electrons consisting of two physical quantities of charge and spin in a ferromagnetic/nonmagnetic junction structure is introduced. Systems containing spin-polarized materials such as ferromagnets provide spin degree of freedom in addition to electric charge. Three types of flow of electrons mixed with spin degrees of freedom are known: electric current, spin polarized current, and pure spin current. In this study, we investigate pure spin current which is the spin current without the electron charge. First, we introduce that the pure spin current is driven by diffusion, then describe the spin absorption effect which is the theme of this research. Finally, we describe a nonlocal method using a lateral spin valve which is a traditional research method of spin current.

2.2 Spin-dependent transport

The flow of electrons with two degrees of freedom of charge and spin is introduced in this section. The electron has two degrees of freedom, Charge -1 and Spin $\pm 1/2$. Therefore, the conducting electrons in the metal are mixed with two types of electrons: charge -1, spin $+1/2$ and charge -1, spin $-1/2$. In this case, in nonmagnetic metal such as copper wire, the two-fluid model is established because the spin diffusion length (several hundred to a few thousand nm) is longer than the mean free path (several nm) of electrons [31, 32]. This is called Mott's two-fluid model, and the conduction channel of electrons is defined as two kinds, up spin channel and down spin channel. Figure2.1 is a schematic illustration showing the flow of electrons in a nonmagnetic and a ferromagnetic material. Because there is no spin polarization for nonmagnetic material, charge flow J_{c} exists but spin flow J_{s} does not exist as shown in Fig.2.1(a). On the other hand, the band structure of the ferromagnet has spin dependent 3d band shift due to exchange interaction [2]. In addition, the 4s electron and the 3d electron coexist, and the electronic state of d electron is reflected in the conduction characteristic of s due to s-d interaction. For these reasons, although 4s electrons with a small effective mass are the main carriers of conduction electrons, their conductivities reflect the band structure of 3d electrons. Therefore, in case of Fig.2.1(b), since the downspin state density of 3d electrons at the Fermi level is larger than the upspin state density, s-d scattering of the downspin electron is affected strongly, resulting in the conductivity of the downspin electrons becomes small. Here, in the two fluid model considering the spin degree of freedom, the electron conductivity σ shows a spin dependence and can be expressed by

the following equation:

$$\sigma = \sigma_{\uparrow} + \sigma_{\downarrow}, \tag{2.1}$$

In such a two-fluid model, the current density J can be divided into a flow of charge and a flow of spin. The flow of charge is called electric current, whereas the flow of spin angular momentum is called spin current. The current density J_{c} and the spin current density J_{s} can be defined by the following equations:

$$\begin{cases} J_{\uparrow} + J_{\downarrow} = J_{\mathrm{c}}, & (2.2) \\ J_{\uparrow} - J_{\downarrow} = J_{\mathrm{s}} & (2.3) \end{cases}$$

Here, $J_{\uparrow}$ is the density of up spin current, and $J_{\downarrow}$ is the density of down spin current.

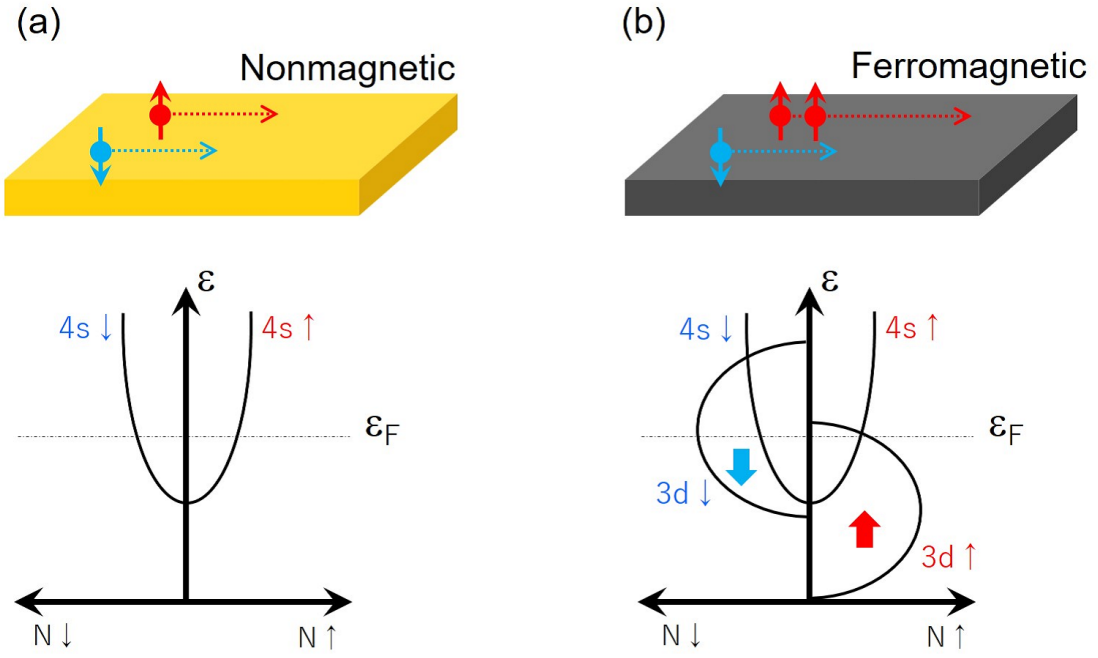

Figure 2.1: (a) Electron motion and band structure in a nonmagnetic material. Because of no exchange splitting of electrons at the Fermi surface, the conductivity of up and down spins are equal. As a result, the current densities of up and down spins are also equal. (b) Electron motion and band structure in a ferromagnetic material. The conductivity for up and down spins are different due to exchange splitting and s-d interaction of 3d electrons. As this result, the current densities of up and down spins are different.

2.3 Spin-dependent electrochemical potential

In order to represent two physical quantities of current and spin current by one equation, the spin dependent electrochemical potential is defined. The total current density in the metal can be expressed by the drift current J_{drift} caused by the electric field E and the diffusion current $J_{\mathrm{diffusion}}$ caused by the accumulation of localized electron density.

$$j_{\uparrow,\downarrow} = j_{\mathrm{drift}} + j_{\mathrm{diffusion}} = \sigma_{\uparrow,\downarrow} E - eD_{\uparrow,\downarrow} \nabla \delta n_{\uparrow,\downarrow}, \tag{2.4}$$

Where, $D_{\uparrow,\downarrow}$ is a diffusion constant and $\delta n_{\uparrow,\downarrow}$ is number of accumulated electrons for up and downspin states. The electric field can be represented by the gradient of the electrostatic potential ($E = -\frac{\partial V}{\partial x}$) , and the accumulated electron density shifts chemical potential from equilibrium($\delta n_{\uparrow,\downarrow} = N_{\uparrow,\downarrow}(E_{\mathrm{F}})\delta\varepsilon$, where the $N_{\uparrow,\downarrow}$ is the density of states in the subband and $\delta\varepsilon$ is the shift in the chemical potential of electrons from its equilibrium value). Considering the Einstein relation $\sigma_{\uparrow,\downarrow} = e^2 N_{\uparrow,\downarrow}(E_{\mathrm{F}}) D_{\uparrow,\downarrow}$, the flow of electrons can be expressed as follows using the electrochemical potential $\mu_{\uparrow,\downarrow}$:

$$j_{\uparrow,\downarrow} = -\frac{\sigma_{\uparrow,\downarrow}}{e} \nabla \left(-eV + \frac{\delta n_{\uparrow,\downarrow}}{eN_{\uparrow,\downarrow}(E_{\mathrm{F}})} \right) = -\frac{\sigma_{\uparrow,\downarrow}}{e} \nabla \left(-eV + \frac{\delta\varepsilon}{e} \right) = -\frac{\sigma_{\uparrow,\downarrow}}{e} \nabla \mu_{\uparrow,\downarrow}, \tag{2.5}$$

2.4 Electrical spin injection

Electrical spin injection is an epoch-making technique for generating pure spin current. It is difficult to observe the spin current because the spin scattering due to the s-d interaction is strong in the ferromagnetic material. Here, let us consider a case where a spin polarized current is caused to flow from a ferromagnet to a nonmagnet electrically by giving a electrical potential difference at the junction. As shown in Fig.2.2, because of no spin polarization between up spin band and down spin band, non-equilibrium

spin accumulates in non-magnetic material ($\delta n_{\uparrow,\downarrow}$). Therefore, a difference in density between up spin and down spin is created in a non-magnetic material. As a result, the total potential of the nonmagnetic material can be expressed by the following equation:

$$\mu_{\uparrow,\downarrow} = -eV + \varepsilon_{\mathrm{F}} \frac{\Delta n_{\uparrow,\downarrow}}{N_{\uparrow,\downarrow}(\varepsilon_{\mathrm{F}})}, \tag{2.6}$$

In the vicinity of the interface of the nonmagnetic material where spins have accumulated, the concentration of up spins is large and that of down spins is small. Therefore, up spin spreads by diffusion to reduce its amount. On the other hand, down spin gathers by diffusion to increase its amount. The spin current is a phenomenon in which up and down spin electrons diffuse in opposite directions, respectively.

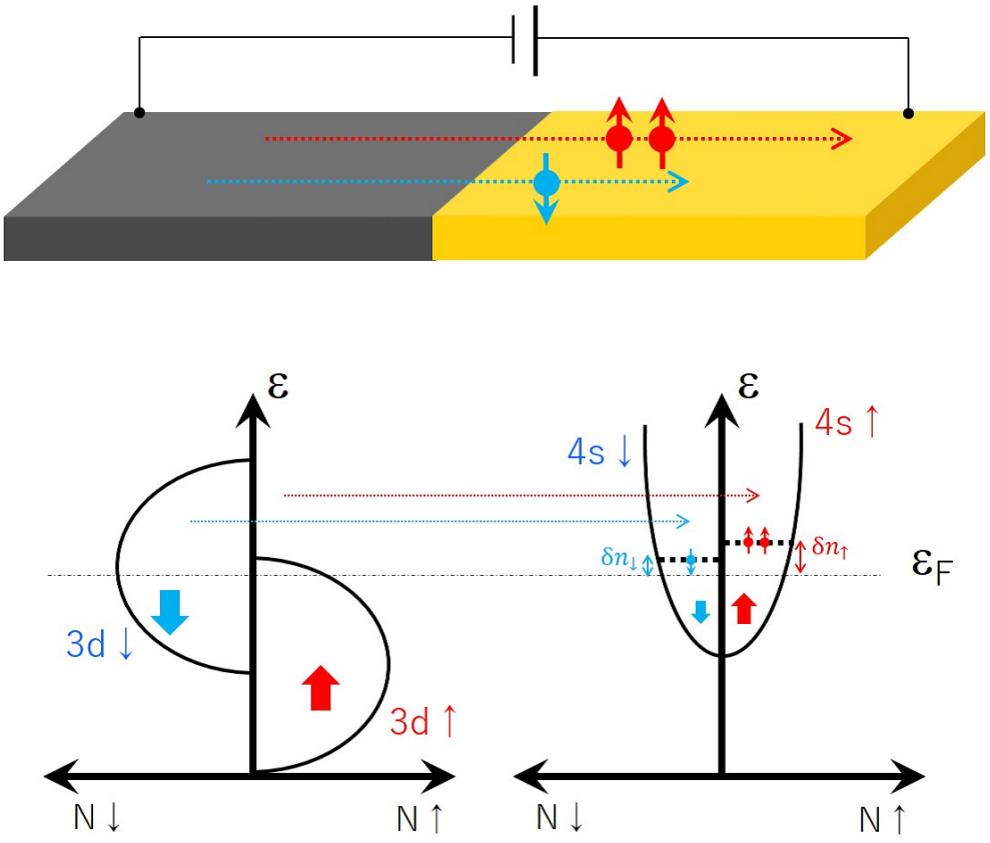

Figure 2.2: Electrical spin injection in a ferromagnetic/nonmagnetic hybrid structure. A electrostatic potential difference is applied to the junction between a ferromagnetic material and a nonmagnetic material, and spin polarized electrons are injected into a nonmagnetic material. A difference in density between up spin and down spin is created in the nonmagnetic material.

2.5 Spin polarized current and pure spin current

In this section, the spin polarized current which is the charge flow together with the spin flow, and the pure spin current which is the flow of the spin without accompany charge are introduced. In the electrical spin injection, the spin current distribution exists in a region where there is no electrical potential difference. In spin current, up spin and down spin propagate by diffusion, respectively, and signs of diffusion directions are different. Therefore, the definition of current density with respect to up spin and down spin is as follows, current density as drift current and spin current density as diffusion current.

$$\begin{cases} j_{\mathrm{c}} = j_{\uparrow} + j_{\downarrow} = 2j_{\mathrm{drift}}, & (2.7) \\ j_{\mathrm{s}} = j_{\uparrow} - j_{\downarrow} = 2j_{\mathrm{diffusion}} & (2.8) \end{cases}$$

The current driving force is the gradient of the electrostatic potential $E(= \nabla V)$ and the driving force of the spin current is the gradient of the spin dependent chemical potential $\nabla\mu_{\uparrow,\downarrow}$. From this, it is understood that the electric current and the spin current are propagated by independent physical laws, respectively. Now, we consider the electric spin injection in the system as shown in Fig.2.3. Since the current flows due to the drift current, it propagates by the electrical potential difference. On the other hand, since the spin current flows by diffusion, it spreads isotropically in the nonmagnetic material channel. Accordingly, the spin current flows in a region not only having an electrical potential gradient but also in a region having no electrical potential gradient. In this way, a spin polarized current flows in a region having an electrostatic potential. On the other hand, in the region without the electrostatic potential, only the flow of spin can be created. This is called pure spin current [12, 14, 15, 33].

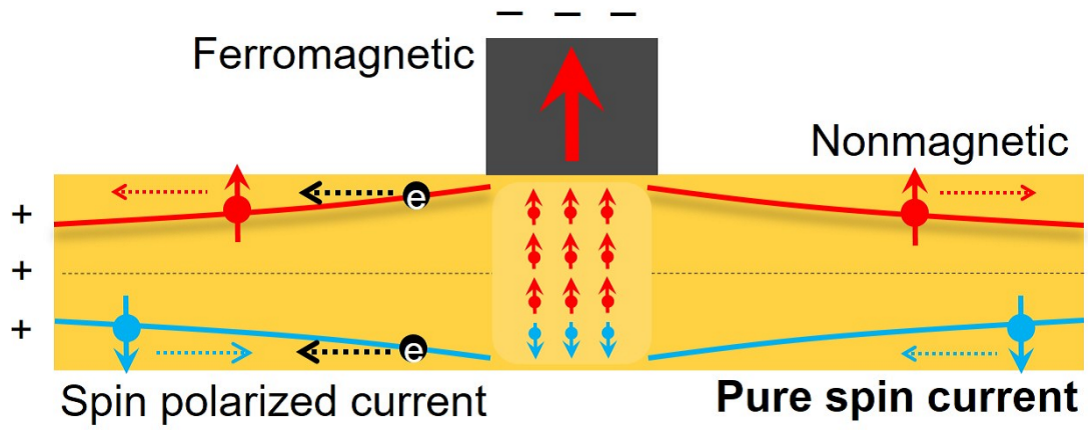

Figure 2.3: Nonequilibrium spin diffusion in a nonmagnetic material. The figure is a schematic illustration when a electrostatic potential difference is applied at the ferromagnetic/nonmagnetic junction. Non-equilibrium spin accumulation is created at the nonmagnetic material. Red (blue) line represents change in chemical potential due to spin accumulation of up (down) spin band. Since non-equilibrium spin flows so as to complement the concentration difference, up spin and down spin diffuse in opposite directions to each other. During diffusion, spin relaxation decreases the difference in density between up spin and down spin with distance. The left hand side of the nonmagnetic material in the figure shows the spin polarized current which has both charge and spin flow. The right hand side of the nonmagnetic material in the figure shows pure spin current which is only the flow of spin.

2.6 Spin relaxation

The pure spin current diffuses into a material with a strong spin relaxation when non-equilibrium spin accumulates. So, the spin flows from the spin accumulation source to a region with strong spin relaxation so that the electric current corresponds to the flow from the + potential to the - potential. The spin relaxation mechanism in the metal is D'yakonov-Perel' mechanism and Elliott-Yafet mechanism.

In the D'yakonov-Perel' mechanism, electrons precess by spin-orbit interaction, and are scattered during the orbital motion resulting in loss of spin information. It is observed in a system with strong spin-orbit interaction. For example, Pt as a heavy metal, or a surface of oxidized copper which is a broken system of space inversion symmetry [34]. In recent years spin relaxation caused by the Kondo effect has been proposed [35,36]. This effect is the central topic of Chapter 6. Additionally, in a ferromagnet, it has a strong spin relaxation occurs due to exchange interaction in addition to spin orbit interaction.

In the Elliott-Yafet mechanism, spin quantization axis is reversed due to the spin orbital interaction during the electron scattering. It is observed in a system with weak spin-orbit interaction. For example, copper as a spin channel. Considering the effect of spin relaxation, the spin relaxation time can be defined as $\tau_{\uparrow,\downarrow}$. Because of no change in the total number of electrons in the relaxation process of the spin current, the spin current can be expressed by the following equation from the relation of spin relaxation:

$$\frac{\partial J_{\uparrow,\downarrow}}{\partial x} = -e\left(\frac{\Delta n_{\uparrow}}{\tau_{\uparrow,\downarrow}} + \frac{\Delta n_{\downarrow}}{\tau_{\downarrow,\uparrow}}\right), \tag{2.9}$$

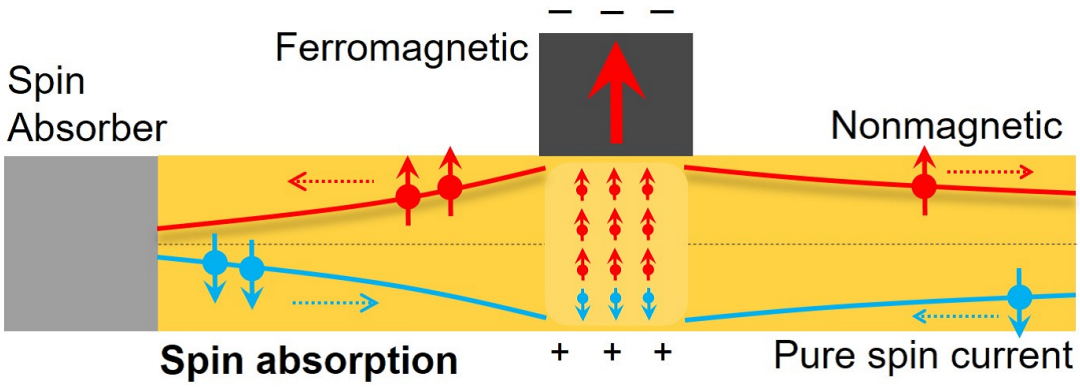

Figure 2.4: Non-equilibrium spin diffusion in a non-magnetic material when spin absorbers are connected. For convenience, the electrostatic potential difference is taken as shown in this figure. A pure spin current spreads in the nonmagnetic material. A strong spin relaxation causes spin absorption effect from the left hand side of the nonmagnetic channel where the spin absorber is connected. As a result, diffusion of the pure spin current is promoted and a lot of pure spin current flows towards the spin absorber.

2.7 Spin absorption effect

As shown in Fig.2.4, the spin absorption effect is a phenomenon in which a spin current is absorbed into a material with a strong spin relaxation [22, 37–40]. Heavy metals and ferromagnets are generally used for spin absorption due to the strong spin relaxation. Since heavy metals have large nuclei, spin orbit interaction causes electrons to dissipate spin current. On the other hand, in ferromagnets, dissipation of the spin current is caused by s-d scattering. Because of these effects spin relaxation becomes stronger, spin current is preferentially absorbed by these materials.

2.8 Spin diffusion equation

Pure spin current is expressed using diffusion equation [19,21,88]. Equations (2.4), (2.9), and equilibrium states of non-equilibrium spin $\frac{N_\uparrow(\varepsilon_F)}{\tau_{\uparrow,\downarrow}} = \frac{N_\downarrow(\varepsilon_F)}{\tau_{\downarrow,\uparrow}}$, the spin current can be expressed as the following equation:

$$\frac{\partial^2 \Delta\mu}{\partial^2 x} = \frac{1}{\lambda}\Delta\mu, \tag{2.10}$$

Here, $\lambda = \sqrt{D\tau_{sf}}$ is the spin-diffusion length, with the spin-relaxation time τ_{sf} and diffusion constant D, which is given by: $1/\tau_{sf} = 1/\tau_{\uparrow,\downarrow} + 1/\tau_{\downarrow,\uparrow}$, $1/D = \sigma/(\sigma_\downarrow D_\uparrow + \sigma_\uparrow D_\downarrow)$ $= N(N_\downarrow/D_\uparrow + N_\uparrow/D_\downarrow)$

2.9 Spin resistance

Let us define the concept of spin resistance as an index of the strength of spin diffusion [21, 41, 88]. So far, although spin current has been characterized by spin relaxation length, it is redefined according to the concept of electric circuit. In other words, we define Ohm's law for spin current in this section. It enables us to quantitatively express the pure spin current as an electrical quantity, which is a non-conserved amount. From equation (2.10), the general solution of the spin-dependent electrochemical potential depending on the spin accumulation can be expressed by the following equation:

$$\Delta\mu = \Delta\mu_+ \exp\left(\frac{x}{\lambda}\right)\Delta\mu_- \exp\left(-\frac{x}{\lambda}\right), \tag{2.11}$$

Consequently, the spin current driven by this potential can be expressed by the following equation:

$$I_{\mathrm{s}} = \left(-\frac{\sigma_{\uparrow}}{2e}\frac{\partial \mu_{\uparrow}}{\partial x} + \frac{\sigma_{\downarrow}}{2e}\frac{\partial \mu_{\downarrow}}{\partial x} \right) S = \frac{(1-P^2)\sigma_{\mathrm{F}} S}{2\lambda} \left[\frac{\Delta\mu_{-}}{e} \exp\left(-\frac{x}{\lambda}\right) - \frac{\Delta\mu_{+}}{e} \exp\left(\frac{x}{\lambda}\right) \right] \tag{2.12}$$

Here, $P = (\sigma_{\uparrow} - \sigma_{\downarrow})/(\sigma_{\uparrow} - \sigma_{\downarrow})$ is the spin polarization, S is the cross-sectional area of the spin channel, and λ is the spin diffusion length. Here, these coefficients $R_{\mathrm{F}}^{\mathrm{s}} \equiv 2\rho\lambda_{\mathrm{F}}/[S(1-P^2)]$ are defined as spin resistances. As a result, the spin current can be represented as follows:

$$I_{\mathrm{s}} = \frac{1}{R_{\mathrm{F}}^{\mathrm{s}}} \left[\frac{\Delta\mu_{-}}{e} \exp\left(-\frac{x}{\lambda}\right) - \frac{\Delta\mu_{+}}{e} \exp\left(\frac{x}{\lambda}\right) \right] \tag{2.13}$$

From the above equation, the spin current can be understood by the spin accumulation voltage which decreases exponentially with the distance with the spin resistance as a coefficient. Here, since the spin polarization is 0 for the nonmagnetic material, the spin resistance in a nonmagnetic channel can be expressed as $R_{\mathrm{N}}^{\mathrm{s}} \equiv 2\rho\lambda_{\mathrm{N}}/S$.

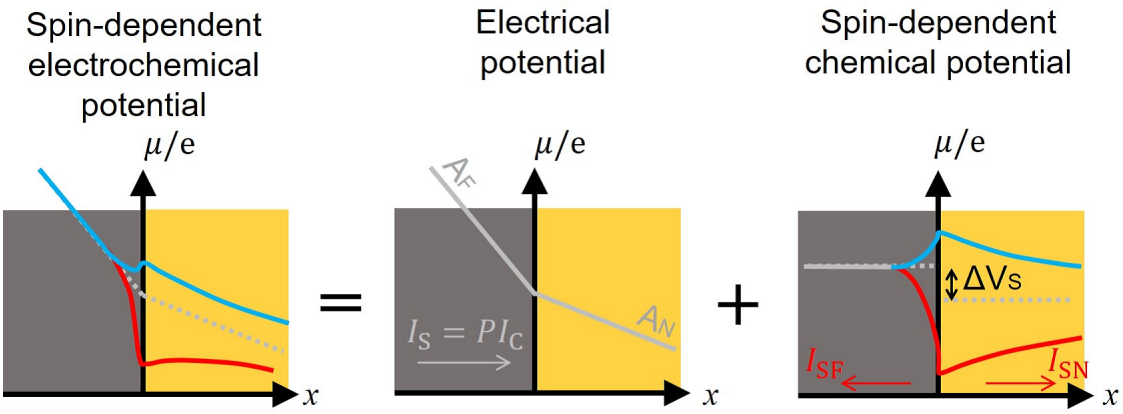

Figure 2.5: Spin-dependent electrochemical potential diagram when electrical spin injection is performed. The spin-dependent electrochemical potential can be considered separately for the electric circuit and the spin accumulation circuit.

2.10 Spin accumulation voltage by spin injection

The injected spin current density is quantitatively expressed using electrical physical quantities. The spin accumulation created by spin injection is represented by the voltage. Therefore, when a current flows from a ferromagnetic material to a non-magnetic material, the resistance increases at the interface. As shown in Fig.2.5, the electrochemical potential diagram can be divided into electrostatic potential and spin-dependent chemical potential: First of all, let us pay attention to the electric circuit by the electrostatic potential. The total current $I_c = \frac{S}{e}\left(\sigma_\uparrow \frac{\partial \mu_\uparrow}{\partial x} + \sigma_\downarrow \frac{\partial \mu_\downarrow}{\partial x}\right)$ when a potential difference is applied to the ferromagnetic/nonmagnetic interface is constant regardless of position, and if it is far away from the interface, it is also to be constant $\frac{\partial \mu_{\uparrow,\downarrow}}{\partial x} = A$. Therefore, the gradient of the potential indicated by the electric circuit in the figure 2.5 can be

expressed by the following equation:

$$\begin{cases} A_{\mathrm{F}} = \dfrac{eI_{\mathrm{c}}}{S}\dfrac{1}{\sigma_{\mathrm{F}}}, & (2.14) \\ A_{\mathrm{N}} = \dfrac{eI_{\mathrm{c}}}{S}\dfrac{1}{\sigma_{\mathrm{N}}} & (2.15) \end{cases}$$

On the other hand, in order to consider the voltage generated by the pure spin current, the change of the spin dependent chemical potential should be considered. When a potential difference is applied to the ferromagnetic/nonmagnetic junction, the spin current flows to the ferromagnetic material and the nonmagnetic material respectively. Therefore, the combined spin resistance of the injector junction can be expressed by the following parallel circuit:

$$R_{\mathrm{s}} = \frac{R_{\mathrm{s1}}R_{\mathrm{s2}}}{R_{\mathrm{s1}} + R_{\mathrm{s2}}}, \tag{2.16}$$

Therefore, the detected spin voltage ΔV_{s} and the increase in resistance caused by spin accumulation at the spin injection junction R_{SL} can be expressed by the following equations:

$$\begin{cases} \Delta V_{\mathrm{s}} = \dfrac{\lambda_{\mathrm{F}}\lambda_{\mathrm{N}}P^2 I_{\mathrm{c}}}{S[\lambda_{\mathrm{F}}\sigma_{\mathrm{N}} + (1-P^2)\lambda_{\mathrm{N}}\sigma_{\mathrm{F}}]}, & (2.17) \\ R_{\mathrm{SL}} = \dfrac{\lambda_{\mathrm{F}}\lambda_{\mathrm{N}}P^2}{S[\lambda_{\mathrm{F}}\sigma_{\mathrm{N}} + (1-P^2)\lambda_{\mathrm{N}}\sigma_{\mathrm{F}}]} & (2.18) \end{cases}$$

Since the ferromagnetic material at the injector has a small spin resistance, most of the spin current is reabsorbed by the ferromagnetic material, and the amount of the generated spin current is small [42]. The spin resistance of a ferromagnetic material depends on the spin polarization, and when a CoFe-based alloy which is a high spin polarized material is used, the spin resistance of the ferromagnetic material increases and the spin generation efficiency also increases.

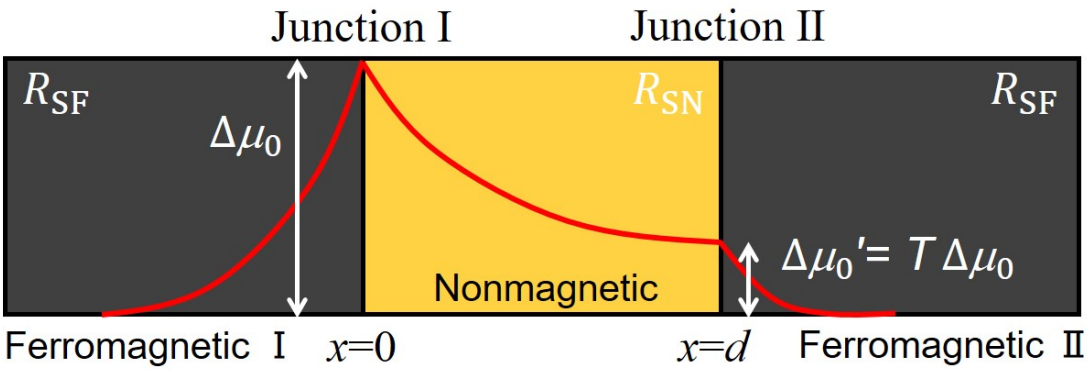

Figure 2.6: Spin-dependent electrochemical potential diagram in a FM/NM/FM junction structure. Red line represents change in chemical potential due to spin accumulation of up spin band. Accumulated pure spin current at the Junction I. ($\Delta\mu_0$) diffuses into the Ferromagnetic I. and the Nonmagnetic channel by the spin relaxation effect. The pure spin current reached at the Junction II. has a spin accumulated voltage $\Delta\mu_0'$ which is characterized by a transmission coefficient (T) and an accumulated pure spin current at the Junction I. ($\Delta\mu_0$).

2.11 Spin accumulation voltage due to spin absorption

Let us consider the spin accumulation voltage in the laminated structure composed of ferromagnetic spin injection source/nonmagnetic spin channel/ferromagnetic spin absorber. Spin accumulation created at the junction I. and spin current is absorbed into the junction II. as shown in Fig. 2.6. The spin current generated at the junction I. can be understood by a series circuit of a nonmagnetic spin channel and a ferromagnetic spin absorber. The spin accumulation and the spin current at the junction I., spin accumulation and spin current at the junction II. and each boundary condition with $x = 0, d, \infty$

can be expressed by equations shown as below:

$$\begin{cases} \Delta\mu(x) = A\exp\left(-\dfrac{x}{\lambda_{\mathrm{N}}}\right) + B\exp\left(\dfrac{x}{\lambda_{\mathrm{N}}}\right), & (2.19) \\ I_{\mathrm{S1}}(x) = \dfrac{1}{eR_{\mathrm{SL}}}\left[A\exp\left(-\dfrac{x}{\lambda_{\mathrm{N}}}\right) - B\exp\left(\dfrac{x}{\lambda_{\mathrm{N}}}\right)\right], & (2.20) \\ \Delta\mu(x) = C\exp\left(-\dfrac{x-d}{\lambda_{\mathrm{N}}}\right) + D\exp\left(\dfrac{x-d}{\lambda_{\mathrm{N}}}\right), & (2.21) \\ I_{\mathrm{S2}}(x) = \dfrac{1}{eR_{\mathrm{SL}}}\left[C\exp\left(-\dfrac{x-d}{\lambda_{\mathrm{N}}}\right) - D\exp\left(\dfrac{x-d}{\lambda_{\mathrm{N}}}\right)\right], & (2.22) \end{cases}$$

$$\begin{cases} \Delta\mu_0 = A + B, & (2.23) \\ \Delta\mu_0' = A\exp\left(-\dfrac{d}{\lambda_{\mathrm{N}}}\right) + B\exp\left(\dfrac{d}{\lambda_{\mathrm{N}}}\right) = C + D, & (2.24) \\ \dfrac{1}{eR_{\mathrm{SL}}}\left[A\exp(-\dfrac{d}{\lambda_{\mathrm{N}}}) - B\exp(\dfrac{d}{\lambda_{\mathrm{N}}})\right] = \dfrac{1}{eR_{\mathrm{SR}}}(C-D), & (2.25) \\ \mathrm{D} = 0, & (2.26) \end{cases}$$

Here, R_{SF} and R_{SN} are the spin resistance of the ferromagnetic material and the spin resistance of the non-magnetic material, respectively. Also, $\Delta\mu_0$ and $\Delta\mu_0'$ are the spin-dependent electrochemical potentials at junctions I. and II., respectively. From the above relationship, the transfer coefficient T and the combined spin resistance R_{SR} at the nonmagnetic spin channel/ferromagnetic spin absorber junction can be expressed by the following equations, respectively:

$$\begin{cases} T = \dfrac{\Delta\mu_0'}{\Delta\mu_0} = \dfrac{R_{\mathrm{SN}}}{R_{\mathrm{SN}}\cosh\left(\frac{d}{\lambda_{\mathrm{N}}}\right) + R_{\mathrm{SF}}\sinh\left(\frac{d}{\lambda_{\mathrm{N}}}\right)}, & (2.27) \\ R_{\mathrm{SR}} = \dfrac{\Delta\mu_0}{eI_s(0)} = \dfrac{R_{\mathrm{SN}}\sinh\left(\frac{d}{\lambda_{\mathrm{N}}}\right) + R_{\mathrm{SF}}\cosh\left(\frac{d}{\lambda_{\mathrm{N}}}\right)}{R_{\mathrm{SN}}\sinh\left(\frac{d}{\lambda_{\mathrm{N}}}\right) + R_{\mathrm{SF}}\cosh\left(\frac{d}{\lambda_{\mathrm{N}}}\right)}, & (2.28) \end{cases}$$

Therefore, using above equations, the spin accumulation voltage at the spin injection junction and the spin absorption junction can be expressed by the following equations:

$$\begin{cases} \Delta\mu_0 = I_{\mathrm{s}}R_{\mathrm{s}} = PI\dfrac{R_{\mathrm{SL}}R_{\mathrm{SR}}}{R_{\mathrm{SL}}+R_{\mathrm{SR}}}, & (2.29) \\ \Delta\mu_0' = \dfrac{eP_{\mathrm{F}}R_{\mathrm{F}}^2R_{\mathrm{N}}I_{\mathrm{c}}}{4R_{\mathrm{F}}(P_{\mathrm{F}}+P_{\mathrm{N}})(\cosh\left(\frac{d}{\lambda_{\mathrm{N}}}\right) + \sinh\left(\frac{d}{\lambda_{\mathrm{N}}}\right) + R_{\mathrm{N}}^2\sinh\left(\frac{d}{\lambda_{\mathrm{N}}}\right)}, & (2.30) \end{cases}$$

2.12 Quantitative detection of spin accumulation by lateral spin valve

A method for experimentally evaluating of the generated pure spin current is described in this section [12–16]. By using the ferromagnetic/nonmagnetic/ferromagnetic junction structure, the spin current density can be quantitatively evaluated. As shown in Fig. 2.7(a), by preparing the lateral structure, it is possible to create a region where no electrostatic potential exists. As discussed previously, this structure is called lateral spin valve, and it can not only generate a pure spin current but also helps us experimentally estimate the spin accumulation voltage. Considering the pure spin current where is injected from the ferromagnetic material FM I. is absorbed by the ferromagnetic material FM II. Because of the continuity of the chemical potential, the diffused pure spin current is absorbed from NM to FM I.. Here, since the spin current injected into the NM and the magnetization of the FM II. is oriented in the same direction, many spins of the injected spin current flow through the FM II. with a slight potential energy difference. On the other hand, the minority spins are relaxed while changing the potential energy strongly so as to satisfy $I_{\rm c} = 0$, resulting in the flowing spin current forming equilibrium with the potential energy. At this time, the potential energy stabilizes at 0 V, because the nonmagnetic material is stable in the same state of up spin and down spin. Therefore, when spin polarized direction of the detected spin current and the magnetization direction of the detector are the same direction, a positive voltage $V_{+}^{\uparrow\uparrow} - V_{-}^{\uparrow\uparrow}$ is observed at the detector. On the other hand, if one side of the FM is inverted, the detected spin current and the magnetization direction of the detector become antiparallel, and a negative

voltage $V_{+}^{\downarrow\downarrow} - V_{-}^{\downarrow\downarrow}$ is observed. Since a single magnetic domain structure is generally used as FM, the obtained spin signal has a steep signal change as shown in Fig. 2.7(b). As a result, the observed signal depends on the parallel and antiparallel states of the magnetizations direction between the injector and the detector $V_{+}^{\uparrow\uparrow} - V_{+}^{\downarrow\downarrow}$. Since the signal is proportional to the amount of the applied current, the amplitude of the signal is divided by the applied current usually. This is called a spin signal, which represents an amount of the spin current density. The spin signal can be expressed by the following equation:

$$R_{\mathrm{s}} = \frac{2P}{eI_{\mathrm{c}}}\Delta\mu_0' = \frac{P_{\mathrm{F}}^2 R_{\mathrm{F}}^2 R_{\mathrm{N}}}{2R_{\mathrm{F}}(P_{\mathrm{F}} + P_{\mathrm{N}})(\cosh\left(\frac{d}{\lambda_{\mathrm{N}}}\right) + \sinh\left(\frac{d}{\lambda_{\mathrm{N}}}\right) + R_{\mathrm{N}}^2 \sinh\left(\frac{d}{\lambda_{\mathrm{N}}}\right)}, \tag{2.31}$$

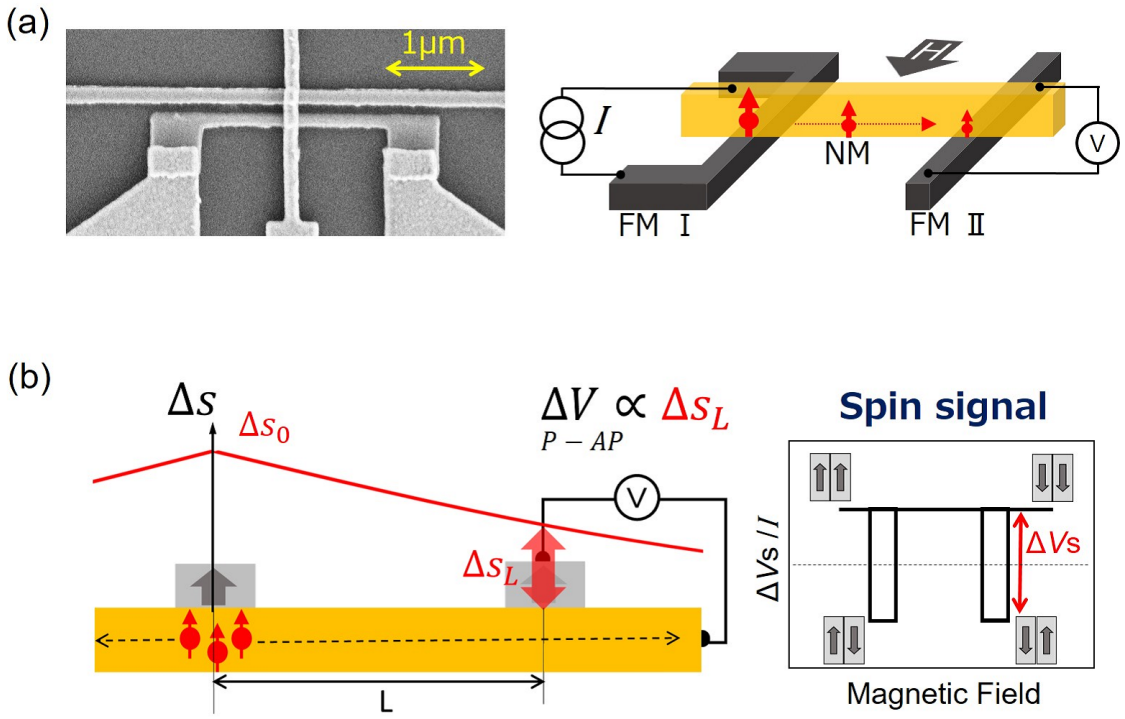

Figure 2.7: Scanning electron microscope image and schematic illustration of the lateral spin valve structure (a). Also, a schematic illustration of spin current density change from the spin accumulated junction to the spin detected junction, and spin signal (b). The spin signal can be observed by inverting the magnetization of FM injector and FM detector. The amplitude of the spin signal represents the spin current density reaching at the detector.

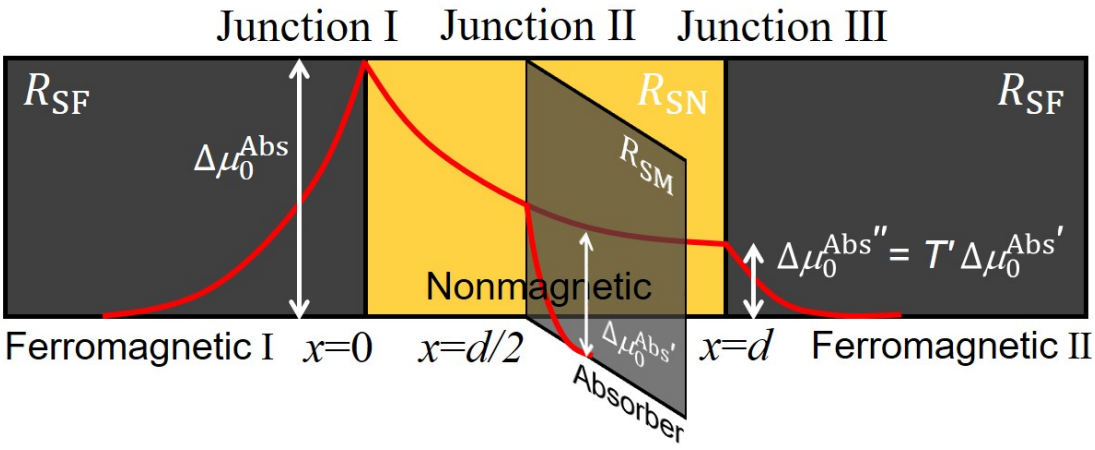

Figure 2.8: Spin-dependent electrochemical potential diagram in FM/NM/FM/NM/FM junction structure. Red line represents change in chemical potential due to spin accumulation of up spin band.

2.13 Quantitative detection of spin accumulation in a lateral spin valve including a spin absorber

Let us consider the spin accumulation voltage in the laminated structure consisting of FM/NM/FM/NM/FM [21,88]. As shown in the figure 2.8 spin accumulation generated at junction I., and spin absorption occurs at junction II. and junction III.. The spin accumulation voltage generated at the junction III. is as follows:

$$R_s = \frac{2P}{eI_c}\Delta\mu_0^{Abs''} = \frac{4P_{F2}\,R_M R_F}{R_N\left[\cosh\left(\frac{d}{\lambda_N}\right)-1\right] + 2R_M \sinh\left(\frac{d}{\lambda_N}\right) + 2R_F\left(1+\frac{R_F}{R_N}\right)\left(1+2\frac{R_M}{R_N}\right)\exp\left(\frac{d}{\lambda_N}\right) - 2R_F}, \quad (2.32)$$

Here, R_{SM} is the spin resistance of the spin absorber. Also, $\Delta\mu_0^{Abs}$, $\Delta\mu_0^{Abs'}$, $\Delta\mu_0^{Abs''}$ is the spin-dependent electrochemical potential for junction I., II., and III..

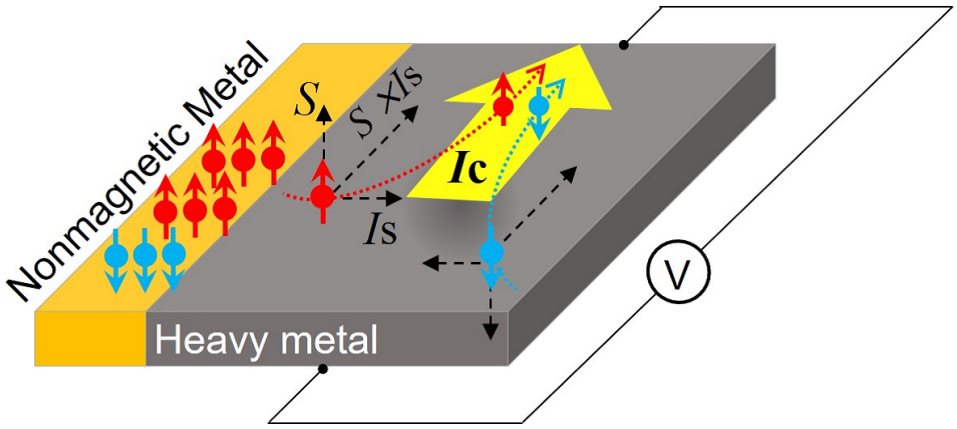

Figure 2.9: Schematic illustration of the inverse spin Hall voltage detection. Up spin and down spin receive forces in the direction of $S \times I_s$ due to the spin orbit interaction. Since up spin and down spin flow in the same direction, electric current is generated. This is called an inverse spin Hall effect, and it enables us to convert the spin current into an electric current.

2.14 Quantitative detection of spin accumulation by inverse spin Hall effect

Another method for quantitatively evaluating the spin current density is the inverse spin Hall effect [14,43–48]. When observing the inverse spin Hall effect, heavy metals are used as spin absorbers as shown in the figure 2.9. Since heavy metals have large nuclei, the orbit of conduction electrons are bent by an effective electric field. This Hamiltonian can be expressed by the following equation:

$$\mathcal{H} = \frac{e\hbar^2}{4m^2c^2}\frac{1}{r}\frac{dV(r)}{dr}\boldsymbol{s}(\boldsymbol{r}\times\boldsymbol{p}) \equiv \lambda \boldsymbol{s}\cdot\boldsymbol{L}, \tag{2.33}$$

Here m is the effective mass of electrons, c is the speed of light, V (r) is the spherical symmetry potential of the atom, $\boldsymbol{s}$ is the electron spin quantum number, $\boldsymbol{L}$ is the orbital angular momentum of the atom. As the above equation shows, the sign of the Hamiltonian depends on the inner product of the spin quantum axis and the spin orbital angular momentum. In addition, the spin current is a phenomenon in which up spin and down spin diffuse in opposite directions. Therefore, in heavy metals, up spin and down spin trajectories are bent. As a result, up spin and down spin diffuse in the same direction as shown in Fig. 2.9. Electrically evaluation of the spin current density can be realized using this effect. The magnitude of inverse spin Hall current is defined by the following equation:

$$\boldsymbol{s} \times \boldsymbol{I}_{\mathrm{s}} = \boldsymbol{I}_{\mathrm{c}} \tag{2.34}$$

This enables to detect the spin information without using the ferromagnetic detector, leading to the simplification of the device structure and its integration.

Chapter 3

Device fabrication and transport measurement

3.1 Introduction

In this section, the device fabrication techniques and equipments used in this research are described. The device fabrication techniques used in this study are lift-off method and etching method. For patterning the circuit, we used an electron beam lithography system. For depositing the metal, an electron beam evaporation, a resistance heating vapor deposition, a magnetron sputtering, and an Ar ion milling equipment were used. The method of preparing the sample used in each experiment will be described again in the experiment method section of each chapter.

3.2 Microfabrication technique used in this research

3.2.1 Lift-off method and Etching method

The sample preparation in this study was carried out by repeating lift-off method and etching method for several times. The flow of each processing steps for the lift-off and etching methods are shown in Fig. 3.1. A lift-off method is a technique for fabricating

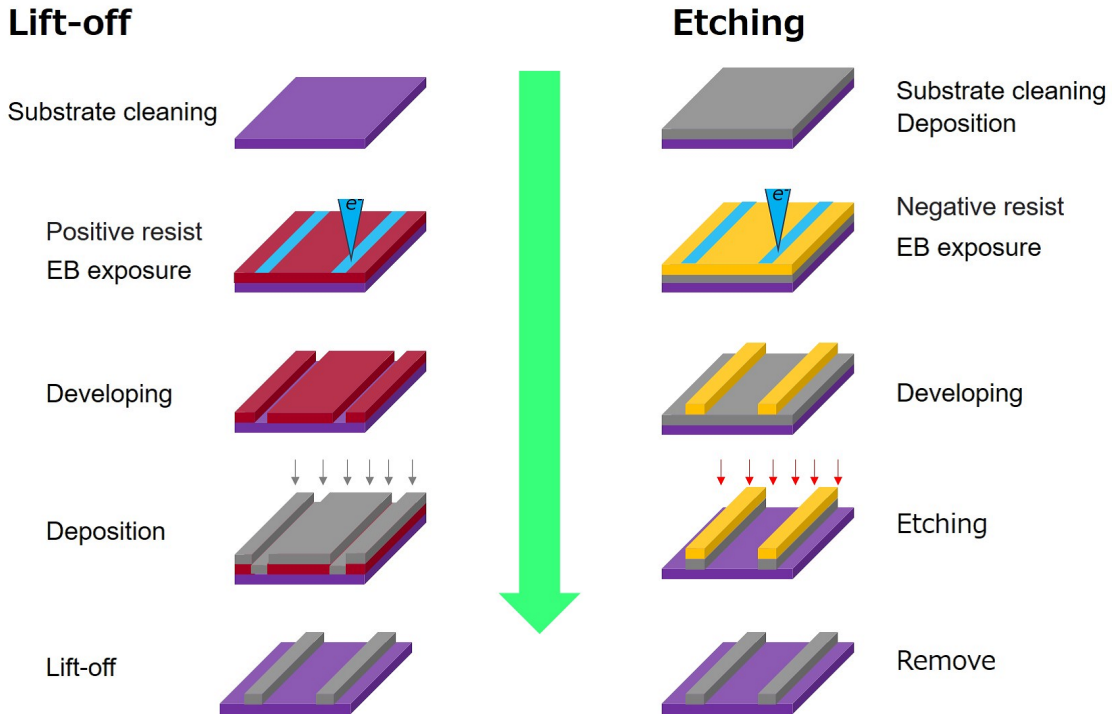

Figure 3.1: Lift-off method Etching method

a desired circuit by irradiating an electron beam to a highly sensitive positive resist. A positive resist on a substrate is dissociated a combination of polymers by applying an electron beam. A portion where an electron beam is irradiated is dissolved by immersing it in a developer, so that a circuit mask is completed. Then, by depositing a metal and immersing it in a remover, only the drawn metal remains. Using this process, we can

fabricate a sample with a submicron order channel width. In the sample preparation of this study, the lift-off method was used for fabrication of ferromagnetic thin wires and nonmagnetic thin wires. On the other hand, the etching method is a technique for fabricating a desired circuit by irradiating an electron beam onto a negative resist. By immersing the sample in the developer, the area to which the electron beam is applied is solidified and the other area is peeled off. Thereafter, a desired circuit can be formed by removing the resist of no irradiated areas with the electron beam by an Ar ion milling machine. In the preparation of the sample of this study, the etching method was used to prepare ferromagnetic dots of the nanopillar lateral spin valve which is describing in Chapter 3. The flow chart is shown in Fig. 3.2, and the procedure for fabricating the lateral spin valve and the nanopillar-based lateral spin valve are shown below. And the flow chart for the nanopillar-based lateral spin valve is shown in Fig. 3.3.

3.2.2 Fabrication of ferromagnetic thin wire

1. First, a resist film was formed on a thermally oxidized silicon substrate by using a spin coater, where ZEP 520 A for a positive type resist was applied, and rotate this sample at the rotation speed of 5000 rpm.

2. In order to sinter the resist, it was heated with hot plate at 180 degree for 120 seconds.

3. In order to prevent charge-up during electron beam writing, spread Espacer uniformly with the spin coater 3000 rpm.

4. Patterning by electron beam, we used ELS-7800 manufactured by ELIONIX, where

the acceleration voltage of the electron beam was 80 kV, the current amount was 0.1nA, and the dose amount was 2.4 μsec/dot. The current amount of 0.1nA was used to prevent the expansion of the channel width due to the proximity effect.

5. Developing the substrate by immersing it in developer and rinse.

6. Depositing the ferromagnetic metal using ultrahigh vacuum electron beam evaporation equipment.

7. Lift-off treatment was carried out by immersing in ZDMAC which is a remover.

3.2.3 Fabrication of nonmagnetic thin wire

1. First, a resist film was formed on a substrate prepared in subsection 3.2.2 by using a spin coater, where ZEP 520 A for a positive type resist was applied, and rotate this sample at the rotation speed of 3000 rpm.

2. In order to sinter the resist, it was heated with hot plate at 180 degree for 60 seconds. The reason for reducing the heating time is to prevent deterioration of the ferromagnetic thin wire.

3. In order to prevent charge-up during electron beam writing, spread Espacer uniformly with the spin coater 3000 rpm.

4. Patterning by electron beam, we used ELS-7800 manufactured by ELIONIX, where the acceleration voltage of the electron beam was 80 kV, the current amount was 4.0nA, and the dose amount was 0.05 μsec/dot. However, the current amount was 0.1nA, and the dose amount was 2.4 μsec/dot for drawing of channel thin lines.

5. Developing the substrate by immersing it in developer and rinse.

6. Depositing the nonmagnetic metal using ultrahigh vacuum Joule evaporation equipment.

7. Lift-off treatment was carried out by immersing in ZDMAC which is a remover.

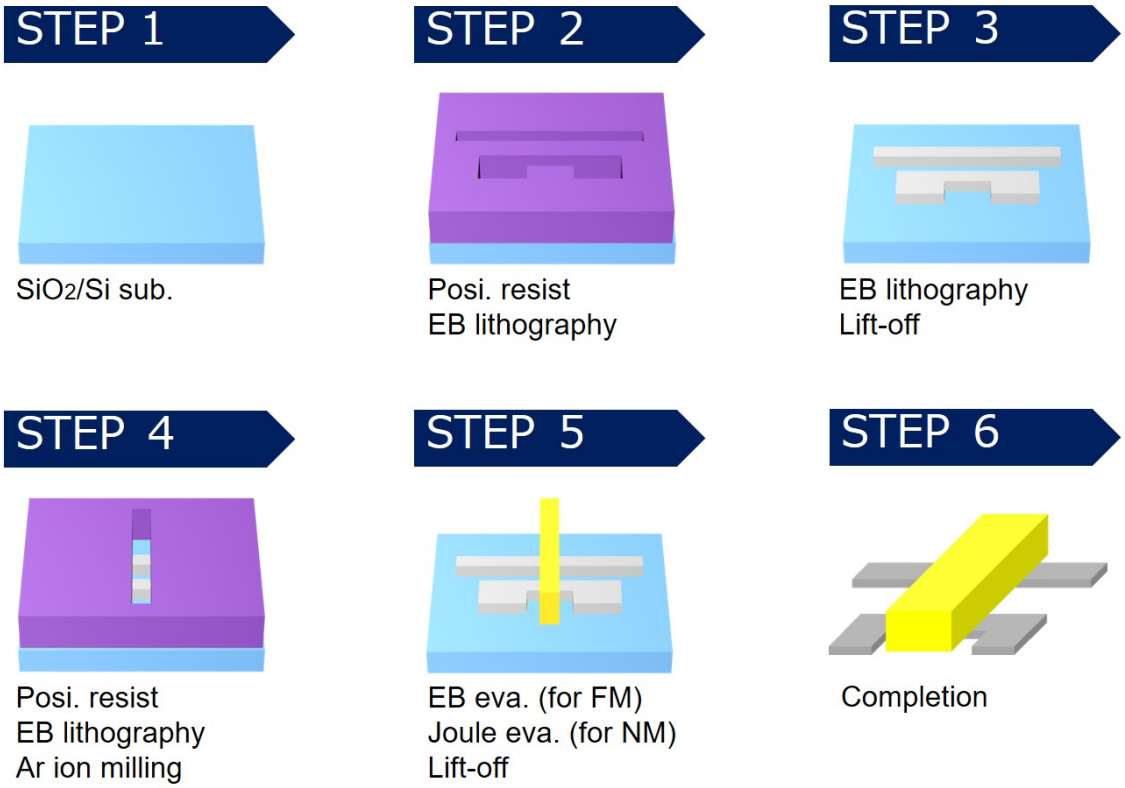

Figure 3.2: Fabrication flowchart for the lateral spin valve.

3.2.4 Fabrication of ferromagnetic dots

1. A two-layer film of Cu/Py was deposited on a thermally oxidized silicon substrate by using an ultrahigh vacuum evaporation equipment.

2. A resist film was prepared using a spin coater, where TGMR for a negative type resist was applied, and rotated this sample at the rotation speed of 3000 rpm. In order to strengthen a connection with TGMR, HMDS was uniformly coated with spin coater 3000 rpm in advance.

3. In order to sinter the resist, it was heated with hot plate at 110 degree for 90 seconds.

4. Patterning by electron beam using ELS-7800 manufactured by ELIONIX, where the acceleration voltage of the electron beam was 80 kV, the current amount was 0.05nA, and the dose amount was 2.6 μsec/dot.

5. In order to further strengthen the area to which the electron beam was applied, it was heated with hot plate at 120 degree for 90 seconds as a pre-bake.

6. Developing the substrate by immersing it in developer and rinse.

7. Milling the metal film with dotted resist by Ar ion milling.

8. TGMR was peeled off by immersing it in 1-methyl-2-pyrrolidone as a remover.

Figure 3.3: Fabrication flowchart for the nanopillar-based lateral spin valve.

3.3 Sample fabrication machines

3.3.1 Electron beam lithography

An electron beam lithography is an equipment that fabricates a desired submicron circuit by irradiating an electron beam of an extremely short wavelength. The illustration of internal system with an exterior photo is shown in Fig. 3.4 By applying an acceleration voltage of 80 kV to the thermal field emission electron gun, it enable to realize minimum beam diameter of 2 nmϕ, and one can obtain a sample with thin line width of 10 nm or less. The intensity of the electron beam can be controlled using a focusing lens and a movable diaphragm. The beam can be rounded by the astigmatism corrector, and focus

and position are adjusted by an electrostatic deflector and objective lens. The position of the stage can be accurately adjusted by using the laser length measuring system. It has also a secondary electron detector and has a function as a scanning electron microscope.

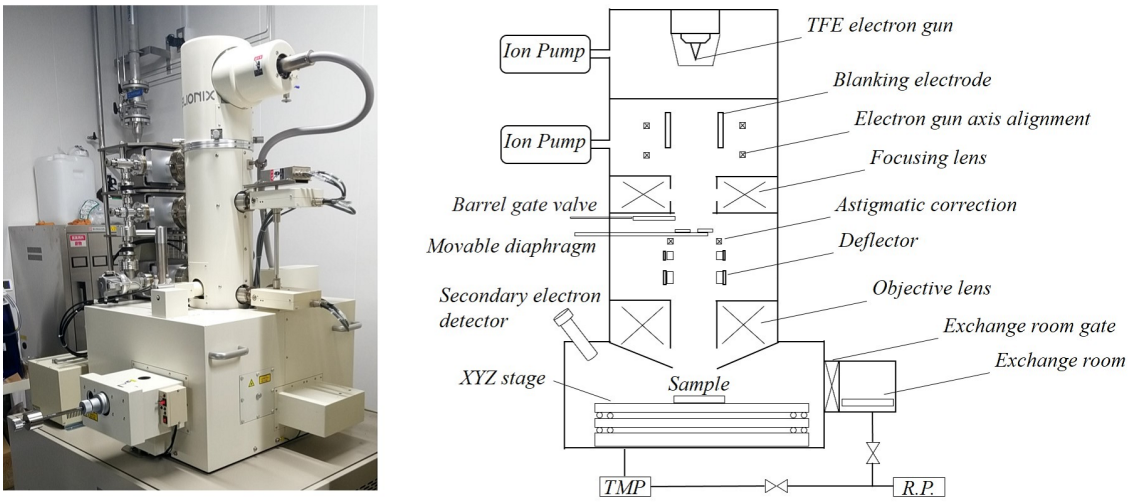

Figure 3.4: Electron beam lithography

3.3.2 Ultra-high vacuum quadruple electron beam evaporation system

An electron beam evaporation is an evaporation method using an electron beam. The illustration of internal system with an exterior photo is shown in Fig. 3.5. The vapor deposition source of electron beam equipment used in this study is a quadruple independent control type. The target metal is placed on a water-cooled hearth made of a refractory metal and is deposited by irradiating with an electron beam. Since heat is applied locally, it is possible to deposit a material with a high melting point. To prevent corruption of quality, a stainless steel chamber with less gas discharge from the inner

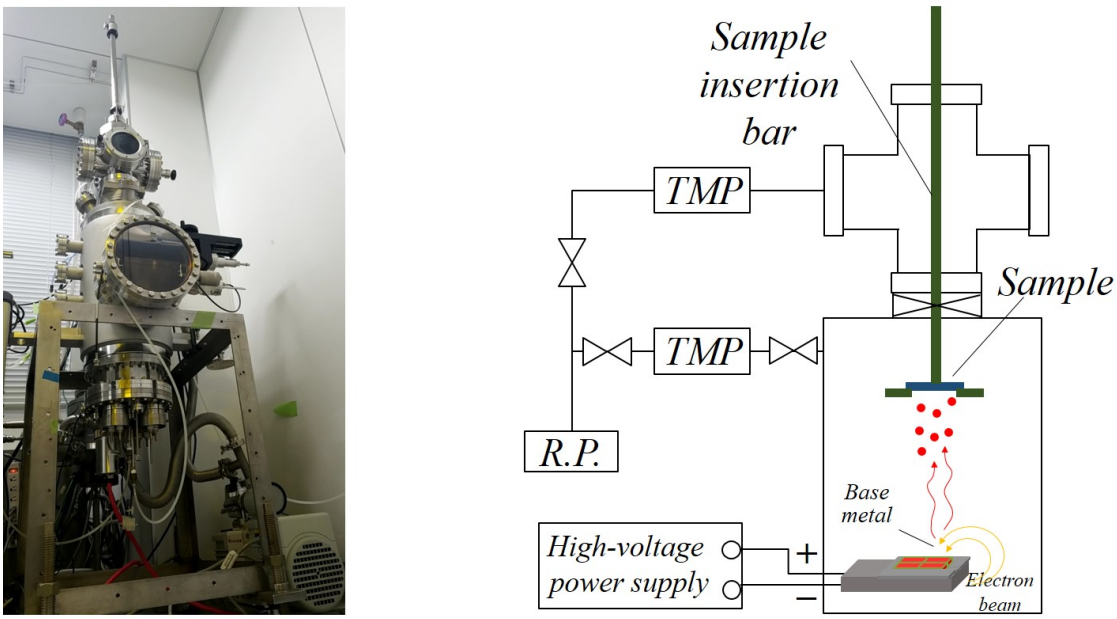

Figure 3.5: Ultra-high vacuum quadruple electron beam evaporation system

wall has been used. The equipment used in this study enables ultrahigh vacuum of 10^{-9} Torr by exhausting with oil rotary pump (RP), turbo molecular pump (TMP). In this research, this equipment has been used for depositing NiFe (Permalloy: Py).

3.3.3 Ultra-high vacuum resistance heating vapor deposition system

The resistance heating deposition method is a vapor deposition technique by melting a metal placed on a refractory plate using Joule heating. The resistance heating vapor deposition system is shown in Fig. 3.6. The material of the boat was applied W which has a sufficiently high melting point and does not alloy with Cu. The experimental equipment used in this study is a composite equipment capable of resistive heating evaporation, electron beam evaporation and ion milling. The equipment enables ultrahigh vacuum of

10^{-9} Torr by exhausting with RP, TMP, and a Cryo Pump (CP). The present equipment was used for vapor deposition of Cu. In addition, in order to make the highly transparent interfaces at each junction, the low voltage Ar ion milling was carried out. This is also equipped with a triplet electron beam evaporation system. In experiments, it was used for the deposition of CoFeAl (CFA) alloys.

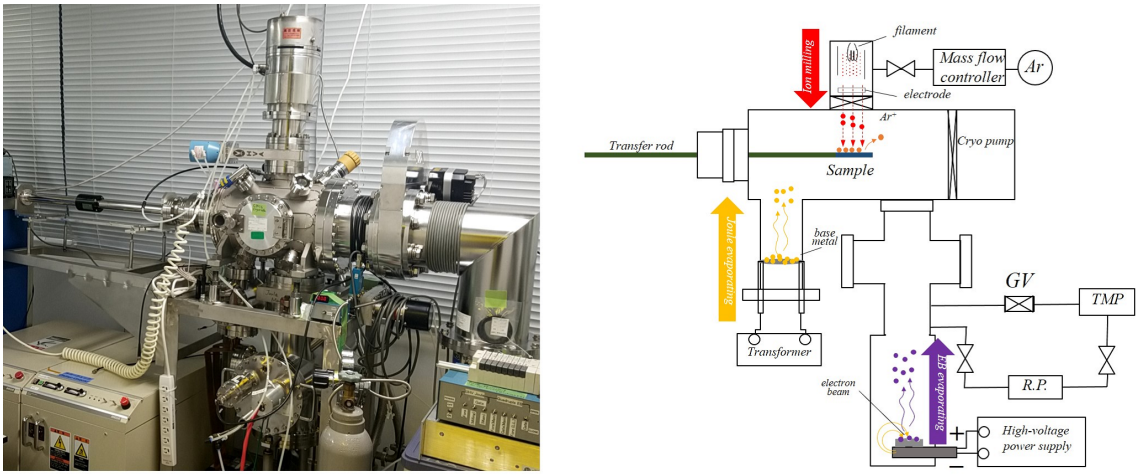

Figure 3.6: Ultra high vacuum resistance heating vapor deposition system.

3.3.4 High vacuum magnetron sputtering equipment

Sputtering is a technique of depositing a metal by colliding with an ionized Ar gas and a target constituting a desired metal. The sputtering system is shown in Fig. 3.7. This method enable to deposit a metal having a strong adhesion uniformly on a large area with almost no change in the composition ratio of the target. Also, since it does not require dissolution of the target, it can be used for a wide range of metals regardless of melting point. This sputtering machine is possible with pressure of 10^{-8} Torr order, and in this research we used this equipment depositing for SiO_2.

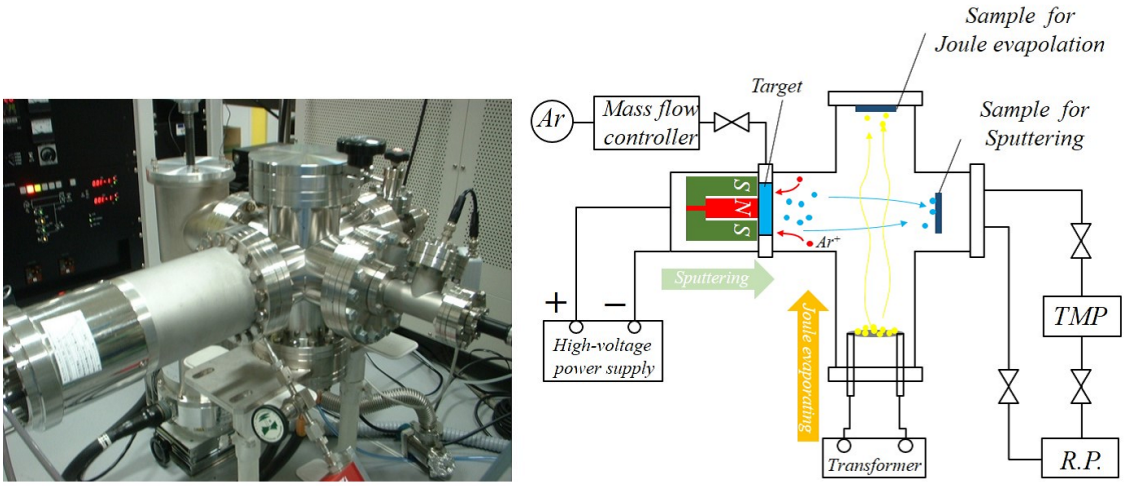

Figure 3.7: High vacuum magnetron sputtering equipment

3.3.5 Ar ion milling machine

Ar ion milling is a technique of milling a metal by colliding with an ionized Ar gas. The Ar ion milling machine shown in Fig. 3.8. An electric current is applied in the filament to take out thermoelectrons, and these are accelerated by the anode voltage and collide with the neutral molecules to ionize Ar. When the number of Ar ions increases, the gas in the ion gun becomes a plasma state, and the whole is at an equipotential. Only the ions are accelerated by the electric field between the screen electrode and the accelerating electrode, and the Ar ions are extracted, so that atoms on the surface of the sample are knocked out. In this research, Ar ion milling was used for fabricating the nanopillar-based lateral spin valve.

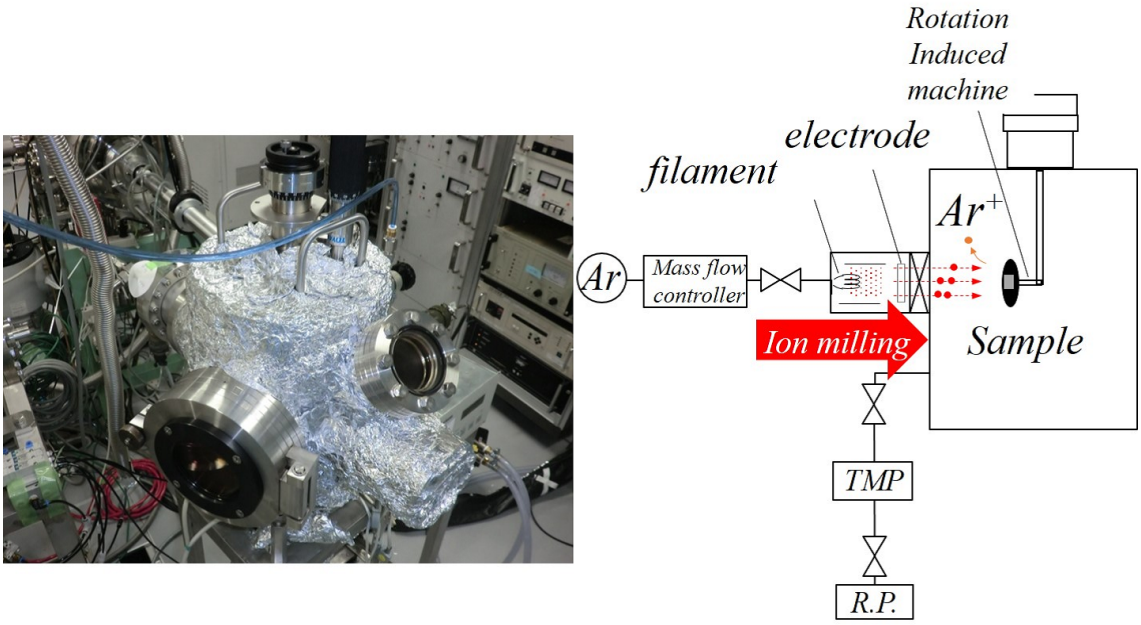

Figure 3.8: Ar ion milling machine

3.3.6 Scanning electron microscope

A scanning electron microscope is a microscope which is observed by detecting the emitted electron: secondary electrons, backscattered electrons, transmitted electrons, X-rays, cathode luminescence (fluorescence), internal electromotive force. A photo graph and a schematic illustration of its detection systems are shown in Fig. 3.9. Both the SE2 detector and the In-Lenz detector detect irregular information of secondary electrons of the sample. In-Lenz detects secondary electrons with relatively low energy. In general, the shortest wavelength of visible light is about 400 nm, and it is impossible to observe the microscopic asperity structure. An electron microscope enables observation with high resolution using an ultra short wavelength characteristic of an electron which can not be realized by an optical microscope. In this study, the present equipment was used

to observe a fine structure of a few hundred nm.

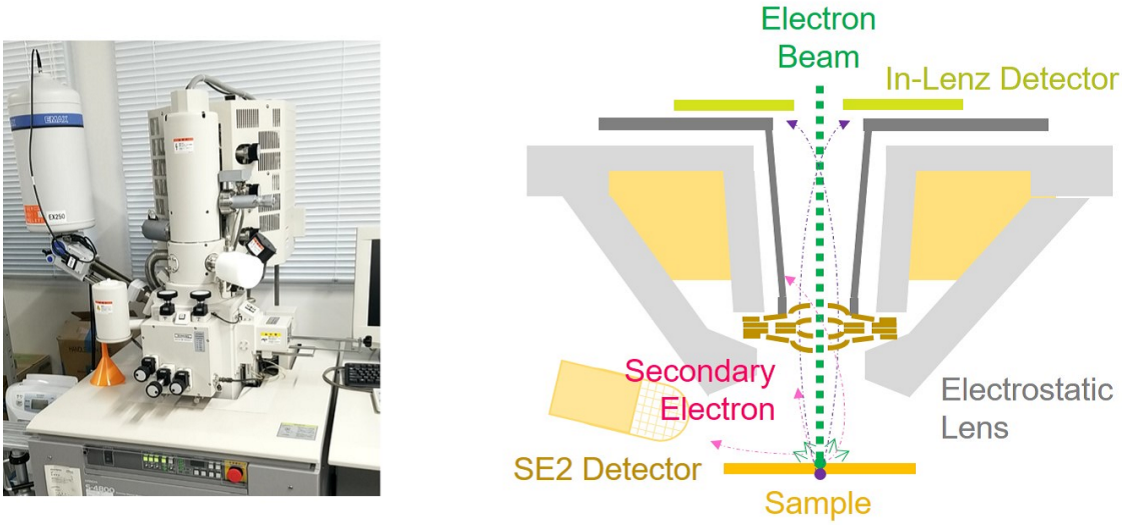

Figure 3.9: Scanning electron microscope

3.4 Sample evaluation equipment used in this study

3.4.1 Magnetic transport characteristics measurement system

A magnetic transport characteristics measurement system is a equipment for measuring the spin signal of a fabricated sample. The AC current is obtained by applying the voltage $V_{\text{p-p}}$ of 173 Hz from the oscillator via the resistance of 5.6 kΩ. At the same time, a voltage measurement terminal of V_+, V_- is provided at another terminal of the sample and it is connected to the differential amplifier. Since the signal to be measured is weak, the differential amplifier amplifies the voltage ΔV of $V_+ - V_-$. In addition, the filter (173 Hz band pass) and the amplifier filter can more amplify ΔV with reducing noise. Finally, read the ΔV using the digital multimeter which is amplified by the lock-in amplifier. Two multimeters show the real part and the imaginary part of the electric resistance (impedance), respectively, and the real part is a so-called ordinary resistance. Letting the sample resistance be R,

$$I_{\text{eff}} = \frac{1}{2\sqrt{2}} \frac{V_{\text{p-p}}}{5600 + R}$$

where, I_{eff} was taken as the effective value of I. Since $5600\Omega \gg R$ in the above equation, approximating 5600Ω yields I_{eff}. Therefore, from the Ohm's law, the resistance of the sample can be measured by $R = \Delta V / I_{\text{eff}}$. On the other hand, the external magnetic field was controlled by the DC current through the electromagnet coil. A bipolar power supply is used as the current source, and the generated current can be controlled by the control voltage. In this study, we used two kinds of low temperature measurement environments such as liquid nitrogen cooling device and liquid helium freezing device shown in Fig. 3.10.

MR measurement system
Cooling by liquid nitrogen

MR measurement system
Cooling by liquid helium

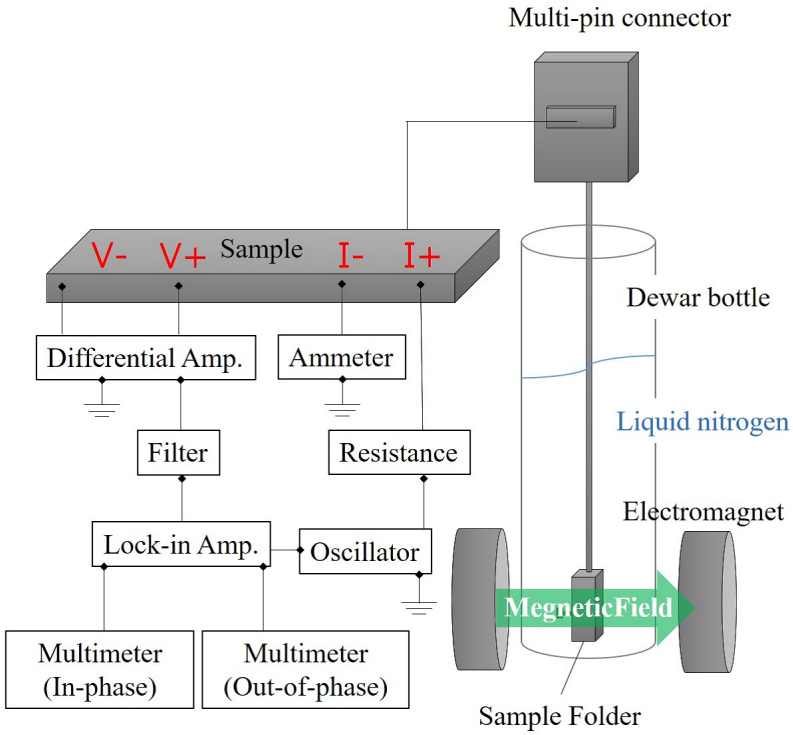

Figure 3.10: Magnetic transport characteristics measurement system

Chapter 4

Geometrical dependence of spin current absorption into a ferromagnetic nanodot

4.1 Introduction

Efficient manipulation of the spin current is a key ingredient for realizing next-generation spintronic devices with ultralow electric power consumption [49–52]. Because spin current diffuses by driving force of a gradient of the spin-dependent electrochemical potential, the spin current is absorbed into a material with a strong spin relaxation. This phenomenon is called spin absorption effect, and high spin absorption efficiency is required as one of the methods to control spin current. An ideal experimental platform for studying the spin absorption effect is provided by using a lateral spin valve. The lateral spin valve enables generation, control and detection of spin current. In addition, since it

has a spin channel width shorter than the spin diffusion length, it has been regarded as ideal one-dimensional spin diffusion so far. However, the spin absorption effect studied by the lateral spin valve has been limited to one-dimensional diffusion. In recent years, spin injection into various materials has been demonstrated [27–30, 53]. In addition, various types of spin devices using spin current have been proposed [12–16, 54–56]. In this context, it is important to study the spin absorption effect in a complex junction system with three-dimensional geometry.

In this study, we investigate the spin absorption effect in various geometries. First, we investigate the spin absorption effect using a specialized sample composed of small ferromagnetic dots and large two-dimensional nonmagnetic spin channel. This structure has large asymmetry between the ferromagnetic and nonmagnetic materials, a large chemical potential gradient is realized at the ferromagnetic/nonmagnetic junction. Therefore, the spin injection efficiency in this structure is increased, which has been demonstrated in previous studies [33, 64, 65]. However, the spin absorption efficiency in nano-pillar based lateral spin valves has not yet been evaluated. Since the large effective cross section for a two-dimensional nonmagnetic film decreases the effective spin resistance of the nonmagnetic channel, the spin absorption efficiency may decrease. In the present study, we experimentally evaluate the spin current absorption efficiency in the nano-pillar-based lateral spin valve. In addition, we also explore the better structure for realizing the efficient spin absorption.

4.2 Spin absorption characteristic in a nanopillar-based lateral spin valve

We have fabricated a nano-pillar-based lateral spin valve consisting of five ferromagnetic nanodots formed on a uniform nonmagnetic film. First, 200-nm-thick Cu and 20-nm thick Permalloy (Py) films were deposited by electron-beam evaporation on a thermally oxidized Si substrate at the base pressure of 4×10^{-9}Torr. Subsequently, electron-beam lithography was performed to form the elliptical-shaped resist masks. The Ar ion milling process has been performed to make the Py nano-pillar structures, followed by the SiO_2 sputtering. After making the contact holes in the SiO_2 insulating layer, the top Cu electrodes were formed by the conventional lift-off process. Thus, the array of the ferromagnetic nanodots was formed on the two-dimensional uniform nonmagnetic Cu film, as schematically shown in Fig.4.3. Here, the desired lateral dimensions for the Py1, Py2, Py3, and Py4, which were diagonally located on the Cu film, are approximately 120nm $\times$ 180nm. The desired dimension of the middle Py dot (Py5) is 120nm $\times$ 350nm, respectively. All the measurements in this study have been performed at 77K. Here, the resistivity for the Py is 24 $\mu\Omega$cm at 77K and that for Cu is 1.6 $\mu\Omega$cm at 77 K. First, we evaluated the spin injection and detection efficiency for each dot by measuring the nonlocal spin valve signals, which is a barometer for the lateral spin transports, with various probe configurations. Here, we fixed the voltage probe to the middle dot (Py5). The spin injection was performed from one of the diagonally located dots (Py1, Py2, Py3, or Py4). Since the Py5 is located at the shortest distance from each ferromagnetic dot, we only consider the spin injector and detector (Py5) by neglecting the influence

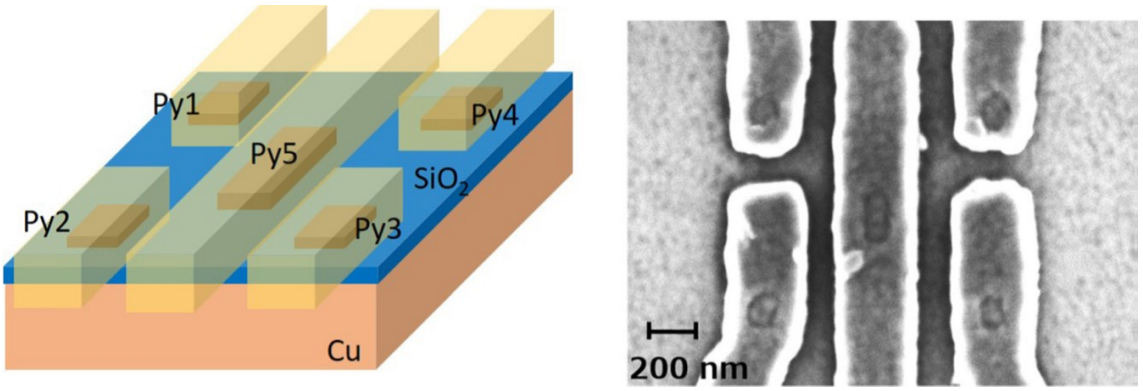

Figure 4.1: Scanning electron microscopy image of the fabricated nano-pillarbased lateral spin valve with the multi spin injectors together with a schematic illustration for the fabricated lateral spin valve. The top and bottom electrodes are electrically connected via the Py nanopillars, and other regions are separated by a 100-nmthick SiO2 insulating layer.

of the additional ferromagnetic dots. In this case, we can adapt the following basic equation for the nonlocal spin signal $\Delta R_{\rm s}$ commonly used in a conventional lateral spin valve [88]:

$$R_{\rm s} = \frac{P^2 R_{\rm PyIPyD} R_{\rm Cu}}{2R_{\rm Py}(P_{\rm Py}+P_{\rm Cu})(\cosh{(L/\lambda_{\rm Cu})}+\sinh(L/\lambda_{\rm Cu}))+R_{\rm Cu}^2\sinh(L/\lambda_{\rm Cu})}, \qquad (4.1)$$

Here, $\Delta R_{\rm s}$ corresponds to the overall change of the nonlocal voltage divided by the excitation current. P is the spin polarization for the injector or detector. d is the center-center distance between the injector and detector. λ_N is the spin diffusion length for the nonmagnetic channel, in this case Cu. $R_{\rm FI}$, $R_{\rm FD}$, and $R_{\rm N}$ are the spin resistances for the injector, detector, and nonmagnetic channel. The spin resistance is defined by $2\rho\lambda/(S(1-P^2))$, where ρ and S are, respectively, the electrical resistivity and the effective

cross section for the spin current [21].

Figure.4.2 shows the spin valve signals for four different configurations. The nonlocal spin signals exhibit clear spin-valve effects corresponding to either parallel (high) or antiparallel (low) state. Here, the negative and positive resistance changes correspond to the magnetization reversals for the spin injector and the detector, respectively. Although the desired distance between the injector and detector is fixed to be 650 nm in all configurations, the magnitudes of the spin signals are distributed from 0.57 mΩ to 0.70 mΩ. This difference may be due to the distributions of the lateral dimensions for the Py injectors and detectors, leading to the dispersion of the spin resistances for the injector and detector. Indeed, we can confirm from the SEM image that the Py3 has a relatively small lateral dimension compared to other Py dots. We also mention that the effective distance between the injector and detector has a small difference, leading to the distribution of the spin signal. Therefore, we believe that the difference in the spin signals is not caused by the material parameters such as uniformity and interface condition but by the dispersion of the geometrical parameters in the device.

In the above analysis, we neglected the influence of the other ferromagnetic dots on the spin current distribution. However, the obtained spin signal was smaller than the previously reported device with a similar lateral dimension [64]. This is because the spin current distribution is affected by other ferromagnetic dots. To clarify the influence of the multi spin injectors and to analyze the spin absorption efficiency due to the Py5, we evaluate the nonlocal spin valve signal with various probe configurations. Here, we compare the nonlocal spin valve signals between two configurations. One is the nonlocal spin valve measurement using Py1 and Py4 and the other one is that using Py1 and

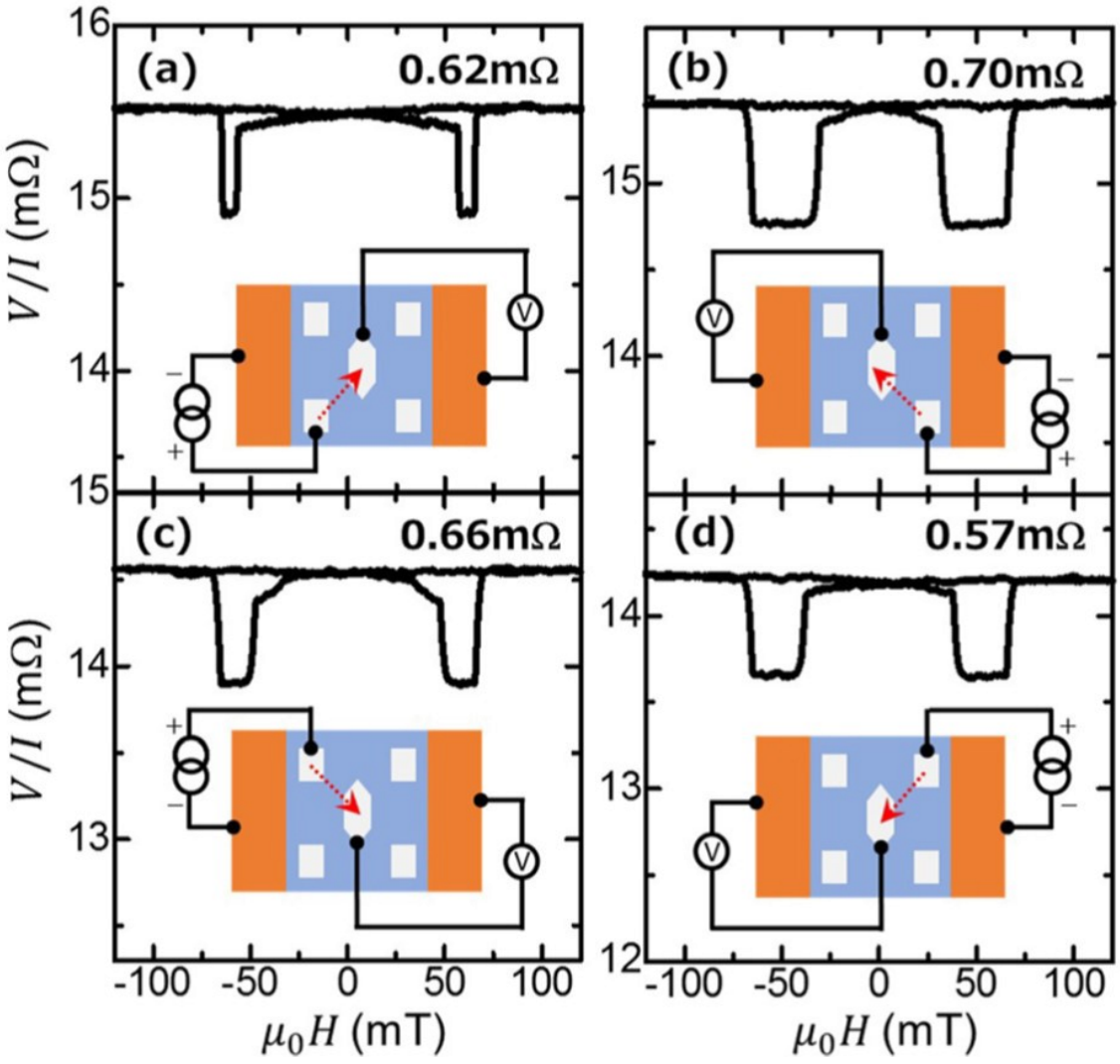

Figure 4.2: Nonlocal spin valve signals by using the Py5 detector with various spin injectors measured at 77 K. The inset shows a schematic illustration of the probe configuration and the obtained spin signal.

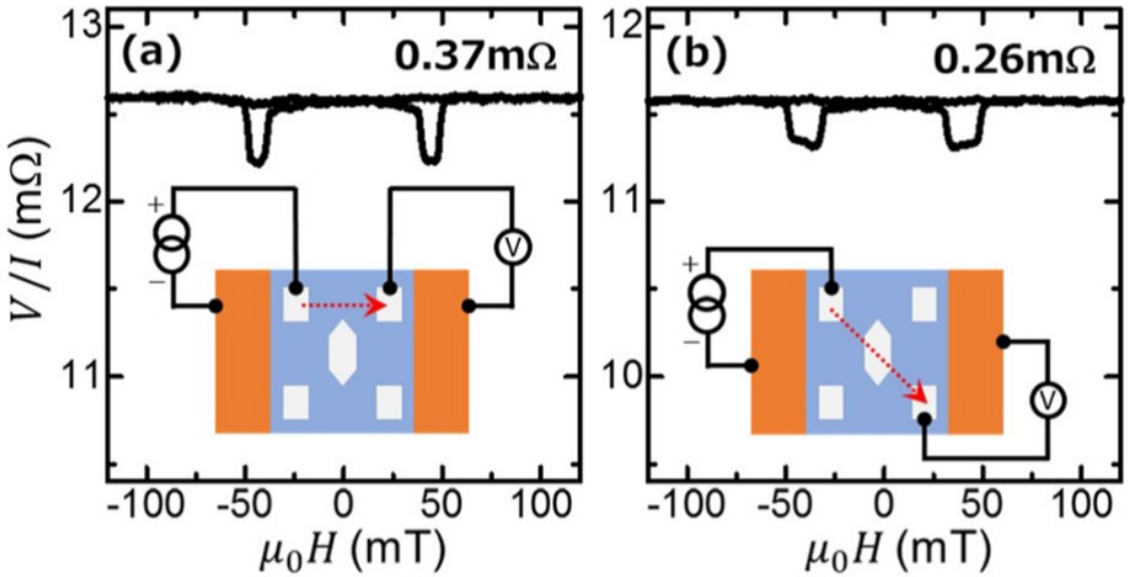

Figure 4.3: (a) Nonlocal spin valve signal by using the Py1 injector and Py4 detector. (b) Nonlocal spin valve signal by using the Py1 injector and Py3 detector. Here, Py 5 is placed at the middle between Py1 and Py3.

Py3. Here, it should be noted that in the latter configuration, a middle ferromagnetic dot (Py5) is located in between Py1 and Py4. Therefore, we expect that the significant reduction of the spin signal is expected because of the spin current absorption effect into Py5. As in Fig.4.3(a), the obtained spin signal using Py1 and Py4 is 0.37 mΩ , which is smaller than the value expected from the previous nanopillar lateral spin valve [64]. Moreover, as in Fig. 3(b), we obtain 0.26 mΩ, which is comparable to the spin signal in Fig.4.3 although a spin absorber is located at the center of the injector and detector. These results imply that the spin current absorption exists in both configurations.

To survey the probe-configuration dependence of the spin signal, we propose two different models based on the one dimensional spin diffusion model [68]. In the first

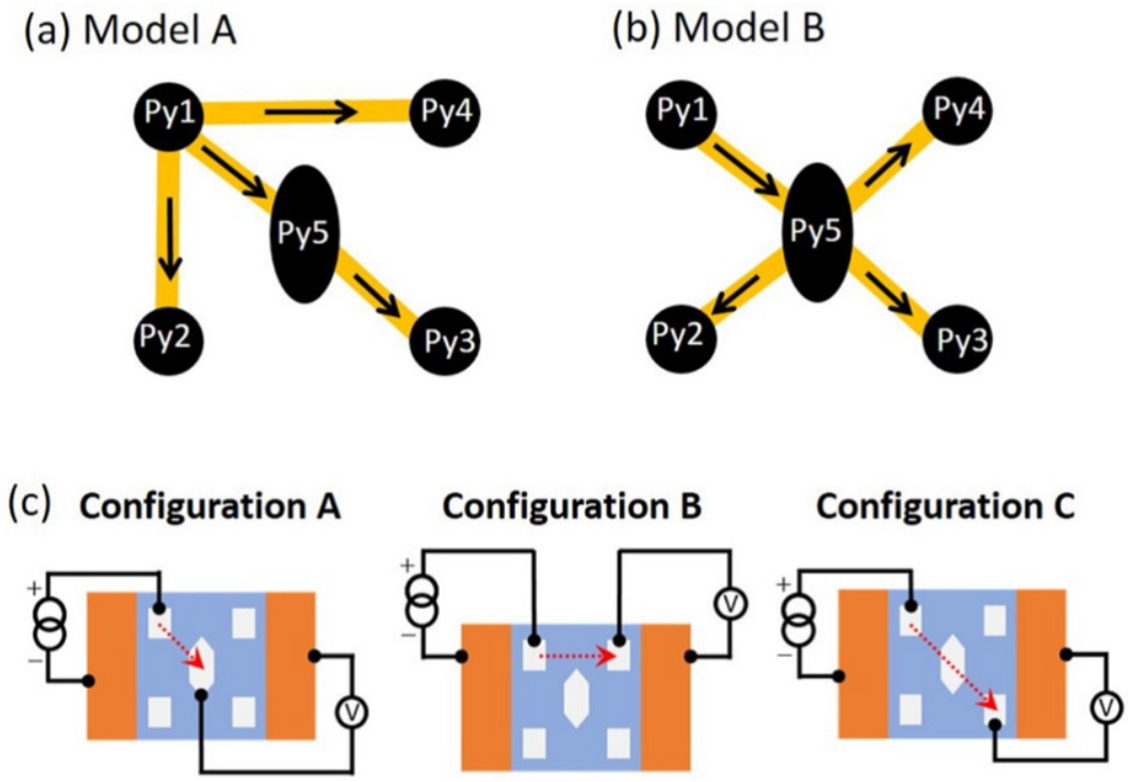

Figure 4.4: Schematic illustrations for two different spin diffusion models: (a) model A and (b) model B. (c) Schematic illustrations for the representative probe configurations A, B, and C.

model (model A), we consider the spin absorption effect only in the spin current diffusion along the diagonal direction, as conceptually shown in Fig.4.4(a). Here, we neglect the influence of the middle spin absorber on the spin diffusion to Py2 and Py3. In this case, by using $\rho_{\rm Py}\lambda_{\rm Py}/\rho_{\rm Cu}\lambda_{\rm Cu} = 0.2$, which is approximately equal to the ratio of the spin resistance for the ferromagnetic dot to that for the nonmagnetic Cu film [88], we can calculate the spin signals $\Delta R_{\rm s}^{\rm A}$, $\Delta R_{\rm s}^{\rm B}$, and $\Delta R_{\rm s}^{\rm C}$ for the configurations A, B, and C shown in Fig.4.4(c). From the calculation, we obtained the following relationship of the

spin signals:

$$\Delta R_{\mathrm{s}}^{\mathrm{B}} = 1.41\Delta R_{\mathrm{s}}^{\mathrm{A}}, \Delta R_{\mathrm{s}}^{\mathrm{C}} = 0.25\Delta R_{\mathrm{s}}^{\mathrm{A}} \tag{4.2}$$

Although the second relationship is reasonable, the first relationship is quite far from the experimental result, indicating invalid situation of the proposed model. To improve these discrepancies, we proposed another model (model B), in which we consider the spin absorption effect due to the middle Py dot for all branches. By using the same values of $\rho_{\mathrm{Py}}\lambda_{\mathrm{Py}}/\rho_{\mathrm{Cu}}\lambda_{\mathrm{Cu}}$ as in model A, we obtain the following relationship for the spin signals:

$$\Delta R_{\mathrm{s}}^{\mathrm{B}} = 0.65\Delta R_{\mathrm{s}}^{\mathrm{A}}, \Delta R_{\mathrm{s}}^{\mathrm{C}} = 0.32\Delta R_{\mathrm{s}}^{\mathrm{A}} \tag{4.3}$$

These values show reasonable consistency with the experimental results, indicating that the middle ferromagnetic dot acts as a good spin absorber even in the nanopillar-based lateral spin valve because of its large lateral dimension of the Py dot. However, because of the small spin resistance of the quasi-two-dimensional Cu film, the absorption efficiency is smaller than the conventional lateral spin valve [69].

4.3 Spin current absorption through side surface

In order to increase the spin absorption efficiency, the spin resistance for the spin absorber should be much smaller than the spin resistance for the nonmagnetic channel. Since the spin resistance is inversely proportional to the cross section, increasing the effective cross section is one of the ways for improving the absorption efficiency [21]. By increasing the lateral dimension of the F dot or F/N junction size, one can reduce the spin resistance for the spin absorber [38]. However, increasing the lateral dimension does not improve the

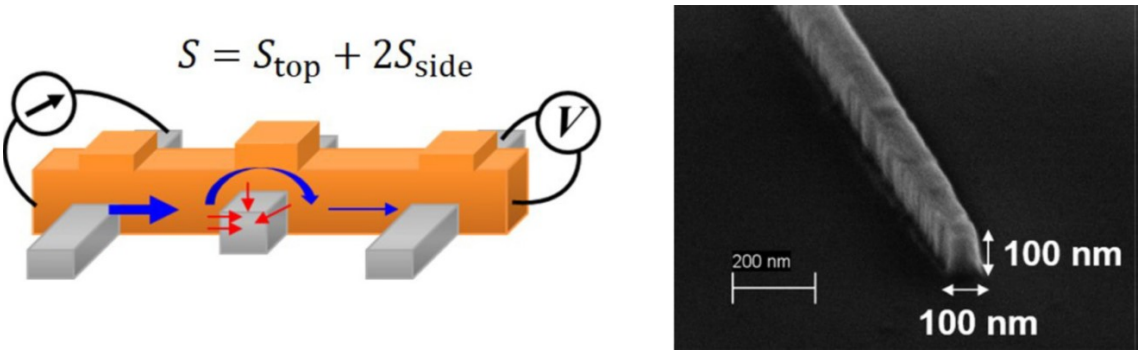

Figure 4.5: Schematic illustration for the spin absorption measurement together with the cross-sectional SEM image of the 100-nm-thick Py nanowire.

density of the spin current and is not suitable for nano-sized spin devices from the view point of the device integration. To improve the absorption efficiency, we focus on the spin absorption from the side surface, which is another way for increasing the effective cross section for the spin current.

To investigate the spin current absorption from the side surface, we have fabricated the lateral spin valves with middle ferromagnetic dots with different dot thicknesses, as schematically shown in Fig.4.5. Here, we have prepared 20-, 40-, and 100-nm-thick ferromagnetic middle dots. We believe that the side surface of the thick ferromagnetic dot was cleaned by the conventional Ar ion milling because of the forward tapered cross section of the ferromagnetic dot as shown in Fig.4.5 (b). In addition, the deposition rate of the Cu was 0.5 nm/s to obtain a better surface covering around the Py dot.

The absorption efficiency for each device has been evaluated by comparing the spin signal to that without the middle absorber. Figures 4.6(a) and 4.6(b) show the typical results of the spin current absorption. We have clearly observed the significant reduction

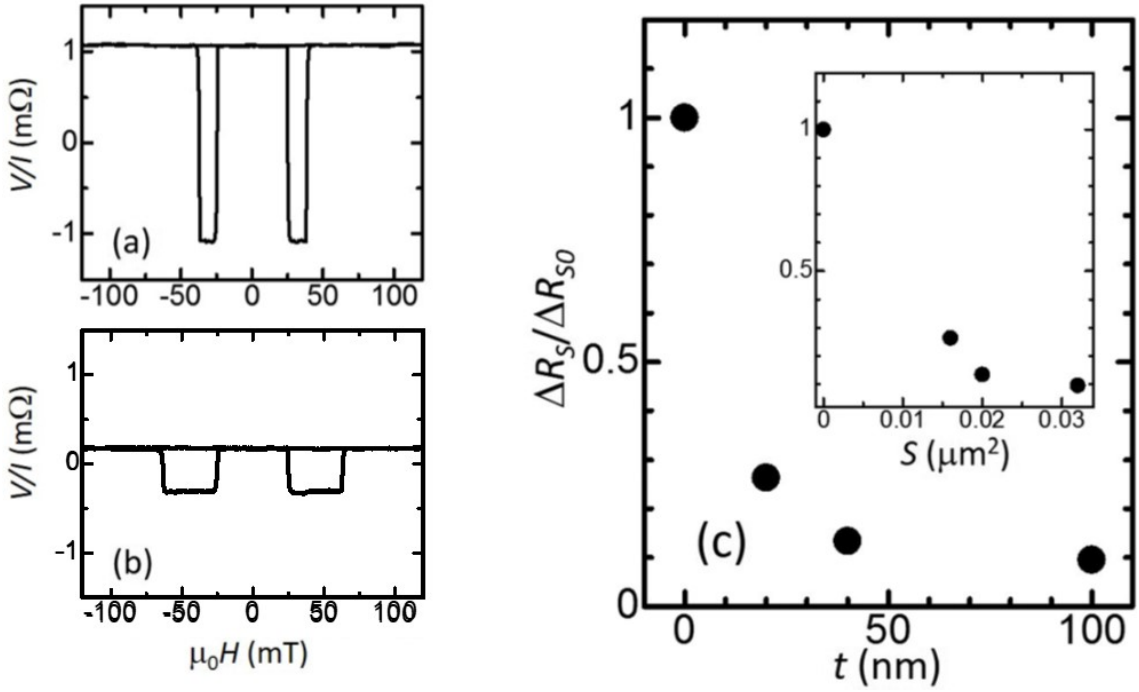

Figure 4.6: Spin absorption effect in a conventional lateral spin valve. Nonlocal spin valve signal (a) without and (b) with the 40-nm-thick Py dot. (c) Reduction of the spin valve signal as a function of the dot thickness. The inset of (c) is the reduction of the spin valve signal as a function of the effective junction size of the spin absorber.

of the spin signal. Moreover, as can be seen in Fig. 4.6(c), it was confirmed that the reduction of the spin signal increases by increasing the dot thickness. This implies that the side surface of the middle ferromagnet acts as an efficient spin absorber [38, 39]. To clarify the influence of the spin absorption from the side surface, we replot the ratio of the spin signal as a function of the effective cross section in the inset of Fig. 4.6(c). Here, the effective cross section is the sum of the top surface and two side surface areas. A large reduction of the spin signal was observed at $S \approx 0.02\mu\mathrm{m}^2$. To understand this behavior,

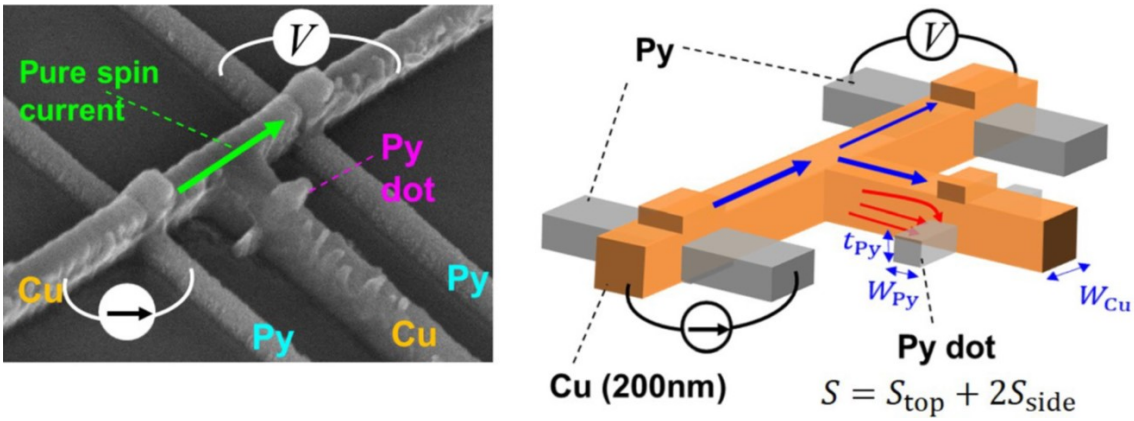

Figure 4.7: Scanning electron microscopy image of the modified lateral spin valve together with the schematic illustration of the fabricated device.

we may have to take into account the influence of the geometrical disorder, which may induce the additional spin-flip scattering, when the thickness of the middle ferromagnetic dot increases. However, since the influence of the geometrical scattering also increases with increasing the thickness, we cannot distinguish the origin of the reduction.

To exclude the influence of the geometrically induced scattering, we have developed a modified lateral spin valve consisting of a T-shaped Cu channel shown in Fig. 4.7. Here, the spin absorber is placed under the branch of the Cu channel. Therefore, the spin current diffusing into the Py detector is not affected by the geometrical disorder of the spin absorber. Here, we have fabricated the modified lateral spin valves with the different dot thicknesses, 10, 30, 60, 80, and 100 nm. The spin absorption efficiency is evaluated from the comparison of the spin signal with and without the ferromagnetic dot.

Figures 4.8(a) and (b) show the spin signals with and without the ferromagnetic

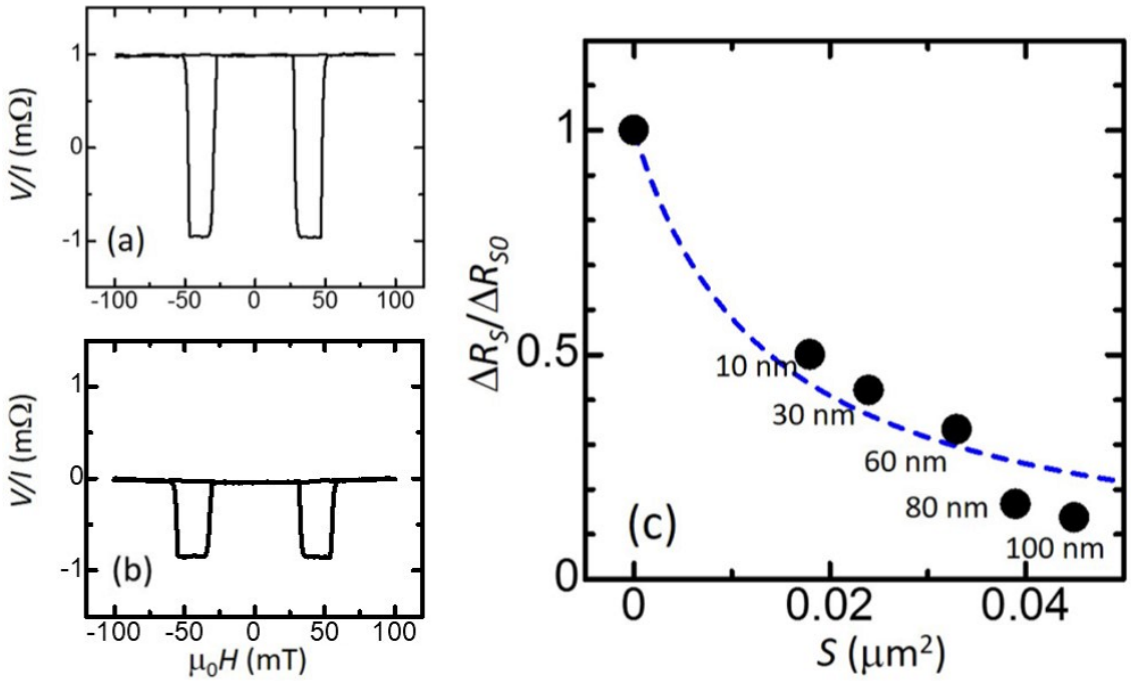

Figure 4.8: Spin absorption effects in a modified lateral spin valve. Nonlocal spin valve signal (a) without and (b) with the 30-nm-thick Py dot. (c) Reduction of spin valve signal as an effective junction size of the Py-dot.

absorber, respectively. Here, the spin signal without the absorber is slightly smaller than that in Fig. 4.6(a), indicating that the influence of the additional Cu branch is small in the spin diffusion in the Cu channel. However, we have clearly observed the reduction of the spin signal in Fig. 4.8(b) by putting the Py dot in the branch because of the spin absorption effect. Moreover, as shown in Fig. 4.8(c), the spin signal monotonically decreases by increasing the dot thickness. This is a strong evidence that the pure spin current is efficiently absorbed from the side surface of the ferromagnetic dot similarly to the top surface. Here, we analyze the spin absorption efficiency in the modified lateral spin valve. Based on the one dimensional spin diffusion model, the spin signal $\Delta R_{\rm s}$ with

the middle absorber can be approximately calculated as follows [21, 88]:

$$R_{\mathrm{s}} \approx \frac{(PR^{\mathrm{S}}_{\mathrm{Py}})^2 R^{\mathrm{S}}_{\mathrm{Abs}}}{R^{\mathrm{S}}_{\mathrm{Cu}}(R^{\mathrm{S}}_{\mathrm{Cu}}(1-\cosh(\mathrm{d}/\lambda_{\mathrm{Cu}}))+2(\mathrm{R}^{\mathrm{S}}_{\mathrm{Py}}+\mathrm{R}^{\mathrm{S}}_{\mathrm{Abs}})\sinh(\mathrm{d}/\lambda_{\mathrm{Cu}}))}, \tag{4.4}$$

where $R^{\mathrm{S}}_{\mathrm{Py}}$, $R^{\mathrm{S}}_{\mathrm{Cu}}$, and $R^{\mathrm{S}}_{\mathrm{Abs}}$ are the spin resistances for Py, Cu, and the middle spin absorber, respectively. P is the spin polarization for the Py. d is the distance between the injector and detector. It should be noted that in this kind of lateral spin valve based on the metallic wires, $R^{\mathrm{S}}_{\mathrm{Cu}}$ is much larger than $R^{\mathrm{S}}_{\mathrm{Abs}}$ and $R^{\mathrm{S}}_{\mathrm{Py}}$. Since the spin absorber is placed in the Cu branch at a small distance from the intersection, we neglect the spin relaxation in the Cu branch. In order to consider the influence of the absorber thickness, we assume that the effective cross section for the spin resistance is given by $S_{\mathrm{top}} + 2S_{\mathrm{side}}$, where S_{side} is $w_{\mathrm{Cu}}t_{\mathrm{dot}}$, as schematically shown in the inset of Fig. 4.8(c). Using the above assumption, we tried to reproduce the reduction of the spin signal observed in Fig. 4.8.

The fitted curve roughly reproduces the experimental results. However, the reduction rate significantly increases at t >80 nm. The reason for this deviation is unclear at the moment but further reduction from the theoretical calculated value indicates that the side surface is an efficient current absorber for the diffusive spin current. It should also be mentioned that the expanded one-dimensional spin resistor model may be useful for more quantitative understanding [39, 70].

4.4 Verification of transverse spin current generation in a T-shaped lateral spin valve structure

As shown in Fig.4.8(b), modulation of the background of the spin signal was observed in the T-shaped geometric lateral spin valve structure. On the other hand, this modulation

has not been observed in the conventional lateral spin valve structure. Therefore, we believe a spin absorption of non-collinear component occurred in the spin absorber of the T-shaped lateral spin valve. Since the spin polarization of the transverse spin current is 0 relative to the spin absorber, the non-collinear spin absorption efficiency increases by considering the definition of the spin resistance. Because of its geometrical flexibility of the T-shaped lateral spin valve, the polarized direction of the absorbed spin current changes with respect to the relative angle of magnetization as the magnetization direction of the spin absorber rotates. As a result, it is considered that the spin absorption efficiency has changed and the background of the spin signal is modulated. If the non-collinear spin current is absorbed by the absorber, the inverse spin Hall effect can be observed as a voltage. Here, we observed the inverse spin Hall voltage by replacing the Py spin absorber of the T-shaped lateral spin valve with a Pt. The inverse spin Hall voltage is generated, when the direction of spin diffusion is perpendicular to polarization of spin current [14, 43–48]. Therefore, if inverse spin Hall voltage is detected, the existence of transverse spin current can be confirmed. However, since the inverse spin Hall voltage is generally smaller than the spin signal, it is difficult to detect with the same device structure. Therefore, we apply a CoFeAl (CFA) alloy of highly spin polarized material as the ferromagnet of the spin injection/detection terminal. It is known that the spin signal significantly increases by using CFA alloy [71].

The CFA alloys were deposited using an electron beam evaporation at the base pressure of 6×10^{-9} Torr, and the Pt fine wire was fabricated at the base pressure of 7×10^{-9} Torr using an ultrahigh vacuum sputtering. After that, interface cleaning was carried out using low acceleration voltage Ar ion milling, and Cu channel deposition was

performed at the base pressure of 6×10^{-9} Torr. The film thickness and line width for both CFA and Pt are 40 nm and 120 nm, respectively. And, the film thickness and line width for Cu are 200 nm and 120 nm. The distance between the CFA spin injector and the CFA spin signal detector is 250 nm, and the distance between the CFA spin injector and the inverse spin Hall Pt detector is 500 nm.

Figure4.9 shows the measurement results together with the SEM image of the fabricated device and its measurement circuit. First, in order to confirm the amount of generated spin current, clear spin signal of 2.2 mΩ at room temperature and 4.9 mΩ at low temperature has been observed. Then, we measured the inverse spin Hall voltage. Clear hysteresis of 0.09 mΩ at room temperature and 0.24 mΩ at low temperature has been observed. Therefore, we conclude that the spin current absorbed into the Pt spin absorber is a transverse spin current.

4.5 Summary

We have investigated the spin absorption properties in nano-pillar-based and nanowire-based multi-terminal lateral spin valves. Although the spin absorption efficiency in the nano-pillar-type device was smaller than that in the conventional wire-type device, the absorption rate in the nano-pillar device was increased by increasing the junction size similarly in the conventional devices. However, the spin absorber had to have a large lateral dimension in order to maintain the large spin absorption efficiency. To obtain a large spin absorption efficiency with a small lateral dimension, we proposed the spin absorption effect from the side surfaces of a thick ferromagnetic dot. However, it was indicated that the spin current causes the geometrically induced scattering as the spin

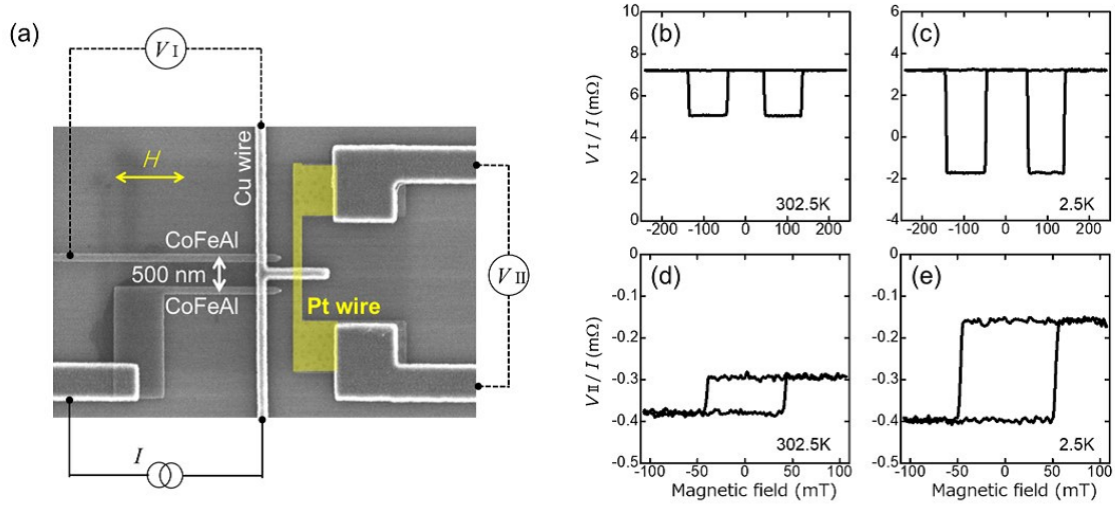

Figure 4.9: (a)Scanning electron microscopy image of the fabricated sample together with probe configurations. Nonlocal spin valve signal (b) at room temperature and (c) at 2.5K. Inverse spin Hall signal (d) at room temperature and (e) at 2.5K.

absorber becomes thicker. In order to evaluate the spin absorption efficiency through the side surface properly, a modified lateral spin valve with a T-shaped nonmagnetic wire has been proposed. First, we confirmed that the geometric spin scattering effect becomes very small by using this structure. Then, we clearly demonstrated that the spin absorption from the side surface was consistently enhanced by increasing the junction area of the side surface. In addition, modulation of the spin absorption efficiency caused by the rotation of the magnetization of the spin absorber was observed. It was confirmed that the absorbed spin current was a transverse spin current by detecting the inverse spin Hall effect.

Chapter 5

Modulation of spin absorption effect by direction control of spin polarization

5.1 Introduction

In the previous chapter, we confirmed that the spin current absorption efficiency changes according to the relative angle between the magnetization of spin absorber and the spin vector of spin current. The magnitude of spin absorption can be characterized by spin resistance. Spin resistance is defined by $2[1/(1-P^2)]\rho\lambda_{\mathrm{s}}/S$, where $P, \rho, \lambda_{\mathrm{s}}$, and S are the spin polarization, the electrical resistivity, the spin diffusion length, and the effective cross section for the spin current [21,41]. When the magnetization of the spin absorber is parallel or antiparallel to the injected spins (longitudinal spin absorption), the effective spin polarization is the same as that of the bulk spin polarization. This situation is

known as a collinear configuration, corresponding to most of the experimental situations in the lateral spin-valve structures reported so far [12–16, 21, 41, 72]. On the other hand, when the magnetization of the spin absorber is normal to the direction of the spin current (transverse spin absorption), the effective spin polarization becomes zero [74]. Since the spin resistance decreases with a decrease in the spin polarization, the spin resistance for the transverse spin current should be smaller than that for the longitudinal spin current. This means that the spin absorption efficiency can be tuned by the relative angle between the injected spin and the magnetization of the spin absorber.

Magnetic domain structures in nano-structured ferromagnets are known to be controlled by patterning their own shapes [75–77]. Patterned domain structures can also be utilized for the electrodes in nano-spintronic devices, especially in lateral configurations [12–16, 54–56]. When the width of a ferromagnetic strip is a few hundred nanometer or less, the magnetization in the strip is strongly restricted along the wire direction [78, 79]. Therefore, except for the wire end, a fully magnetized state can be realized even in the absence of the external magnetic field. This uniform domain structure with bistable characteristic is suitable for the electrode of the electrical spin injection and detection in the laterally configured spintronic devices because the effective spin polarization of the electrode is given by the vector sum of the spin directions underneath the injecting and detecting junctions [74]. Moreover, the junction size and the interval between the spin injector and detector can be minimized by using parallelly configured two ferromagnetic narrow strips with a orthogonally connected nonmagnetic strip [80]. Thus, the precise manipulation of the domain structure is key for the efficient operation in lateral spin devices. Here we conceived a V-shaped lateral spin valve structure. The

V-shaped lateral spin valve structure has a spin injection terminal shaped into a V shape. In this structure, the magnetization direction of the spin injector is oriented along the end of the V shape. Therefore, it is expected that transverse spin current is generated in the nonmagnetic spin channel without applying an external magnetic field. Using spin Hall effects (SHEs) and its inverse effect, the electric current can be converted directly to the spin current and vice versa [14, 43–48]. The vector relationship, in which the spin current vector induced by the SHE is proportional to the cross product between the spin and current vectors [43, 44]. This enables to detect the spin information without using the ferromagnetic detector, leading to the simplification of the device structure and its integration. The ferromagnetic electrode with the perpendicular anisotropy enables the electrical detection of the SHE in the absence of the magnetic field [48]. Here, we first confirmed that a transverse spin current is generated by a V-shaped lateral spin valve by detecting the inverse spin Hall effect. Then, we directly compare the spin absorption efficiency for the transverse spin current to that for the longitudinal one by using the specially developed lateral spin valve.

5.2 Transverse spin current generation using a V-shaped lateral spin valve structure

Our lateral spin device consists of V-shaped ferromagnetic permalloy (Py) wires and a Pt strong spin absorber bridged by a nonmagnetic Cu strip, as shown in Fig 5.1 (a). For the measurement of the inverse SHE, pure spin current was created by means of the nonlocal spin injection from the ferromagnetic wire and is injected into the Pt wire by

using the spin absorption effect. It should be noted that the flowing (vector) direction for the spin current in the Pt wire is almost parallel to the z axis because the absorbed spin current is immediately relaxed by the strong spin-orbit interaction in the Pt [21,41]. Therefore, the x component of the spins is required to induce the inverse SHE along the Pt strip. In the V-shaped wire, when the strong magnetic field is applied along the x direction, all of the magnetizations are aligned with the x direction. Importantly, the magnetizations around the corner maintains the applied field direction (x direction) even at the remanent state [81]. Figure5.1 (b) shows the numerically calculated domain structure of the V-shaped Py wire with 80 nm in width and 30 nm in thickness at the remanent state after the application of the horizontal magnetic field by using the object-oriented micromagnetic frame network (OOMMF). Here, we use typical Py parameters with the exchange constant 1.3×10^{-12}J/m and the saturation magnetization 1 T. The cell size and the damping parameter are 10 nm and 0.01, respectively. At the corner of the V-shaped wire, horizontally aligned magnetizations have been clearly confirmed. Therefore, when the injecting junction is fabricated on the corner of the V-shaped wire, the inverse spin Hall voltage along the Pt wire can be induced even at the zero magnetic field by using in-plane magnetized ferromagnetic Py electrode.

The present device has been fabricated by the conventional lift-off process with electron-beam lithography. Here, the V-shaped Py wires, 30 nm in thickness, have been deposited by the electron-beam evaporator at the base pressure of 5×10^9 Torr. Figure5.1 (c) shows a magnetic force microscopy (MFM) image of a simultaneously fabricated V shaped wire, which was observed in the absence of the magnetic field after the application of the magnetic field along x direction. The observed image reveals that the

desired domain structure shown in Fig 5.1 (b) was formed at the corner of the V-shaped wire. The Pt absorber, 10 nm in thickness, and a Cu strip, 100 nm in thickness, are fabricated by the electronbeam and Joule evaporations, respectively. Here, in order to make the highly transparent interfaces at each junction, the low voltage Ar ion milling was carried out. The electrical resistivities for the Py, Cu, and Pt are 25.0, 2.5, and 18.4 $\mu\Omega$cm respectively, at room temperature, and 20.6, 1.2, and 14.3 $\mu\Omega$cm, respectively, at 77 K. The inverse SHE was measured with the probe configuration shown in Fig 5.1 (a). Here, the spin Hall voltage was measured by a standard current-bias lock-in technique using 173 Hz sinusoidal constant current with the magnitude of 200 μA.

Figures 5.1 (d) and 5.1 (e) show the inverse spin Hall signals as a function of the external magnetic field along the x direction measured at room temperature and 77 K, respectively. The signals exhibit the rectangular hysteresis loops revealing the bistable inverse spin Hall voltages in the absence of the magnetic field. Here, the overall resistance changes were 0.07 mΩ at RT and 0.18 mΩ at 77 K, which are comparable to those in the previous reports [47,83]. The spin Hall conductivity for the Pt can be estimated from the overall resistance changes. However, the quantitative evaluation of the spin Hall angle is still under discussion. This is because many spin-dependent experimental parameters such as the spin polarization for the ferromagnetic Py electrode and the spin diffusion lengths for Py, Cu, and Pt are required for calculating the spin Hall conductivity from the present experiment [47, 83]. Especially, the spin diffusion length for the Pt strongly influences the estimation of the spin Hall conductivity [84]. Moreover, the significant reduction of the spin Hall voltage due to the shunting effect from the Cu wire was pointed out recently [83]. Since the quantitative estimation of the spin Hall conductivity is not

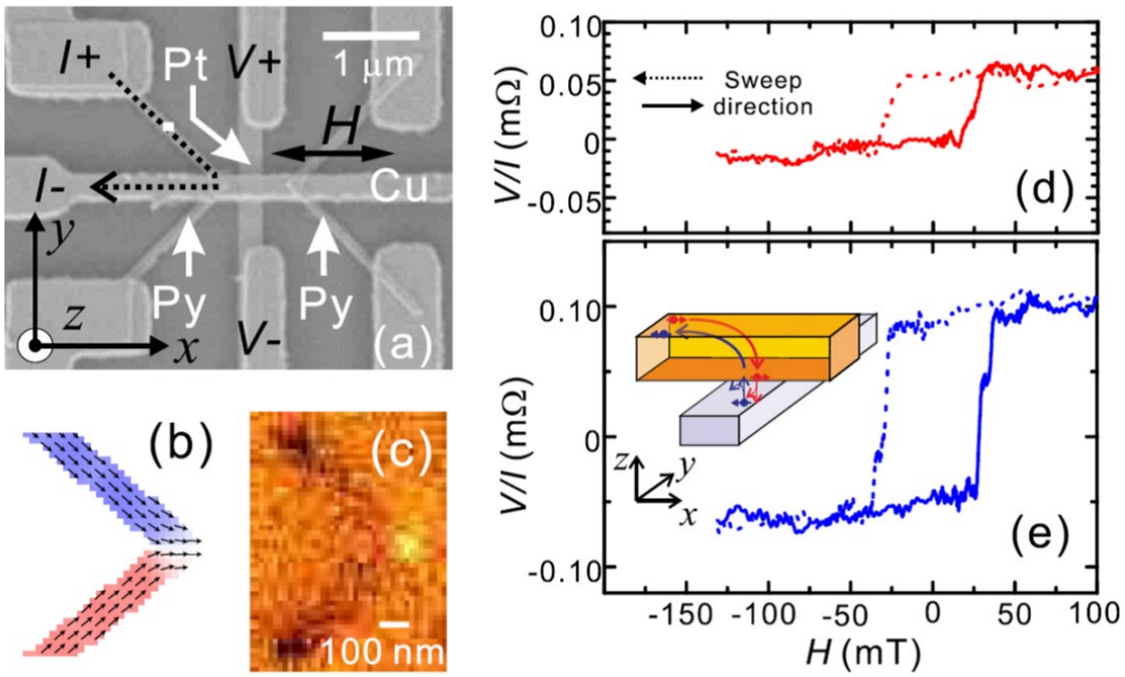

Figure 5.1: (a) Scanning electron microscope image of the fabricated lateral spin Hall device consisting of V-shaped ferromagnetic Py wires and a Pt strip bridged by a Cu strip together with the probe configuration for the inverse SHE measurement. (b) Calculated magnetic domain structure of the V-shaped Py wire at the remanent state using micromagnetic simulation. (c) MFM image of the V-shaped Py wire at the remanent state after the application of the inplane magnetic field along the x axis. Inverse spin Hall signals as a function of the in-plane magnetic field along the x axis measured at RT (d) and at 77 K (e). The inset of (e) shows the schematic illustration for the generation principle of the inverse SHE in the Pt strip.

main subject in the present paper, we do not calculate the spin Hall conductivity for our Pt strip. However, we expect the same order of the spin Hall conductivity because the magnitude of the overall resistance change and the electrical resistivity for the Pt are in the same range as those in the previous reports.

We then performed an inverse SHE measurement using another V-shaped wire. Figure 5.2 (a) shows the field dependence of the inverse spin Hall voltage, exhibiting a similar rectangular hysteresis loop with the overall resistance change of 0.1 mΩ. This is because the flowing direction of the spin current in the Pt does not depend on the position of the spin injector [47]. The magnitude of spin signal smaller than that in Fig 5.1 (d) is due to the longer interval between the Pt and V-shaped wires than the previous one. We also performed nonlocal spin valve measurements using the ferromagnetic V-shaped injector and detector shown in the inset of Fig 5.2 (b). The nonlocal spin signals exhibit the clear spin-valve effects corresponding to either parallel (high) or antiparallel (low) state as in Fig 5.2 (b). However, the magnitude was much smaller than that for the conventional lateral spin valve without a Pt insertion because of the strong spin current absorption [21, 41]. These results are clear evidence that the voltage induced in the Pt wire under the nonlocal spin injection is due to the inverse SHE of the Pt wire induced by the pure spin current.

The direct SHE and the reciprocal relationship between the direct and inverse SHEs have been demonstrated by using a similar designed lateral spin Hall device with a different sample dimension [47]. Figure 5.3 (a) shows the probe configuration for the direct SHE measurement, in which the spin accumulation in the Cu strip induced by the direct SHE of the Pt was nonlocally detected by the V-shaped ferromagnetic voltage

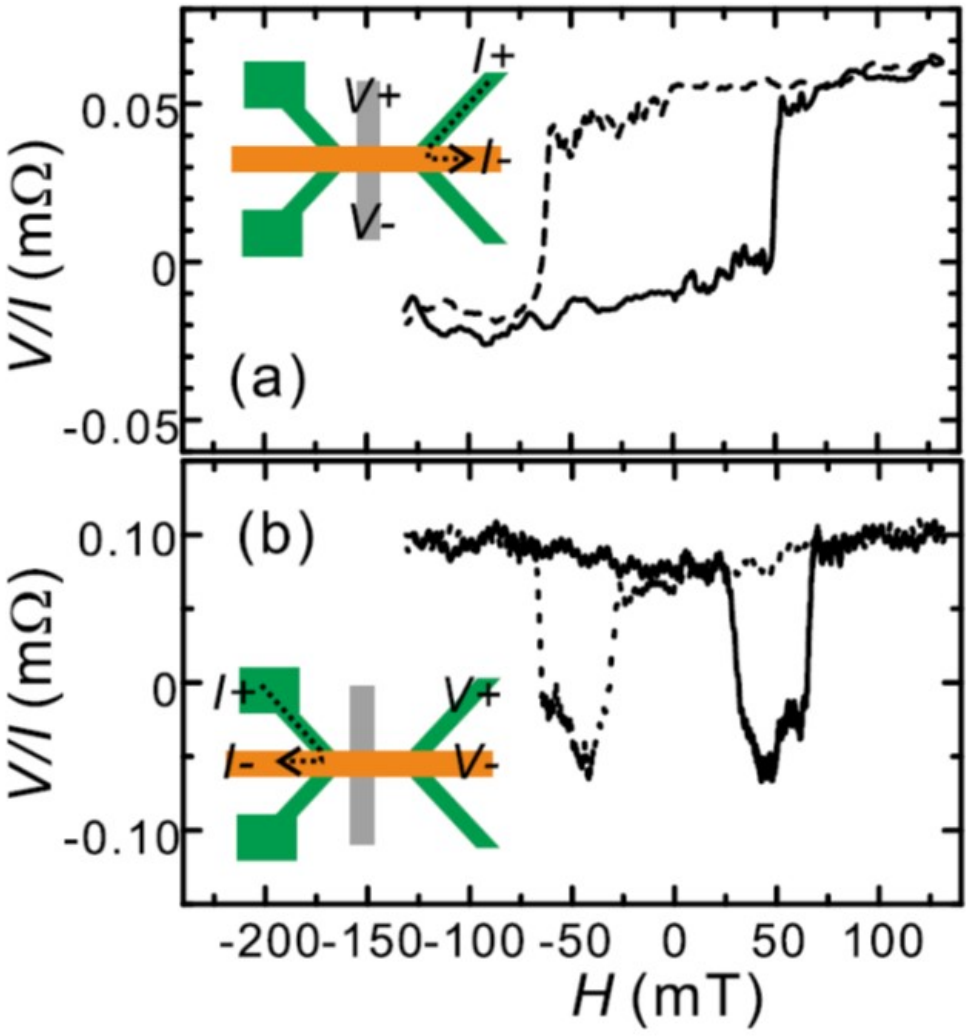

Figure 5.2: (a) Field dependence of the inverse spin Hall signal using another V-shaped spin injector at the opposite side. (b) Nonlocal spin valve signal using the V-shaped Py injector and detector with a Pt insertion. The insets of both figures represent the probe configurations for the measurements.

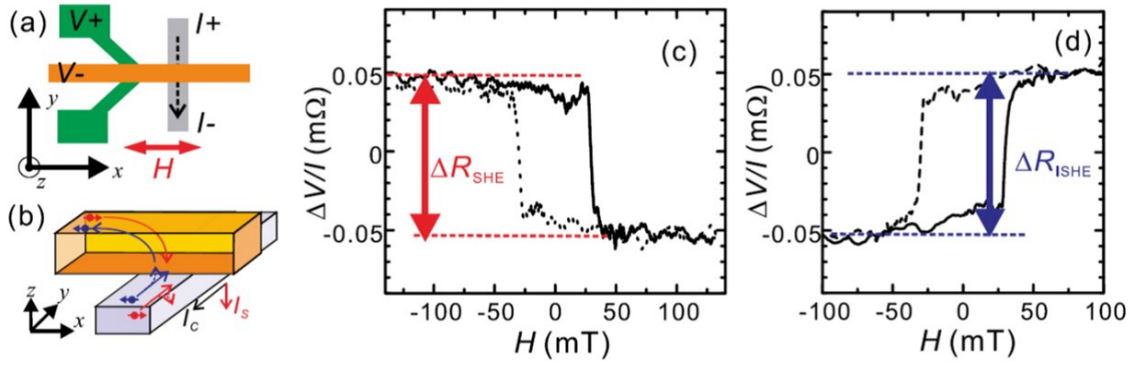

Figure 5.3: Schematic illustrations of the device for the direct SHE together with the probe configuration for the measurement (a) and the induced mechanism of the direct SHE (b). (c) Spin Hall signal as a function of the in-plane magnetic field along x axis. (d) Inverse spin Hall signal as a function of the in-plane magnetic field for the same sample. In order to directly compare the resistance changes between two measurements, the offset resistances of 100 $\mu\Omega$ and 20 $\mu\Omega$ were subtracted from (c) and (d), respectively.

probe (Fig 5.3 (b)). As shown in Fig 5.3 (c)), a rectangular hysteresis loop with the opposite polarity was clearly confirmed in the field dependence of the direct SHE. By interchanging the current and voltage probes, the inverse SHE was also measured, as shown in the inset of Fig 5.3 (d). The overall resistance change equal to that for the direct SHE clearly indicates the verification of the reciprocal relationship between the spin and charge currents.

Finally, we study the angular dependence of the inverse spin Hall signal under the nonlocal spin injection from the V-shaped wire. Figures 5.4 (a) and 5.4 (b) show the field dependences of the inverse spin Hall signals for $\phi \sim 30°$ and $\phi \sim 90°$, respectively. Here, ϕ is the in-plane angle of the external magnetic field with respect to the Cu

wire direction. Two step resistance changes observed in Fig 5.4 (a) can be explained by the separate irreversible switchings of the upper and lower magnetic wires. At the intermediate state, the spin Hall signal becomes almost zero. This is because the average of the x component for the magnetizations at the corner is nearly zero at the intermediate state, as schematically shown in the inset of Fig 5.4 (a). The gradual reduction of the spin Hall signal after the second resistance jump is due to the gradual rotation of the magnetizations toward the external magnetic field. On the other hand, in the spin Hall signal at $\phi \sim 90^\circ$ shown in Fig 5.4 (b)), a finite spin Hall voltage appears around $H \approx 40$ mT. This means that a magnetic domain wall was nucleated at the corner because of the difference of the switching field between upper and lower wires, as schematically shown in the inset. The sign of the finite spin Hall signal depends on the chirality of the domain wall [85], meaning that the spin Hall measurement is useful for sensitive detections of nano-sized magnetic domain structures. According to this result, the polarization direction of the generated spin current depends on the magnetization direction of the V-shaped ferromagnetic spin injector, and it was confirmed that this device structure can generate the transverse spin current.

5.3 Longitudinal and transverse spin current absorptions in a lateral spin-valve structure

In the previous section, we found that the V-shaped lateral spin valve can generate the transverse spin current. Here, to evaluate the longitudinal and transverse spin current absorptions precisely, we developed a lateral spin valve (LSV) using the V-shaped fer-

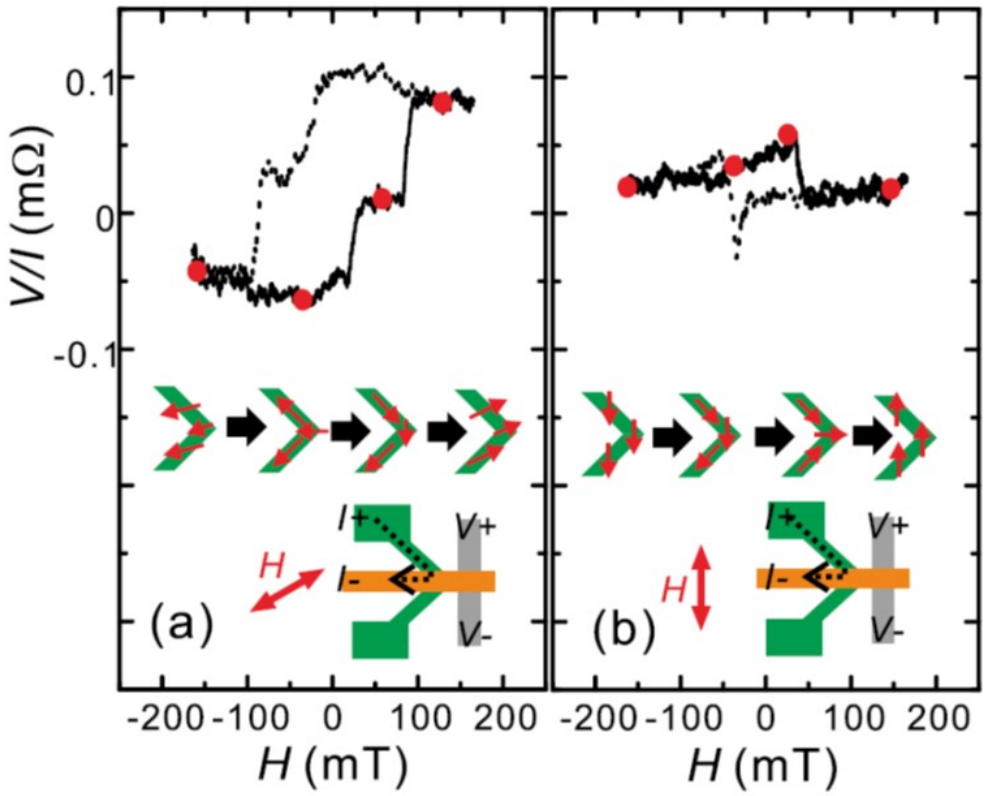

Figure 5.4: Inverse spin Hall signal as a function of the external magnetic field at $\phi \sim 30°(a)$ and $\phi \sim 90°$ (b). The insets show the expected magnetic domain structures for the V-shaped Py wire.

romagnetic injector and detector, as shown in Fig. 5.5. Here, one V-shaped wire (right side) was connected to a large pad at the wire end in order to assist the magnetization reversal. Therefore, the switching field for the right-hand-side V-shaped wire is smaller than that for the left-hand-side one. A ferromagnetic strip, which plays the role of the spin absorber, is located in the middle of the V-shaped wires. The three ferromagnetic Permalloy (Py) wires are bridged by a nonmagnetic Cu strip. It should be noted that the V-shaped Py wires are connected to the Cu strip at the corners of the V-shaped wires. Therefore, the directions of the injecting and detecting spins reflect the domain structures at the corners. When a strong magnetic field is applied to the sample along the x direction, all of the magnetizations in the V-shaped wires and the strip are aligned along the x direction, as shown in Fig. 5.5(b). In this situation, the direction of the generated spins in the Cu strip is parallel to the magnetization of the spin absorber. This situation corresponds to the longitudinal spin current absorption. On the other hand, when the magnetic field decreases to zero, the domain structure of each ferromagnetic wire reflects its own shape, as shown in Fig. 5.5(c). The magnetization of the middle strip is aligned with the wire direction (y direction) because of the shape anisotropy. However, the magnetizations of the V-shaped wire around the corner maintain the field direction (x direction) even at the remanent state [81]. Although two types of domain walls—transverse and vortex—can exist in ferromagnetic wires, the transverse domain wall is known to be stabilized in the present experimental geometry and magnetic configuration [86]. In fact, we confirmed the formation of the transverse domain wall by means of a magnetic force microscope observation [87]. In this situation, the injecting spin is perpendicular to the magnetization of the spin absorber, meaning the transverse

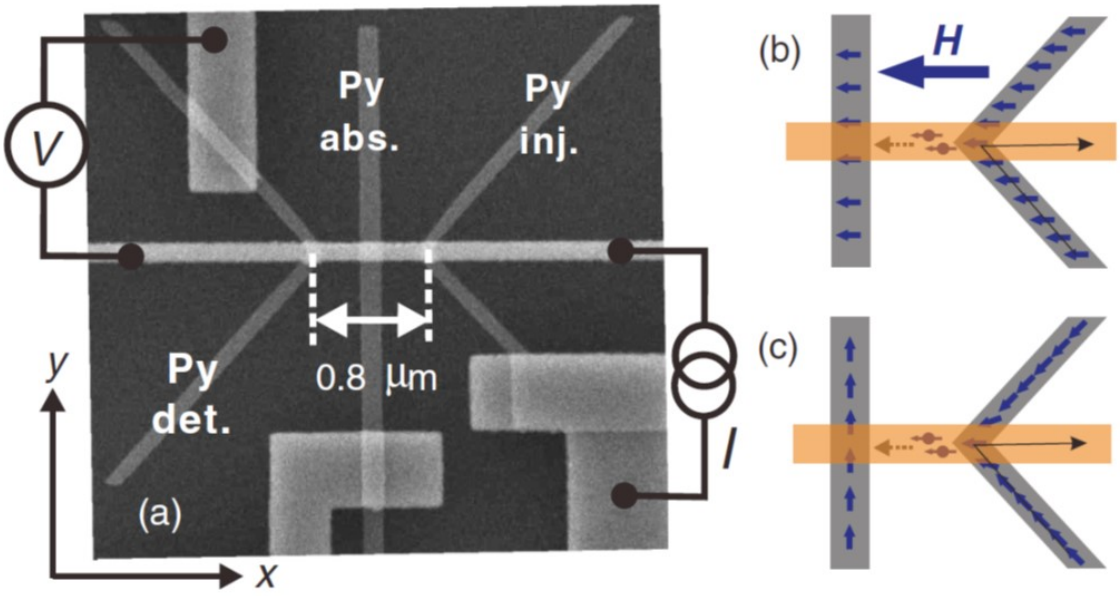

Figure 5.5: (a) Scanning electron microscope (SEM) image of the specially fabricated Py/Cu lateral spin valve consisting of two V-shaped nanowires with a middle strip. Expected domain structures in the Py wires and spin accumulation in a Cu channel for the longitudinal configuration (b) and the transverse configuration (c).

spin current absorption. Note that the magnetic configuration between the injector and the detector should still be parallel at the remanent state. Therefore, the difference in the spin signal between the two situations should mainly be caused by the change of the spin resistance for the middle Py wire. By comparing the nonlocal spin voltages between the two situations, we can evaluate the longitudinal and transverse spin current absorptions precisely.

The LSV for the present study has been fabricated by the conventional liftoff process with electron beam lithography. Here, the three Py wires, 30 nm in thickness, have been deposited by the electron-beam evaporator at a base pressure of 5×10^{-9} Torr. Then, a Cu strip, 150 nm in thickness, has been deposited by Joule evaporation at a base pressure of 2×10^{-8} Torr. Prior to the deposition, the surfaces of the Py wires were well cleaned by low-voltage Ar ion milling. We also fabricated a V-shaped LSV without the middle Py wire. Here, the resistivity for the Py is 22 $\mu\Omega$cm at 77 K and that for Cu is 1.2 $\mu\Omega$cm at 77 K. The nonlocal spin-valve signal has been measured by a standard current-bias lock-in technique at 77 K.

First, we measured the nonlocal spin-valve signal in a V-shaped LSV without a middle strip in order to confirm the magnetization configuration between the V-shaped spin injector and the detector during the field sweep along the x direction. As can be seen in Fig. 5.6, we obtained a clear bipolar signal reflecting the parallel and antiparallel configurations with the magnitude ΔR_s of approximately 1.18 mΩ [12]. Here, in the antiparallel configuration, the righthand-side V-shaped wire was switched because of the large pad connected at the wire end. The signal was found to decrease slightly with a decrease in the magnetic field from the fully parallel state, although the domain structure

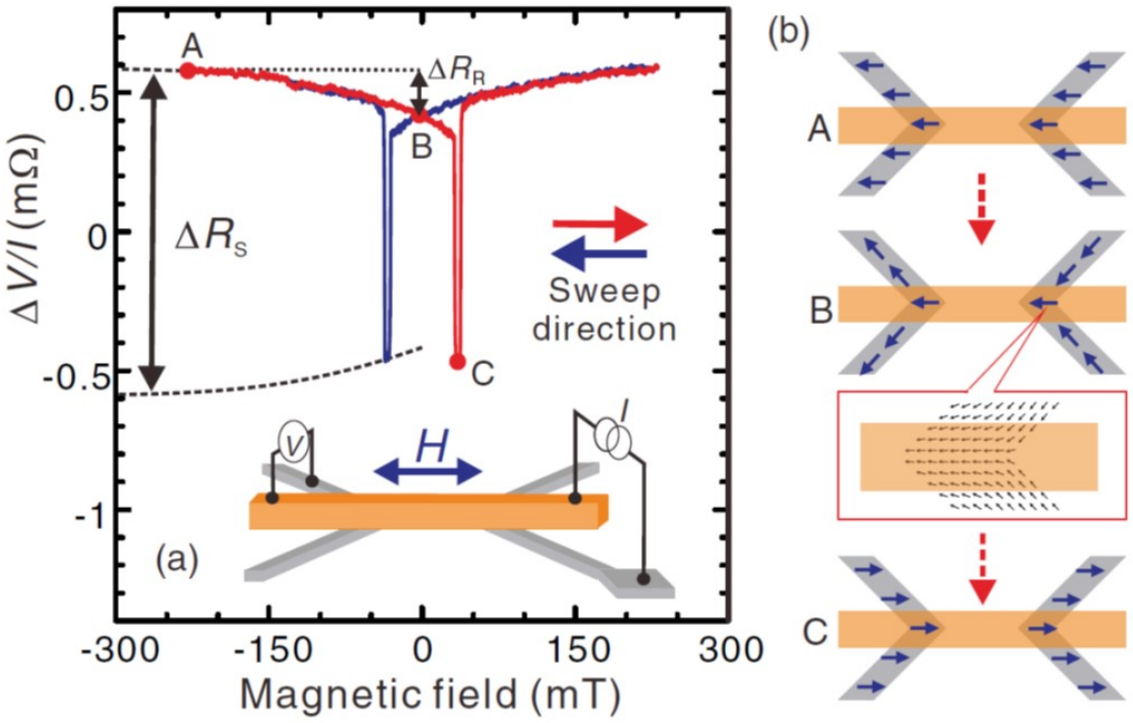

Figure 5.6: (a) Nonlocal spin valve signal in a Vshaped lateral spin valve without the middle spin absorber. The magnetic field is applied along the x direction (parallel to the Cu strip). (b) Schematic illustrations for the domain structures of the V-shaped injector and detector at the fully parallel (A), the remanent (B), and the quasi-anti-parallel (C) states.

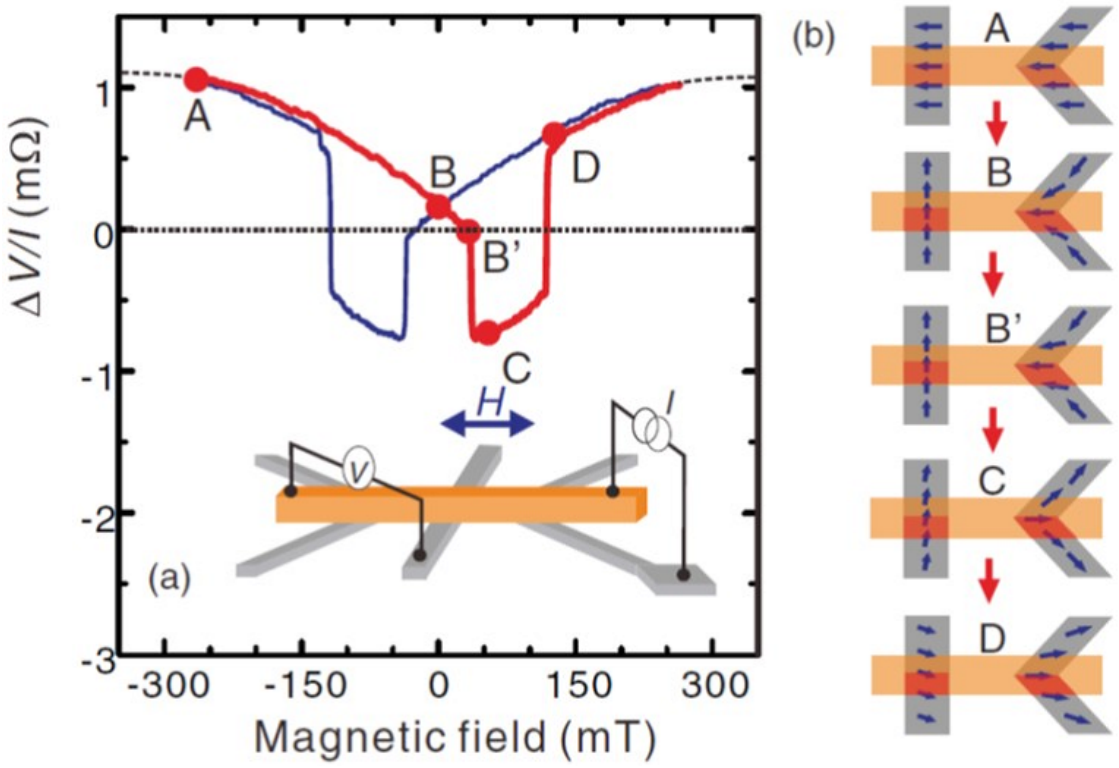

Figure 5.7: Detailed spin structure around the injecting junction of the V-shaped ferromagnetic wires obtained from the micromagnetic simulation.

at the corner was not switched. The gradual signal change between the fully parallel and the remanent states was 0.14 mΩ, corresponding to 24 % of that at the fully parallel state. This reduction can be understood by the slight deviation from the fully uniform domain structure. We numerically calculated the detailed domain structure of the V-shaped wire from the micromagnetic simulation [82]. As shown in Fig. 5.7, most of the spins around the corner are aligned along the x direction even at the remanent state. However, some of the spins deviate slightly from the x direction. Since the spin accumulation in the nonmagnet is given by the average of the vector sum of the injecting spins [74],

the small nonuniformity of the domain structure reduces the effective spin polarization of the injecting spins. A similar reduction of the effective spin polarization has to be considered in the detection of the spin accumulation using the V-shaped ferromagnetic wire. We calculated the average x component of the normalized spins n_x at the lower half of the corner of the V-shaped wire from the numerical result of the micromagnetic simulation, and we found that n_x is given approximately by 0.87. Since the spin signal is proportional to the product of the effective spin polarizations for the injector and the detector [21, 41, 88], the reduction ratio of the spin signal at the remanent state is given by $n^2 \times (0.76)$. Thus, the 24 % reduction observed in the spin signal is quantitatively explained by the slight deviation from the uniform domain structure at the corner of the V-shaped wire. This confirms the validity of the assumption that the magnetization of the injector and the detector is roughly in parallel at the remanent state.

Next, we evaluate the spin transports in the V-shaped LSV with a middle Py strip. Before showing the spin absorption experiment, we measure the nonlocal spin signal using the V-shaped spin injector and the spin detector of the middle Py strip. This enables us to roughly estimate the relative angle between the injected spin from the V-shape wire and the magnetization of the middle Py wire. Figure 5.8(a) shows the spin signal as a function of the external magnetic field along the x direction. The field dependence of the spin signal exhibits a very unconventional change. This can be explained by considering the hard-axis magnetization reversal process of the ferromagnetic middle strip and the small inhomogeneous current distribution in the injecting junction at the corner of the V-shaped ferromagnetic wire. Here, we discuss the field dependence of the spin signal with the forward sweep. When the negative magnetic field is sufficiently

large, both magnetizations of the spin injector and detector align along the direction of the magnetic field (A). Therefore, the spin signal almost takes the value at the parallel state. When the negative magnetic field decreases, the injecting spin remains in the $-x$ direction, as explained in the previous paragraph. On the other hand, the magnetization of the middle strip starts to rotate to its easy axis (B). Here, the rotation direction of the middle strip is determined from a small y-axis component of the external magnetic field due to the experimental misalignment (less than $\pm 5^{\circ}$). It should be noted that the spin signal at the remanent state takes the middle value between the parallel and antiparallel states. This means that the relative angle is almost 90°, indicating that the transverse spin current is absorbed into the middle Py wire. However, the spin signal at zero magnetic field shows a small positive value. This can be explained by the small inhomogeneous current distribution in the injecting junction in the half-probe configuration [89, 90]. In the present probe configuration, the spin accumulation injected from the lower half of the corner of the V-shaped wire is mainly detected by the middle Py strip. This results in a small $+y$ component of the spin accumulation, as schematically shown in Fig. 5.8(b). Since the spin signal is given by the inner vector product between the accumulated and detected spins, the small y component of the spin accumulation induces a small positive spin signal. According to the micromagnetic simulation, when the positive magnetic field increases, the area for the spins aligned along the x direction is found to be wider with an increase in the positive magnetic field before the switching. This is because the magnetization reversal process is caused by switching the direction of the domain wall at the corner, and this feature well explains the experimental fact that the spin signal approaches zero at the positive magnetic field just before the switching

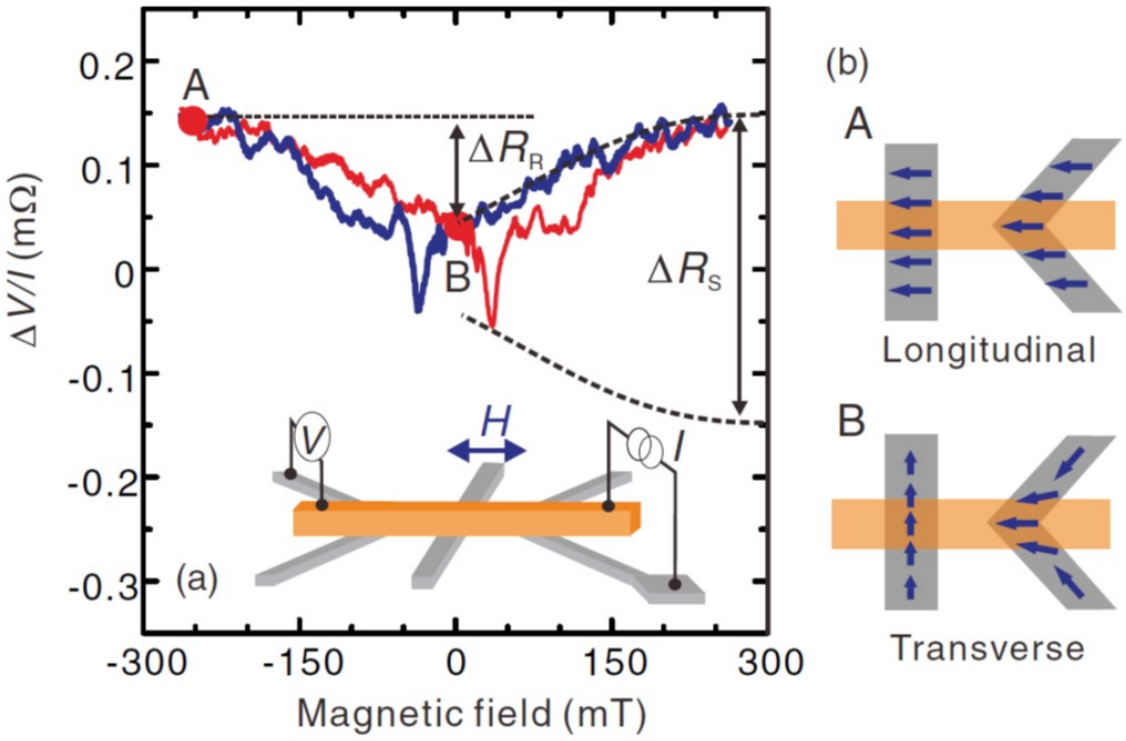

Figure 5.8: (a) Nonlocal spin valve signal using the V-shaped Py injector and detector with the middle Py absorber under the magnetic field along the x direction (parallel to the Cu strip). (b) Schematic illustrations for the domain structures of the V-shaped injector, detector, and absorber at the fully parallel (A) and the remanent (B) states.

(B'). The micromagnetic simulation also shows that the spin direction in the lower half tends to align along the wire direction. This spin structure change explains the negative abrupt change of the spin signal (C). By further increasing the magnetic field, the spin signal shows a large positive jump (D). This is due to the irreversible switching of the middle Py strip, which is a typical feature of the rotation magnetization process for the hard axis [91,92]. Thus, the unusual field dependence of the spin signal can be explained by the magnetization rotation of the middle Py strip and the small inhomogeneity of the spin injection.

We then study how the transverse spin current is absorbed by the middle Py wire by measuring the nonlocal spin signal with the V-shaped injector and detector. As shown in Fig. 5.8(a), the overall resistance change was estimated to be 0.3 mΩ, which is strongly reduced from the V-shaped LSV without the middle Py insertion. This is due to the spin absorption effect in the middle Py strip [21, 41]. The spin signal gradually decreases with a decrease in the magnetic field. This feature is also observed in the V-shaped LSV without the middle Py wire. However, ΔR_{R} is 0.11 mΩ, corresponding to approximately a 73 % reduction from the spin signal at the fully parallel state. This reduction is much larger than that in the LSV without the middle Py. As explained in the previous paragraph, the reduction of the spin signal due to the deviation from the fully parallel state is 24 %. Therefore, we expect that the further reduction of the spin signal at the remanent state is caused by the gradual transition from the longitudinal spin current absorption in the middle Py strip to the transverse spin current absorption.

We analytically calculate the spin absorption efficiency in the middle Py strip for the longitudinal and transverse spin currents. By using the one-dimensional spin-diffusion

model, the ratio of the spin signal with the middle wire, R_s^w, to that without the middle wire, $R_s^{w/o}$, can be calculated as follows [19, 21, 41, 88]:

$$\frac{R_s^w}{R_s^{w/o}} = \frac{2R_{SM}[e^{d/\lambda_{Cu}}(R_{SN}+2R_{SF})+R_{SN}]}{e^{d/\lambda_{Cu}}(R_{SN}+2R_{SF})(R_{SN}+2R_{SM})-R_{SN}(R_{SN}-2R_{SF})} \tag{5.1}$$

where R_{SN}, R_{SF}, and R_{SM} are the spin resistances for the nonmagnetic channel, the ferromagnetic spin injector (or detector), and the middle spin absorber. Here, from our previous experiments, we know $P = 0.35$, $\lambda_{Py} = 5$ nm, and $\lambda_{Cu} = 1300$ nm, which are reasonable values typically reported in Py/Cu LSV systems [12, 15, 73]. By using Eq. 5.1 (1), the ratio R_s^w $/R_s^{w/o}$ for the longitudinal spin current absorption can be calculated to be 0.27. This value well reproduces the experimentally obtained ratio $R_s^w/R_s^{w/o} = 0.3/1.18$. It should also be noted that the overall spin signal observed in Fig. 5.8 (a) can be quantitatively explained by a similar one-dimensional analysis within these parameters [93, 102].

We then calculate the reduction ratio of the spin signal for the transverse spin current absorption. As explained above, the spin accumulation voltage for the transverse configuration shows a 73 % reduction from the fully parallel state with the longitudinal configuration. By considering a 24 % reduction because of the reduction of the effective spin polarization at the remanent state, the ratio of the spin signal for the transverse spin absorber to the original spin signal without the absorber can be estimated to be $(0.3/1.18) \times (1 - 0.73) \times (1/0.76) \approx 0.08$. To quantitatively explain this experimental value, we calculate the reduction ratio of the spin signal for the transverse spin current assuming zero effective spin polarization. However, the value is 0.19, which is not small enough to explain the experimentally observed reduction of the spin signal for the

transverse spin absorption.

To solve this discrepancy, we consider the angular dependence of the spin relaxation length in ferromagnetic metal. In ferromagnetic metals, the spin relaxation length is believed to depend on the relative angle since the spin relaxation can be characterized by the following two situations [94]. One mechanism is spin relaxation due to spin diffusion, where the injecting spin and the magnetization of the spin absorber are in a collinear configuration. This situation corresponds to the longitudinal spin current absorption. The other mechanism is spin relaxation due to the exchange interaction from the local magnetization, where the direction of the spin is normal to the magnetization of the detector (the transverse spin current absorption). Theoretical studies suggest that the spin relaxation length for the transverse spin current is shorter than that for the longitudinal spin current [94–97]. Since the spin resistance is proportional to the spin diffusion length, the shorter transverse spin relaxation length induces a further enhancement of the spin absorption into the middle Py wire. Therefore, the transverse spin relaxation length may explain the reduction of the spin signal at the remanent state quantitatively. Here, we calculate the transverse spin relaxation length in order to reproduce the reduction of the spin signal observed in Fig. 5.8(a). By solving Eq. 5.1, the transverse spin relaxation length can be estimated to be 1.8 nm, which is less than half that of the longitudinal spin relaxation (spin diffusion length). In theoretical studies, the length scale for the transverse spin relaxation is known to depend on the transport mechanism of the conduction electrons. Although the ballistic electron model expects the transverse spin relaxation length [95], which is the same order of the electron Fermi wave length, a length scale of a few nanometers is expected in the diffusive electron

model [98, 99]. Since the spin current in the present lateral structure is caused by the diffusive electrons, the present result is quantitatively explained with the transverse spin relaxation model based on the diffusive transport.

The present method using the lateral spin valve based on V-shaped ferromagnetic wires enables us to evaluate not only the transverse spin diffusion length but also the longitudinal one from a single spin-signal measurement. This is a great advantage compared to the rf spin pumping method, in which the transverse spin diffusion length is estimated from the thickness dependence of the damping constant for several samples. Since the transverse spin diffusion length is an important factor in the spin-transfer torque [100, 101], the technique developed here will be very useful. Another important factor is that the spin absorption efficiency is enhanced by using the transverse spin current because of the reduction in the effective spin polarization and the spin relaxation length. When we use a highly spin polarized material such as Heusler alloys [93,102–105], the absorption efficiency can be strongly modified by changing the relative direction of the spin injector and the spin absorber.

5.4 Summary

We demonstrated that a transverse spin current can be generated using a V-shaped lateral spin valve. First, we confirmed that this device structure can generate spin current of polarized direction component reflecting the magnetic domain structure of V-shaped spin injection terminal. The spin Hall voltage appears even in the absence of the magnetic field and shows the rectangular-shape bistable field dependence. The validity of the observed SHE was also confirmed by changing the probe configuration and the nonlocal

spin valve measurement. In addition, we observed a longitudinal spin absorption and a transverse spin absorption using a V-shaped lateral spin valve. Comparing the longitudinal and transverse spin absorption efficiencies, it was clarified that the transverse spin absorption efficiency is stronger than that for the longitudinal one. Furthermore, from the numerical calculation, we found that the modulation of the spin absorption efficiency depends not only on the spin polarization but also on the spin relaxation length, and the transverse spin relaxation length in the Py is found to be $\lambda = 1.8$ nm.

Chapter 6

Spin absorption effect in ferromagnetic/nonmagnetic bi-layer channel.

6.1 Introduction

Ferromagnetic metal(FM)/nonmagnetic metal (NM) hybrid nanostructures enable us to induce the intriguing electrical transports and magnetization dynamics in association with the spin-dependent transport and the spin momentum transfer [10, 12, 37, 108, 109]. In such phenomena, a spin current, a flow of the spin angular momentum, plays a central role. Therefore, developing the precise control method of the spin current is an important issue for deepening the understanding of the fundamental spin-related physics as well as for further developing the spintronic devices [49–52]. So far, electrical spin injection and detection techniques have been well established with the development of the nano-

fabrication techniques [12, 13]. Especially, the nonlocal scheme enables us to detect tiny spin-related signals by eliminating the charge-current-induced spurious signals.

The lateral spin valve structure provides an ideal platform for investigating the transport properties of the diffusive spin current because of its flexible probe configurations [12–16]. In the lateral structures, the spatial distributions of the non-equilibrium spin current and accumulation in the NM are significantly affected by an additionally connected material when the connected material has a strong spin relaxation compared with the NM [21,41,88]. This is known as the spin absorption effect, where the pure spin current is effectively extracted from the NM. Interestingly, when the spin absorber is a FM, the extraction efficiency depends on the angle between the magnetization direction and the injected spin owing to the following two reasons. One is the difference of the spin relaxation mechanism between the longitudinal and transverse spins [94–97]. In the FM, the transverse spin relaxation time is known to be shorter than the longitudinal one because of the strong exchange interaction [98, 99]. The other one is the spin polarization [74]. The difficulty of the flow of the pure spin current increases with increasing the difference of the electrical conductivity between up and down spins prevents the absorption of the pure spin current. Therefore, the extraction efficiency decreases in the longitudinal configuration. These features can be well characterized by introducing the spin resistance [21, 41, 88]. For the transverse spin current, the effective spin polarization becomes zero and the spin diffusion length is shorter than the longitudinal case. Therefore, the spin resistance for the transverse spin current becomes smaller than the longitudinal one [94–97]. Indeed, the stronger transverse spin current absorptions have been reported experimentally [106]. However, the significant reduction of the spin signal

makes it difficult to detect the difference between the longitudinal and the transverse spin absorption effects precisely. We have recently developed high performance lateral spin valves by employing highly spin polarized electrodes [107]. The magnitude of the spin signal becomes 10 times larger than that of the conventional LSV based on the Permalloy electrodes. This enables us to perform more precise experiments on the spin absorption effect. From this point of view, we investigate the spin absorption property of the Cu/CoFeAl interface and its temperature dependence.

6.2 Anisotropic spin absorption effect in a FM/NM bi-layered channel

We have fabricated a specially developed lateral spin valve consisting of the CoFeAl and Cu on a thermally oxidized Si substrate. The special point of the LSV is that the spin-transport channel is not a Cu monolayer strip, but is the Cu/CoFeAl bilayer strip. Figure 6.1 (a) shows the SEM image of the fabricated device together with the schematic illustration of the device. The CoFeAl electrodes, 100 nm in width and 30 nm in thickness, were bridged by a Cu/CoFeAl bilayer strip. Here, the CoFeAl electrodes have been fabricated by a standard lift-off technique with an e-gun evaporation under the base pressure of 10^{-9} Torr. Here, one electrode has the flat end while the other one is connected to the large electrical pad. These results in the different switching field of the CoFeAl electrodes. The CoFeAl/Cu bilayer strip, 1000 nm in width, has been prepared also by a standard lift-off method. Here, the Cu layer, 200 nm in thickness, was deposited by a Joule evaporation and the CoFeAl, 10 nm in thickness, was deposited by the e-gun

evaporation. The interface between the Cu and CoFeAl in the spin channel has been grown continuously without breaking the vacuum, meaning the transparent interface. In addition, prior to the Cu deposition, the surface of the CoFeAl has been cleaned by the low voltage Ar ion milling in order to obtain the highly transparent interface. The electrical resistivities for CoFeAl and Cu are 45 $\mu\Omega$cm at room temperature and 30 $\mu\Omega$cm at 2.5 K, respectively. Therefore, in the bilayer film, the current flowing in the CoFeAl is negligibly small.

In this LSV, owing to the ferromagnetic capping layer on the Cu channel, we expect the modulation of the spin accumulation originating from the longitudinal and transverse spin absorption. Since the easy axis for the ferromagnetic capping layer is normal to the easy axis of the ferromagnetic electrodes, we can realize both the longitudinal and transverse configuration by sweeping the external magnetic field along the CoFeAl electrode. As shown in Fig. 6.1 (b), when the external magnetic field is sufficiently large, the moderate spin absorption into the capping CoFeAl layer occurs under the longitudinal configuration. In the absence of the magnetic field, the transverse configuration can be realized. Thus, we expect the modulation of spin accumulation with magnetic configuration by the application of external magnetic field.

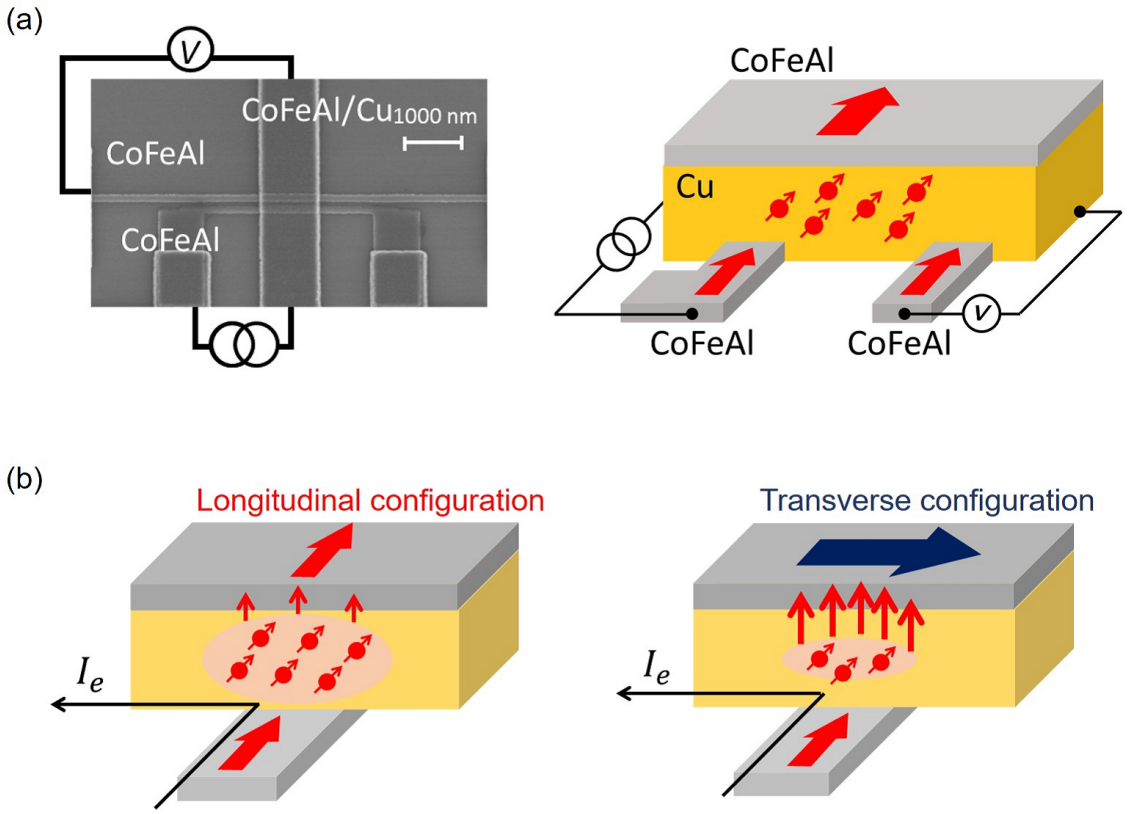

Figure 6.1: (a) Scanning electron microscopy (SEM) image of the fabricated bi-layer type lateral spin valve consisting of ferromagnetic CoFeAl wires bridged by a Cu/CoFeAl by-layer spin channel together with the schematic illustration of the device. (b) Schematic illustration of the longitudinal and transverse spin absorptions.

Figure 6.2 shows a room-temperature nonlocal spin valve signal. We can see clear spin valve signal depending on the parallel and anti-parallel configurations between two CoFeAl electrodes. In addition to the main spin valve signal, we see the gradual field dependence of the spin accumulation signal. This gradual change can be understood by the modulation of the spin accumulation due to the relative angle between the accumulated spin and the magnetization of the capping layer, as explained in Fig. 6.1 (b). Reflecting the parallel and anti-parallel configuration, we can see a gradual change of the base line. So, the base line at the zero magnetic field is 1.52 mOhm while that is 2.46 mOhm at the higher magnetic field. This modulation of the base line can be understood by the anisotropic spin current absorption into the CoFeAl capping layer, as follows. When the magnetic field is sufficiently large, all of the magnetizations align with the direction of the magnetic field. In this case, the accumulated spin is parallel to the magnetization of the spin absorber, namely longitudinal configuration. The magnetizations for each CoFeAl wire starts to rotate to their easy axes with decreasing the magnetic field. So, the magnetizations of the CoFeAl electrodes are normal to the magnetization of the spin absorber. This corresponds to the transverse configuration. As mentioned above, the spin absorption at the transverse configuration is stronger than that at the longitudinal case. Therefore, the detecting spin accumulation at the zero magnetic field becomes smaller than that at the high magnetic field.

From our systematic experiments on the diffusive spin transport in the conventional CoFeAl/Cu lateral spin valve, we know the spin diffusion length and the modulation ratio of the spin signal. So, the transverse spin relaxation length is only the unknown parameter. From the magnitude of the modulation, we can estimate the transverse spin

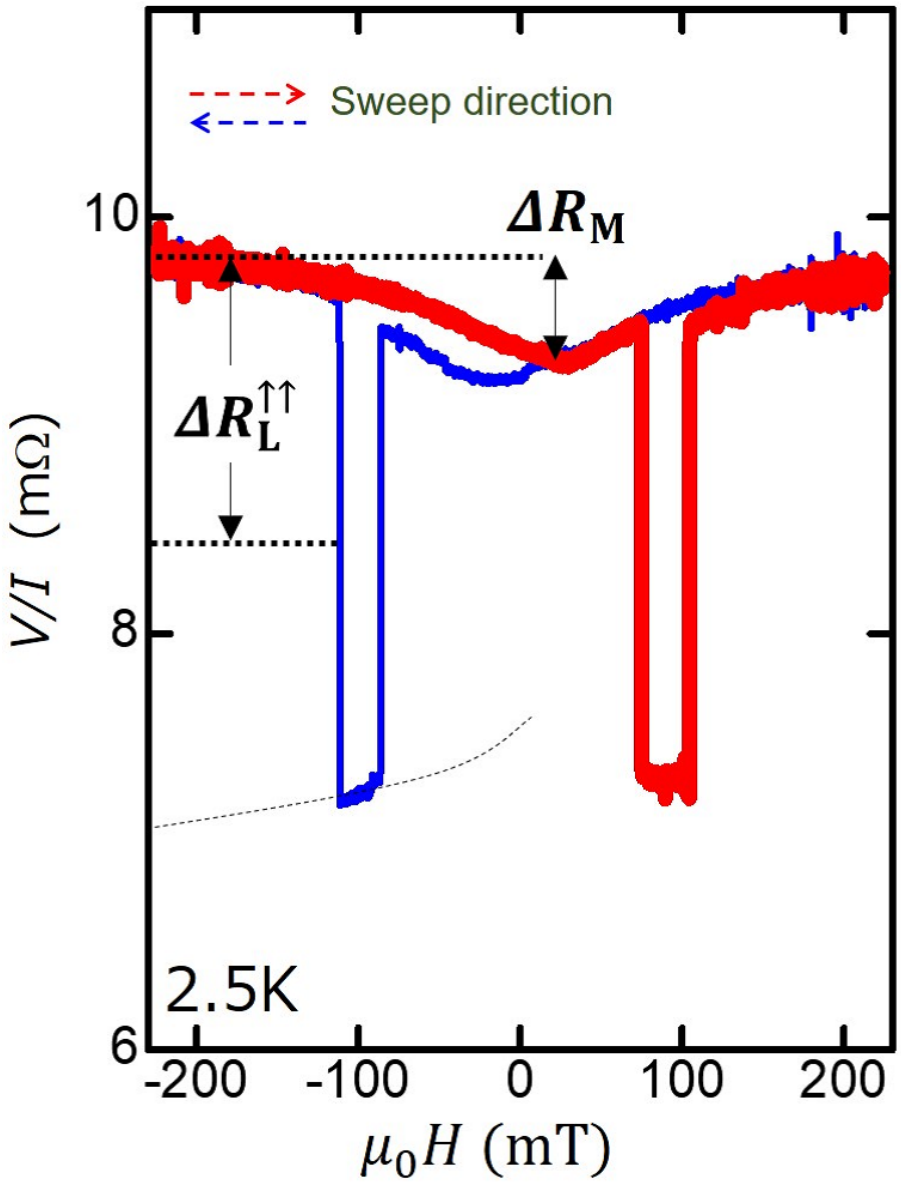

Figure 6.2: Nonlocal spin valve signal in a Cu/CoFeAl bi-layer type lateral spin valve measured at 2.5 K.

relaxation length. The modulation of the spin signal is mainly caused by the spin polarization. The reason for the non-large difference between the longitudinal and transverse spin diffusion length may be related to the amorphous structure of CoFeAl. Since the ferromagnetic absorber has random magnetization, the longitudinal spin diffusion length is too short.

We then measured the temperature dependence of the nonlocal spin valve signal. Since the nonlocal spin signal shows the gradual modulation because of the spin absorption effect, we define the longitudinal and transverse spin signals. In this case, the modulation ratio is given by $\Delta R_{\mathrm{M}}/\Delta R_{\mathrm{L}}^{\uparrow\uparrow}$ in the Fig. 6.2. We can see that the modulation ratio increases with decreasing the temperature. This is because the increment of the mean free path causes the increase in the longitudinal spin diffusion length. In addition, the smaller increase in the electrical spin polarization also contributes to the modulation increase.

6.3 Temperature dependence of the spin signals in a ferromagnetic/nonmagnetic bi-layered channel

We then investigate the temperature dependence of the spin accumulation signal. The width of Cu/CoFeAl wire is reduced to 100 nm, in order to exclude any artifact. Figure 6.3 (a) and (b) show the temperature dependence of the nonlocal spin signal. The modulation ratio seems to increase with decreasing the temperature as expected. However, surprisingly, the spin accumulation signal at low temperature is smaller than that at room temperature. Figure6.3 (c) is the summary of the temperature dependence of the spin accumulation signal. So, the spin accumulation signal takes a maximum value at 180 K. In conventional lateral spin valves, the temperature dependence of the spin accumulation signal shows the monotonic increase with decreasing the temperature because of the suppression of the phono scattering, and the observed non-monotonic feature should originate from the capping layer. It should be noted that the similar non-monotonic temperature dependence has been reported by Refs. [35]. They argue that the unique spin flip scattering is induced by Kondo effect at low temperature. As a result, the spin accumulation signal is smaller than the value at room temperature. However, we want to point out that they have not reported the position dependence of the spin accumulation signal to verify their arguments. Also, the temperature where the spin signal takes the maximum value is far from the temperature of the minimum resistivity. Therefore, the explanation based on the Kondo effect is still a controversial issue.

Here, we provide another argument to explain the non-monotonic temperature dependence of the spin accumulation by using the spin absorption effect. In our sample,

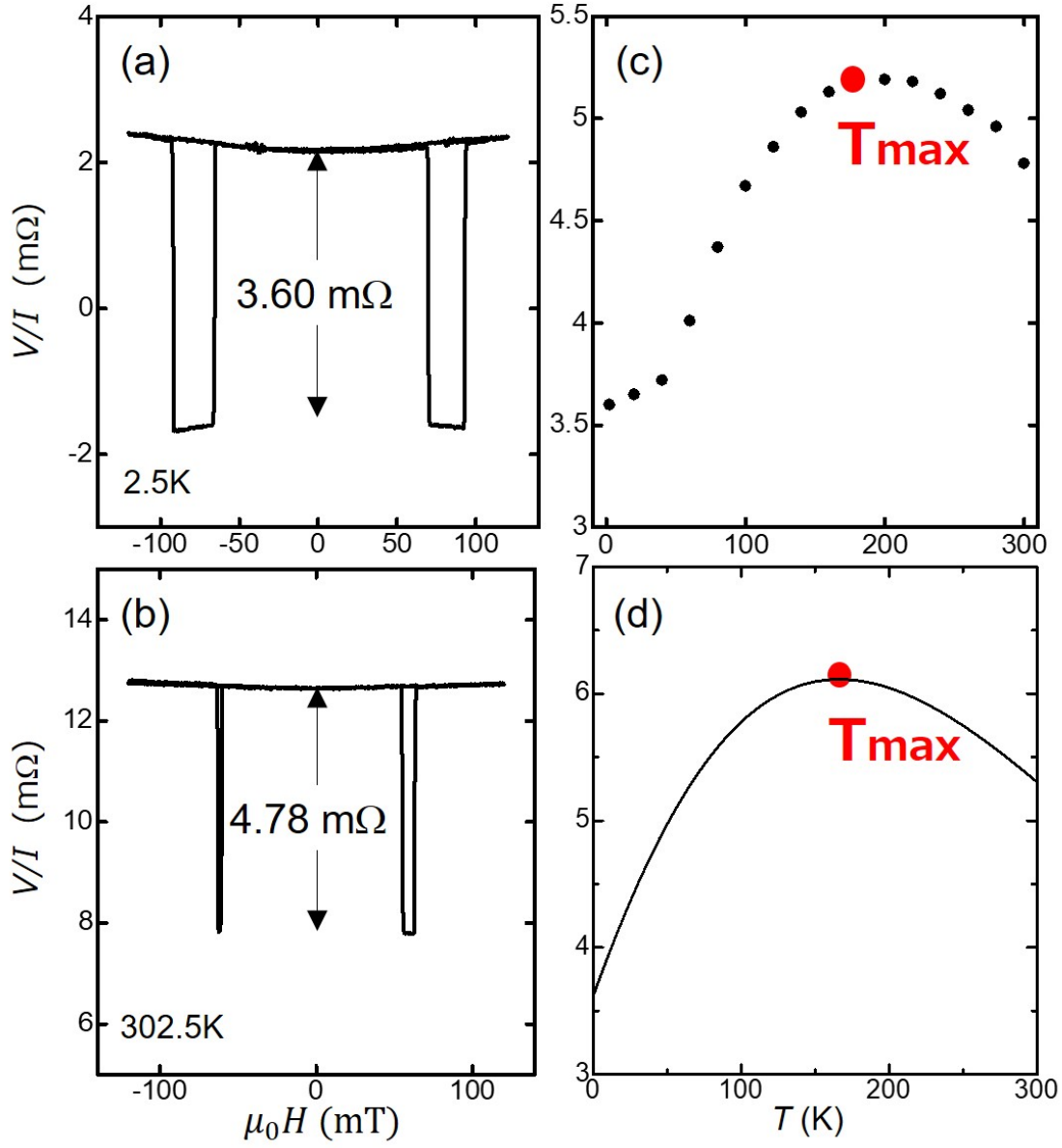

Figure 6.3: Nonlocal spin-valve signals in the lateral spin valve at (a) 2.5 K and (b) 302.5 K. (c) Temperature dependence of the spin signal in the bi-layer device with channel width of 100 nm. (d) Numerical calculation of the temperature dependence of the spin signal.

the junction size between the nonmagnetic channel and the spin absorber is quite large. Especially, the length along the Cu wire is over few microns, which is much longer than the spin diffusion length for the Cu. This means that effective junction size for the spin absorber depends on the temperature. Since the spin diffusion length for the Cu wire increases with decreasing the temperature, the influence of the spin absorber should increase with decreasing the temperature. This may explain the non-monotonic dependence of the spin accumulation signal.

To consider the influence of the spin absorber more quantitatively, we analytically calculate the spin accumulation signal in this system under the framework of the one dimensional spin diffusion model. Here, we consider several paths for the spin diffusion for the non-equilibrium spin accumulation. The first one, say path 1, is the spin re-absorption into the spin injector, which is important factor for the efficient spin injection. The second one, path 2, is the spin diffusion into the spin detector, which is directly related to the spin accumulation signal. The third one, path 3, is the spin absorption into the absorber. This is the most important contribution in the present structure. The final one, path 4, is the spin diffusion into the Cu. For the non-equilibrium spins in the vicinity of the injecting junction, these paths exist in parallel. By defining the spin resistance for each path as $R_{\rm si}$, the total spin resistance is given by the following equation.

$$R_{\mathrm{si}} = \left(\frac{1}{R_1} + \frac{1}{R_2} + \frac{1}{R_3} + \frac{1}{R_4} \right) \tag{6.1}$$

Here, the spin resistance for each path is given by the following equations.

$$\begin{cases} R_1 = \dfrac{2\lambda_{\mathrm{CoFeAl}}\rho_{\mathrm{CoFeAl}}}{(1-P^2)W_{\mathrm{CoFeAl}}W_{\mathrm{Cu}}}, & (6.2) \\ R_2 = R_{\mathrm{Cu}} \dfrac{R_{\mathrm{Cu}}\sinh(L/\lambda_{\mathrm{Cu}}) + R_{\mathrm{CoFeAl}}\cosh(L/\lambda_{\mathrm{Cu}})}{R_{\mathrm{Cu}}\cosh(L/\lambda_{\mathrm{Cu}}) + R_{\mathrm{CoFeAl}}\sinh(L/\lambda_{\mathrm{Cu}})}, & (6.3) \\ R_3 = R_{\mathrm{Cu}} \dfrac{R_{\mathrm{Cu}}\sinh(t/\lambda_{\mathrm{Cu}}) + R_{\mathrm{CoFeAl}}\cosh(t/\lambda_{\mathrm{Cu}})}{R_{\mathrm{Cu}}\cosh(t/\lambda_{\mathrm{Cu}}) + R_{\mathrm{CoFeAl}}\sinh(t/\lambda_{\mathrm{Cu}})}, & (6.4) \\ R_4 = \dfrac{2\lambda_{\mathrm{Cu}}\rho_{\mathrm{Cu}}}{W_{\mathrm{Cu}}t}, & (6.5) \end{cases}$$

Where, W_{CoFeAl} and W_{Cu} are the line width of CoFeAl and the line width of Cu, respectively. And, L is the distance between the injector and the detector, and t is the distance between the injector and the absorber. This synthetic spin resistance can be defined using only path 3, because of its extremely low spin resistance. Path 3 is described by the series connection between the nonmagnetic channel and the ferromagnetic absorber. Since we treat the spin diffusion along the vertical direction, the effective junction size should be given by $W_{\mathrm{Cu}} \times \lambda_{\mathrm{Cu}}$.

Since we know the temperature dependence for each values, we simply input the equation then calculate the spin accumulation signal. Figure 6.3 (d) shows the calculated result on the temperature dependence of the spin accumulation signal. We can clearly confirm that the spin accumulation signal takes a maximum value at the certain temperature. Thus, the non-monotonic temperature dependence of the spin accumulation can be quantitatively explained by properly considering the spin absorption effect.

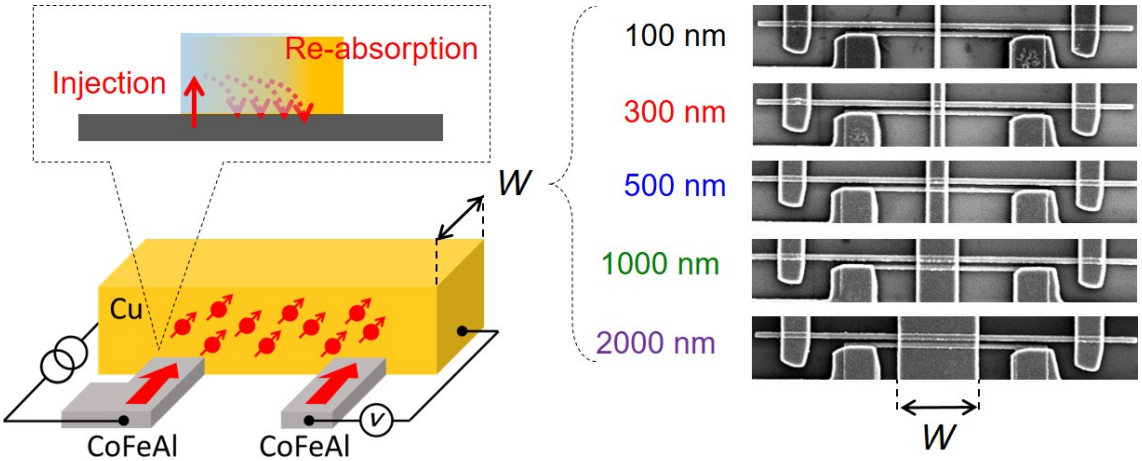

Figure 6.4: Typical schematic illustration of the fabricated lateral spin valve together with the SEM images. The line width of each spin channel was designed from 100 nm to 2000 nm.

6.4 Temperature dependence of the spin signals in conventional lateral spin valves

From the aforementioned analysis, we expect that the similar non-monotonic dependence of the spin accumulation will be observed in the conventional lateral spin valve with the wide Cu channel. This is because the spin injection mainly occurs at the edge of the junction because of the large electrical conductivity difference. As shown in Fig. 6.4, the injected spins from one interface diffuse into the spin detector. However, when the width of the Cu wire is wide, the spin diffuses also along wire width direction. Then, the similar situation will also occur in this structure. Therefore, we expect that the similar non-monotonic temperature dependence will observe also in the conventional lateral spin valve with a wider wire. Here, we have fabricated the lateral spin valves for different

wire widths, 100 nm, 300 nm, 500 nm, 1000 nm and 2000 nm. Then, the temperature dependence of the spin accumulation signals is examined. As can be seen in Fig. 6.5, we can clearly see the non-monotonic dependence of the spin accumulation signal and found that the temperature where the spin accumulation signal takes the maximum value increases with increasing the wire width. This is perfectly consistent with our expectation.

Based on these systematic study, we are able to understand the non-monotonic temperature dependence of the spin accumulation signal without taking into account the additional unique effects such as Kondo effect and surface scattering. Spin absorption effect is quite important to characterize the spin diffusion in the laterally configured ferromagnetic/nonmagnetic hybrid structures.

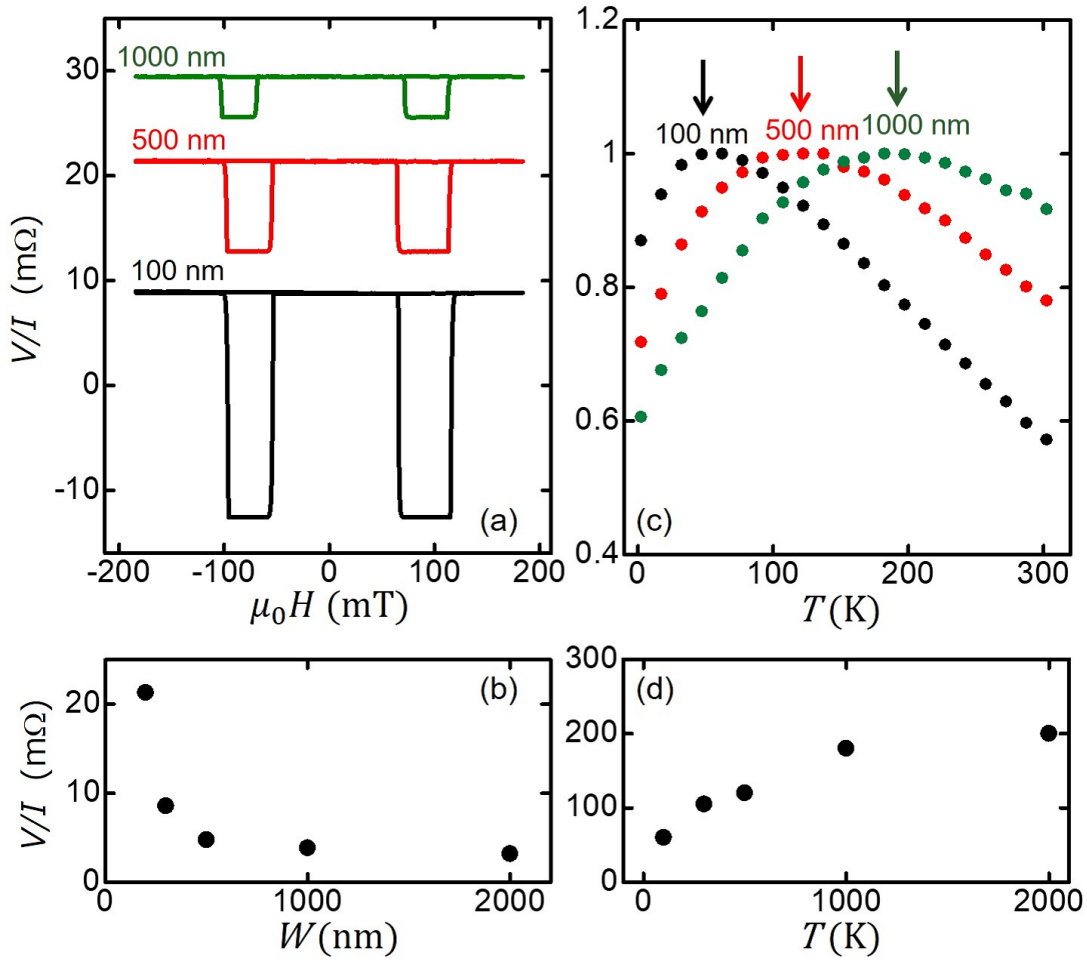

Figure 6.5: (a), (b) Line width dependence of spin signal in the conventional lateral spin valves. (c), (d) Temperature dependence of spin signal in the various line widths.

6.5 Summary

The spin transport properties in a spin valve with ferromagnetic/nonmagnetic bi-layer channel was investigated. It was found that the ferromagnetic channel plays the role of a spin absorber and it is possible to observe the anisotropic spin absorption effect. However, it was found that it is impossible to accurately evaluate the longitudinal and transverse spin relaxation lengths unless the spin absorber has high crystal anisotropy. On the other hand, the temperature dependence of the spin signal showed anomalous behavior. We clarified that the temperature dependence of the spin signal can be explained by modulation of the spin resistance of the whole system caused by the temperature change in the one-dimensional spin diffusion model.

Chapter 7

Conclusion

In this thesis, I have experimentally investigated the spin absorption effect in ferromagnetic/nonmagnetic hybrid nanostructures by taking into account the three dimensional diffusion of the spin current and the non-collinear spin configuration. The major results of the thesis are as follows:

In the first experiments, we have investigated the geometrical contribution in the spin absorption effect. In a nano-pillar-based lateral-spin-valve structure, the spin absorption was found to increase with increasing the lateral dimension of the ferromagnetic dot. However, the absorption efficiency was much smaller than that in a conventional lateral spin valve based on nanowire junctions. This is because the large effective cross section of the two dimensional nonmagnetic film effectively reduces the spin resistance of the nonmagnetic channel. As a result, a relatively large spin current diffuses into the nonmagnetic channel. In a conventional lateral spin valve based on the nanowire junctions, I found that the spin accumulation signal is significantly reduced by increasing the thickness of the ferromagnetic absorber. This can be understood by taking into account

the spin absorption through the side surface of the ferromagnetic dot quantitatively with the spin scattering effect. We showed that the spin scattering effect can be removed by using a T-shaped lateral spin valve in which the spin absorber is located at a position branched from the spin diffusion path. Apart from the spin absorption, the base signal of the nonlocal signal in the T-shaped lateral spin valve exhibits the gradual field dependence. To explain the gradual change, I proposed the anisotropic spin absorption effect originating from the difference between the longitudinal and transverse spin absorption effects.

In the second experiment, we investigate the influence of the relative angle between the direction of the spin current and the direction of the magnetization of the spin absorber on the spin absorption effect. We proposed V-shaped ferrromagnetic injector and detector in order to realize the non-colinear spin configuration. From the spin Hall signal using the Pt detector, we verified that the transverse spin current is really generated from the V-shaped ferromagnetic wire. By extending the experiments with the V-shaped ferromagnetic wires, I examined the spin absorption effects for the longitudinal and transverse spin currents in a Permalloy nanowire. The spin absorption for the transverse spin current was found to be stronger than that for the longitudinal spin current. The result is quantitatively explained by considering the angular dependence of the effective spin polarization with the fact that the transverse spin relaxation length is less than half that of the longitudinal spin relaxation.

In the third experiment, I have developed a novel lateral spin valve consisting of the ferromagentic/nonmagnetic bilayer spin channel with the highly spin-polarized electrodes. A large modulation of the spin valve signal has been observed even at room

temperature and the modulation ratio increases with decreasing the temperature. In this structure, the spin accumulation was found to take a maximum value at 180 K and the room temperature spin signal was larger than that at low temperature. This non-monotonic temperature dependence of the spin accumulation signal can be explained by the considering the three dimensional spin absorption effect.

These findings provide the spin relaxation mechanism in a metallic nanostructures and pave the way for the efficient manipulation of the spin currents.

Bibliography

[1] W. Gerlach and O. Stern, Z. Phys. 9, 349 (1922).

[2] E. C. Stoner, Collective electron specific heat and spin paramagnetism in metals., Proc. R. Soc. A. 154, 656 (1936).

[3] P Grünberg, R Schreiber,Y Pang, MB Brodsky, H Sowers, Layered magnetic structures: Evidence for antiferromagnetic coupling of Fe layers across Cr interlayers., Phys. Rev. Lett. 57, 2442 (1986).

[4] M. N. Baibich, J. M. Broto, A. Fert, F. Nguyen Van Dau, and F. Petroff. Giant Magnetoresistance of (001)Fe/(001)Cr Magnetic Superlattices., Phys. Rev. Lett. 61(21) 2472-2475 (1988).

[5] W. P. Pratt, Jr., S.-F. Lee, J. M. Slaughter, R. Loloee, P. A. Schroeder, and J. Bass, Perpendicular giant magnetoresistances of Ag/Co multilayers., Phys. Rev. Lett. 66, 3060 (1991).

[6] M. A. M. Gijs, S. K. J. Lenczowski, and J. B. Giesbers,Perpendicular giant magnetoresistance of microstructured Fe/Cr magnetic multilayers from 4.2 to 300 K., Phys. Rev. Lett. 70, 3343 (1993).

[7] T. Ono, and T. Shinjo, Magnetoresistance of Multilayers Prepared on Microstructured Substrates., J. Phys. Soc. Jpn. 64, pp. 363-366 (1995)

[8] L. Piraux, J. M. George, J. F. Despres, C. Leroy, E. Ferain, R. Legras, K. Ounadjela, and A. Fert., Giant magnetoresistance in magnetic multilayered nanowires., Appl. Phys. Lett. 65, 2484 (1994).

[9] M. A. M. Gijs, M. T. Johnson, A. Reinders, P. E. Huisman, R. J. M. van de Veerdonk, S. K. J. Lenczowski, and R. M. J. van Gansewinkel, Perpendicular giant magnetoresistance of Co/Cu multilayers deposited under an angle on grooved substrates., Appl. Phys. Lett. 66, 1839 (1995).

[10] Mark Johnson and R. H. Silsbee, Interfacial charge-spin coupling: Injection and detection of spin magnetization in metals., Phys. Rev. Lett. 55, 1790 (1985).

[11] Mark Johnson and R. H. Silsbee. Interfacial charge-spin coupling: Injection and detection of spin magnetization in metals. Phys. Rev. Lett. 55(17):1790-1793 (1987).

[12] F. J. Jedema, A. T. Filip, and B. J. van Wees, Electrical spin injection and accumulation at room temperature in an all-metal mesoscopic spin valve, Nature 410, 345 —348 (2001).

[13] F. J. Jedema, H. B. Heersche, A. T. Filip, J. J. A. Baselmans, and B. J. van Wees, Electrical detection of spin precession in a metallic mesoscopic spin valve, Nature 416, 713—716 (2002).

[14] S. O. Valenzuela, Nonlocal electronic spin detection, spin accumulation and the spin hall effect, Int. J. Mod. Phys. B 23, 2413 (2009).

[15] T. Kimura and Y. Otani, Spin transport in lateral ferromagnetic/nonmagnetic hybrid structures, J. Phys.: Condens. Matter: Spec. Issue. Spin Electron. 19, 165216 (2007).

[16] A. Hoffmann, Pure spin-currents, Phys. Stat. Sol. (c) 4, 4236 (2007).

[17] S. Datta and B. Das., Electronic analog of the electrooptic modulator, Appl. Phys. Lett. 56, 665 (1990).

[18] J.-C. Rojas Sánchez, P. Laczkowski, W. F. Savero Torres, M. Cubukcu, V. D. Nguyen, L. Notin, C. Beigné, C. Vergnaud, A. Marty, M. Jamet, L. Vila, and J. P. Attané, In-plane and out-of-plane spin precession in lateral spin-valves., Appl. Phys. Lett. 102, 132408 (2013).

[19] T Valet and A Fert. Theory of the perpendicular magnetoresistance in magnetic multilayers., Phys. Rev. B 48, 7099, (1993).

[20] S. Takahashi and S. Maekawa, Spin injection and detection in magnetic nanostructures. Phys. Rev. B 67, 052409, (2003).

[21] T. Kimura, J. Hamrle, and Y. Otani, Estimation of spin-diffusion length from the magnitude of spin-current absorption., Multiterminal ferromagnetic/nonmagnetic hybrid structures., Phys. Rev. B 72, 014461 (2005).

[22] T. Yang, T. Kimura, and Y. Otani. Giant spin-accumulation signal and pure spin-current-induced reversible magnetization switching. Nature Physics 4, 851— 854 (2008).

[23] J. Z. Sun, M. C. Gaidis, E. J. ÓSullivan, E. a. Joseph, G. Hu, D. W. Abraham, J. J. Nowak, P. L. Trouilloud, Yu Lu, S. L. Brown, D. C. Worledge, and W. J. Gallagher. A three-terminal spin-torque-driven magnetic switch., Appl. Phys. Lett. 95, 083506 (2009).

[24] B. Behin-Aein, D. Datta, S. Salahuddin, and S. Datta. Proposal for an all-spin logic device with built-in memory. Nature Nanotechnology 5, 266—270 (2010).

[25] T. Kimura, and M. Hara, Nonvolatile multiple-valued memory device using lateral spin valve., Appl. Phys. Lett. 97, 182501 (2010).

[26] Silicon spintronics., Ron Jansen, Nature Materials 11, 400—408 (2012).

[27] K. Kondou, R. Yoshimi, A. Tsukazaki, Y. Fukuma, J. Matsuno, K. S. Takahashi, M. Kawasaki, Y. Tokura and Y. Otani., Fermi-level-dependent charge-to-spin current conversion by Dirac surface states of topological insulators., Nature Physics 12, 1027 —1031 (2016).

[28] Nikolaos Tombros, Csaba Jozsa, Mihaita Popinciuc, Harry T. Jonkman and Bart J. van Wees., Electronic spin transport and spin precession in single graphene layers at room temperature., Nature 448, 571 (2007).

[29] Kohei Ohnishi, Yuma Ono, Tatsuya Nomura and Takashi Kimura, Significant change of spin transport property in Cu/Nb bilayer due to superconducting transition., Scientific Reports 4, Article number: 6260 (2014).

[30] Xianmin Zhang, Shigemi Mizukami, Takahide Kubota, Qinli Ma, Mikihiko Oogane, Hiroshi Naganuma, Yasuo Ando, and Terunobu Miyazaki, Observation of large spin-dependent transport length in organic spin valves at room temperature., Nature Communications 4, Article number: 1392 (2013).

[31] N. F. Mott., The resistance and thermoelectric properties of the transition metals., proc. R. Soc London Ser. A 156, 888 (1936).

[32] A. Fert and I. Campbell, Two-Current Conduction in Nickel. Phys. Rev. Lett. 21, 1190 (1968).

[33] S. Bakaul, S. Hu, and T. Kimura, Large pure spin current generation in metallic nanostructures, Appl. Phys. A 111, 355—360 (2013).

[34] T. Kimura, T. Sato, and Y. Otani, Temperature Evolution of Spin Relaxation in a NiFe/Cu Lateral Spin Valve., Phys. Rev. Lett. 100, 066602 (2008).

[35] L. O'Brien, M. J. Erickson, D. Spivak, H. Ambaye, R.J. Goyette, V. Lauter, P.A. Crowell and C. Leighton, Kondo physics in non-local metallic spin transport devices., Nature Communications 5, 3927 (2014).

[36] K. Hamaya, T. Kurokawa, S. Oki, S. Yamada, and T. Kanashima, Direct evidence for suppression of the Kondo effect due to pure spin current, Phys. Rev. B 94, 140401(R) (2016).

[37] T. Kimura, Y. Otani, and J. Hamrle, Switching magnetization of a nanoscale ferromagnetic particle using nonlocal spin injection, Phys. Rev. Lett. 96, 037201 (2006).

[38] T. Kimura, Y. Otani, and J. Hamrle, Enhancement of spin accumulation in a nonmagnetic layer by reducing junction size, Phys. Rev. B 73, 132405 (2006).

[39] P. Laczkowski, H. Jaffrès, W. Savero-Torres, J.-C. Rojas-Sánchez, Y. Fu, N. Reyren, C. Deranlot, L. Notin, C. Beigné, J.-P. Attané, L. Vila, J.-M. George, and A. Marty, Evaluation of spin diffusion length of AuW alloys using spin absorption experiments in the limit of large spin-orbit interactions, Phys. Rev. B 92, 214405 (2015).

[40] Y. Niimi and Y. Otani, Reciprocal spin Hall effects in conductors with strong spin —orbit coupling: a review, Rep. Prog. Phys. 78, 124501 (2015).

[41] T. Kimura, J. Hamrle, Y. Otani, K. Tsukagoshi, and Y. Aoyagi, Suppression of spin accumulation in nonmagnet due to ferromagnetic ohmic contact., Appl. Phys. Lett. 85, 3795 (2004).

[42] G. Schmidt, D. Ferrand, L. W. Molenkamp, A. T. Filip, and B. J. van Wees, Fundamental obstacle for electrical spin injection from a ferromagnetic metal into a diffusive semiconductor., Phys. Rev. B 62, R4790(R) (2000).

[43] J. E. Hirsh, Spin Hall effect, Phys. Rev. Lett. 83, 1834 (1999).

[44] S. Zhang, Spin Hall effect in the presence of spin diffusion, Phys. Rev. Lett. 85, 393 (2000).

[45] E. Saitoh, M. Ueda, H. Miyajima, and G. Tatara, Conversion of spin current into charge current at room temperature: Inverse spin-Hall effect, Appl. Phys. Lett. 88, 182509 (2006).

[46] S. O. Valenzuela and M. Tinkham, Direct electronic measurement of the spin Hall effect, Nature (London) 442, 176 (2006).

[47] T. Kimura, Y. Otani, T. Sato, S. Takahashi, and S. Maekawa, Room-temperature reversible spin Hall effect, Phys. Rev. Lett. 98, 156601 (2007).

[48] T. Seki, Y. Hasegawa, S. Mitani, S. Takahashi, H. Imamura, S. Maekawa, J. Nitta, and K. Takanashi, Giant spin Hall effect in perpendicularly spin-polarized FePt/Au devices, Nature Materials 7, 125 (2008).

[49] I. Žutić, J. Fabian, and S. Das Sarma, Spintronics: Fundamentals and applications, Rev. Mod. Phys. 76, 323 (2004).

[50] Concepts in Spin Electronics, edited by S. Maekawa (Oxford University Press, 2006).

[51] Spin Current, edited by S. Maekawa et al. (Oxford University Press, 2012).

[52] Handbook of Spin Transport and Magnetism, edited by E. Y. Tsymbal and I. Zutic (CRC, 2011).

[53] Silicon spintronics., Ron Jansen, Nature Materials 11, 400—408 (2012).

[54] D. A. Allwood, G. Xiong, C. C. Faulkner, D. Atkinson, D. Petit, and R. P. Cowburn, Magnetic Domain-Wall Logic, Science 309, 5741, 1688-1692 (2005).

[55] S. S. P. Parkin, M. Hayashi, and L. Thomas, Magnetic Domain-Wall Racetrack Memory, Science 320, 5873, 190-194 (2008).

[56] A. Imre, G. Csaba, L. Ji, A. Orlov, G. H. Bernstein, and W. Porod, Majority Logic Gate for Magnetic Quantum-Dot Cellular Automata, Science 311, 5758, pp. 205-208 (2006).

[57] S. Nonoguchi, T. Nomura, Y. Ando, and T. Kimura, Electrical manipulation of spin polarization and generation of giant spin current using multi terminal spin injectors , J. Appl. Phys. 111, 07C505 (2012).

[58] A. Yamaguchi, T. Ono, S. Nasu, K. Miyake, K. Mibu, and T. Shinjo., Real-space observation of current-driven domain wall motion in submicron magnetic wires, Phys. Rev. Lett. 92, 077205 (2004).

[59] G. S. D. Beach, C. Knutson, C. Nistor, M. Tsoi, and J. L. Erskine., Nonlinear domain-wall velocity enhancement by spin-polarized electric current, Phys. Rev. Lett. 97, 057203 (2006).

[60] Masamitsu Hayashi, Luc Thomas, Charles Rettner, Rai Moriya, Xin Jiang, and Stuart S. P. Parkin, Dependence of current and field driven depinning of domain walls on their structure and chirality in permalloy nanowires, Phys. Rev. Lett. 97, 207205 (2006).

[61] M. Kläui, P.-O. Jubert, R. Allenspach, A. Bischof, J. A. C. Bland, G. Faini, U. Rüdiger, C. A. F. Vaz, L. Vila, and C. Vouille, Direct observation of domain-wall configurations transformed by spin currents, Phys. Rev. Lett. 95, 026601 (2005).

[62] Guido Meier, Markus Bolte, René Eiselt, Benjamin Krüger, Dong-Hyun Kim, and Peter Fischer, Direct imaging of stochastic domain-wall motion driven by nanosecond current pulses, Phys. Rev. Lett. 98, 187202 (2007).

[63] T. Kimura, Y. Otani, I. Yagi, K. Tsukagoshi, and Y. Aoyagi, Spin-current-assisted domain-wall depinning in a submicron magnetic wire, J. Appl. Phys. 94, 7947—7949 (2003).

[64] S. Nonoguchi, T. Nomura, and T. Kimura, Nonlocal spin transports in nanopillar-based lateral spin valve, Appl. Phys. Lett. 100, 132401 (2012).

[65] T. Nomura, K. Ohnishi, and T. Kimura, Large spin current injection in nano-pillar-based lateral spin valve, AIP Conference Proceedings 1763, 020011 (2016).

[66] N. Poli, J. P. Morten, M. Urech, Arne Brataas, D. B. Haviland, and V. Korenivski., Spin injection and relaxation in a mesoscopic superconductor, Phys. Rev. Lett. 100, 136601 (2008).

[67] T. Wakamura, N. Hasegawa, K. Ohnishi, Y. Niimi, and Y. Otani, Spin injection into a superconductor with strong spin-orbit coupling, Phys. Rev. Lett. 112, 036602 (2014).

[68] O. Stejskala, J. Hamrle, J. Pištora, and Y. Otani, Optimization of spin injection and spin detection in lateral nanostructures by geometrical means, J. Magn. Magn. Mater. 414, 132—143 (2016).

[69] Emmanouil Masourakis, Libe Arzubiaga, Goran Mihajlović, Estitxu Villamor, Roger Llopis, Fèlix Casanova and Luis E Hueso., Modulation of spin accumulation by nanoscale confinement using electromigration in a metallic lateral spin valve, Nanotechnology 27, 095201 (2016).

[70] W. Savero Torres, A. Marty, P. Laczkowski, L. Vila, M. Jamet, J-P. Attané, Calculation method of spin accumulations and spin signals in nanostructures using spin resistors, e-print arXiv:1506.01347.

[71] G. Bridoux, M. V. Costache, J. Van de Vondel, I. Neumann, and S. O. Valenzuela. Enhanced spin signal in nonlocal devices based on a ferromagnetic CoFeAl alloy. Appl. Phys. Lett. 99(10):102107, (2011).

[72] S. Garzon, Žutić, and R. A. Webb, Temperature-dependent asymmetry of the nonlocal spin-injection resistance: evidence for spin nonconserving interface scattering, Phys. Rev. Lett. 94, 176601 (2005).

[73] A. van Staa, J. Wulfhorst, A. Vogel, U. Merkt, and G. Meier, Spin precession in lateral all-metal spin valves: Experimental observation and theoretical description., Phys. Rev. B 77, 214416 (2008).

[74] T. Kimura, Y. Otani, and P. M. Levy, Electrical control of the direction of spin accumulation, Phys. Rev. Lett. 99, 166601 (2007).

[75] Magnetic Domains: The Analysis of Magnetic Microstructures, edited by A. Hubert and R. Schäfer, (Springer, Berlin, 1998).

[76] R. P. Cowburn, Property variation with shape in magnetic nanoelements, J. Phys. D 33, R1 (2000).

[77] K. Shigeto, T. Okuno, K. Mibu, T. Shinjo, and T. Ono, Magnetic force microscopy observation of antivortex core with perpendicular magnetization in patterned thin film of permalloy., Appl. Phys. Lett. 80, 4190 (2002).

[78] A. O. Adeyaya, J. A. C. Bland, C. Daboo, D. G. Hasko, and H. Ahmed, Optimized process for the fabrication of mesoscopic magnetic structures, J. Appl. Phys. 82, 469 (1997).

[79] T. Ono, H. Miyajima, K. Shigeto, and T. Shinjo, Appl. Magnetization reversal in submicron magnetic wire studied by using giant magnetoresistance effect ,Phys. Lett. 72, 1116 (1998).

[80] P. Łączkowski, L. Vila, S. Ferry, A. Marty, J.-M. George, H. Jaffrés, A. Albert, T. Kimura, T. Yang, Y. Otani, and J.-P. Attané, Spin signal in metallic lateral spin valves made by a multiple angle evaporation technique, Appl. Phys. Express 4, 063007 (2011).

[81] T. Taniyama, I. Nakatani, T. Namikawa, and Y. Yamazaki, Resistivity due to domain walls in Co zigzag wires, Phys. Rev. Lett. 82, 2780 (1999).

[82] Micromagentic simulations have been performed using OOMMF given by http://math.nist.gov/oommf/. Here, the cell size in the x and y directions is 10 nm and that in the z direction is 30 nm.

[83] M. Morota, Y. Niimi, K. Ohnishi, D. H. Wei, T. Tanaka, H. Kontani, T. Kimura, and Y. Otani, Indication of intrinsic spin Hall effect in 4d and 5d transition metals, Phys. Rev. B 83, 174405 (2011)

[84] L. Liu, R. A. Buhrman, and D. C. Ralph, e-print arXiv:1111.3702.

[85] E. R. Lewis, D. Petit, A.-V. Jausovec, L. O'Brien, D. E. Read, H. T. Zeng, and R. P. Cowburn, Measuring Domain Wall Fidelity Lengths Using a Chirality Filter, Phys. Rev. Lett. 102, 057209 (2009).

[86] M. Klläui, Appl. Head-to-head domain walls in magnetic nanostructures ,J. Phys.: Condens. Matter 20, 313001 (2008).

[87] T. Nomura, S. Nonoguchi, and T. Kimura, Efficient inducement of bistable spin Hall effect using in-plane-magnetized V-shaped ferromagnetic wire., Appl. Phys. Lett. 101, 082403 (2012).

[88] S. Takahashi and S. Maekawa, Spin injection and detection in magnetic nanostructures, Phys. Rev. B 67, 052409 (2003).

[89] T. Kimura, J. Hamrle, Y. Otani, K. Tsukagoshi, Y. Aoyagi, Effect of probe configuration on spin accumulation in lateral spin-valve structure, J. Magn. Magn. Mater. 286, 88 (2005).

[90] J. Hamrle, T. Kimura, Y. Otani, K. Tsukagoshi, and Y. Aoyagi, Current distribution inside PyCu lateral spin-valve devices., Phys. Rev. B 71, 094402 (2005).

[91] E. C. Stoner, E. P. Wohlfarth, A mechanism of Magnetic Hysteresis in Heterogeneous alloys., Physical. Sciences, 240, 826, pp.599-642 (1948).

[92] Yongqing Li, Peng Xiong, Stephan von Molnár, Yuzo Ohno, and Hideo Ohno, Magnetization reversal of iron nanoparticles studied by submicron Hall magnetometry., J. Appl. Phys. 93, 7912 (2003).

[93] K. Hamaya, N. Hashimoto, S. Oki, S. Yamada, M. Miyao, and T. Kimura, Phys. Rev. B 85, 100404(R) (2012).

[94] S. Zhang, P. M. Levy, and A. Fert, Theory of the perpendicular magnetoresistance in magnetic multilayers, Phys. Rev. Lett. 88, 236601 (2002).

[95] M. D. Stiles and A. Zangwill, Anatomy of spin-transfer torque, Phys. Rev. B 66, 014407 (2002).

[96] J. Zhang, P. M. Levy, S. Zhang, and V. Antropov, Identification of Transverse Spin Currents in Noncollinear Magnetic Structures, Phys. Rev. Lett. 93, 256602 (2004).

[97] T. Taniguchi and H. Imamura, Proposal of an experimental scheme for determination of penetration depth of transverse spin current by a nonlocal spin valve., arXiv:1208.3074v1.

[98] T. Taniguchi, S. Yakata, H. Imamura, and Y. Ando, Penetration depth of transverse spin current in ferromagnetic metals., IEEE Trans. Magn. 44, 2636 (2008).

[99] T. Taniguchi, S. Yakata, H. Imamura, and Y. Ando, Determination of penetration depth of transverse spin current in ferromagnetic metals by spin pumping, Appl. Phys. Express 1, 031302 (2008).

[100] L. Berger, Exchange interaction between ferromagnetic domain wall and electric current in very thin metallic films., J. Appl. Phys. 55, 1954 (1984).

[101] J. C. Slonczewski, Current-driven excitation of magnetic multilayers., J. Magn. Magn. Mater. 159, L1 (1996).

[102] T. Kimura, N. Hashimoto, S. Yamada, M. Miyao, and K. Hamaya. Room-temperature generation of giant pure spin currents using epitaxial Co2FeSi spin injectors. NPG Asia Materials, 4(3):e13, March (2012).

[103] I. Galanakis, P. H. Dederichs, and N. Papanikolaou, Slater-Pauling behavior and origin of the half-metallicity of the full-Heusler alloys., Phys. Rev. B 66, 174429 (2002).

[104] T. Block, C. Felser, G. Jakob, J. Ensling, B. Mühling, P. Gütlich, V. Beaumont, F. Studer, and R. Cava, Large negative magnetoresistance effects in Co2Cr0.6Fe0.4Al., J. Solid State Chem. 176, 646 (2003)

[105] G. H. Fecher and C. Felser, Substituting the main group element in cobalt—iron based Heusler alloys: Co2FeAl1 − xSix., J. Phys. D 40, 1582 (2007).

[106] S. Nonoguchi, T. Nomura, and T. Kimura, Longitudinal and transverse spin current absorptions in a lateral spin-valve structure, Phys. Rev. B 86, 104417 (2012).

[107] S. Hu, H. Itoh, T. Kimura., Efficient thermal spin injection using CoFeAl nanowire, NPG Asia Materials, 6, e127 (2014).

[108] M. Tsoi, a. Jansen, J. Bass, W.-C. Chiang, M. Seck, V. Tsoi, and P. Wyder. Excitation of a Magnetic Multilayer by an Electric Current. Phys. Rev. Lett. 81, 493 (1998).

[109] E. B. Myers, D.C. Ralph, J.A. Katine, R.N. Louie, and R.A. Buhrman. Current-Induced Switching of Domains in Magnetic Multilayer Devices. Science, 285, 5429, 867-870, (1999).

Acknowledgement

First of all, I would like to express my gratitude to Prof. Takashi Kimura, Prof. Hirofumi Wada, Prof. Hiromi Yuasa and Assoc. Prof. Takuya Satoh for my defense committee. And, I also would like to express my gratitude to Assoc. Prof. Akihiro Mitsuda as a member of my pre-defence committee. Valuable comments have made the contents of this thesis more fulfilling.

I would like to express my deepest gratitude to Prof. Takashi Kimura as my supervisor. Prof. Kimura has given me guidance on how to act as a researcher and all the skills necessary for performing research. In addition, I have been given a lot of valuable experiences to be properties as a researcher.

I would like to express my gratitude deeply to assist. prof. Kazumasa Yamada and assist. prof. Kohei Ohnishi. Assist. prof. Yamada deepened my thought on physics through discussions on physical phenomena and researches. Assist. prof. Ohnishi has taught me many things about experiment and presentation techniques.

I would like to express my sincere gratitude to Tech. Staff Atsushi Kenjo. He has given me practical knowledges on microfabrication techniques and experimental equipments. Also, we got a great deal of cooperation in assembling experimental equipments.

I would like to express my sincere gratitude to Secretary Mika Ishama. She has assisted me with administrative procedures in carrying out my research, and also she has always encouraged us by sweets etc. to make our laboratory comfortable.

I would like to express my heartfelt gratitude to all the students in our laboratory below. They gave me great supports for my research life:
Hu Shaojie, Xiaomin Cui, Kazuto Yamanoi, Makoto Hidegara, Nagarjuna Asam, Md Kamruzzaman, Thomas Steinle、Yu Takaira, Masatoshi Kawakita, Yuma Ono, Ginga Uematsu, Kyota Okabe, Toshiyuki Ogawa, Yuki Yokotani, Michiko Sakamoto, Yosuke Nakano, Kotaro Okade, Masayuki Ishitaki, Taisei Ariki, Daigo Yano, Hiroto Fujita.

I would like to express my sincere gratitude to teachers, staffs, and students in related research fields. They have given me active discussions and encouragements on my research, and those were strong supports for me.

I would like to express my sincere gratitude to Japanese Society for the Promotion

of Science (JSPS). I got a lot of economic support to conduct this research.

Finally, I would like to express my sincere gratitude to my family who supported me economically and emotionally through my long university life.

Research Activities

7.1 Journal Publication

1. T. Nomura, K. Ohnishi, and T. Kimura, Large spin current injection in nanopillar-based lateral spin valve, AIP Conf. Proc., 1763, 020011 (2016).

2. T. Nomura, K. Ohnishi, and T. Kimura, Geometrical dependence of spin current absorption into a ferromagnetic, J. Appl. Phys., 120, 142121 (2016).

3. T. Nomura, T. Ariki, S. Hu, and T. Kimura, Efficient thermal spin injection in metallic nanostructures, J. Phys. D: Appl. Phys. 50 (2017) 465003 (8pp)

4. T. Nomura, T. Ariki, T. Ogawa, K. Ohnishi, and T. Kimura, Non-monotonic temperature dependence of spin accumulation due to large ferromagnetic contact, (In preparation).

5. Y. Kanda, T. Nomura, T. Kimura, and M. Hara, Geometrical optimization of a local ballistic magnetic sensor, Appl. Phys. Lett., 104, 142408 (2014).

6. K. Ohnishi, Y. Ono, T. Nomura, Significant change of spin transport property in Cu/Nb bilayer due to superconducting transition, Sci. Rep., 4, 6260 (2014).

7. S. Hu, T. Nomura, G. Uematsu, N. Asam, and T. Kimura, First- and second-harmonic detection of spin accumulation in a multiterminal lateral spin valve under high-bias ac current, Phys. Rev. B, 94, 014416 (2016).

8. S. Hu, X. Cui, T. Nomura, T. Min, and T. Kimura, Nonreciprocity of electrically excited thermal spin signals in CoFeAl-Cu-Py lateral spin valves, Phys. Rev. B, 86, 100403(R) (2017).

9. T. Ariki, T. Nomura, K. Ohnishi, and T. Kimura, Effective suppression of thermoelectric voltage in nonlocal spin valve measurement, Appl. Phys. Exp., 10, 063004 (2017).

7.2 Journal Publication (JPN)

1. T. Nomura, T. Kimura, High efficiency generation of spin current using temperature difference, Kyushu University Low Temperature Center Letter, No.11, 2017. 3.

2. T. Nomura, T. Kimura, Generation of spin current by spin-dependent Seebeck effect and its practicality, Magne 12-5 Topics, 2017. 8.

7.3 International Conference Presentation

1. T. Nomura and T. Kimura, Spin precession due to in-plane magnetic field in a CoFeAl/Cu/CoFeAl metallic lateral spin valve, IUMRS-ICA, Fukuoka, Japan, 24th-30th Augast 2014, Poster presentation

2. T. Nomura, G. Uematsu, and T. Kimura, Thermally-driven spin injection and spin-injection-induced heat ejection, International Workshop "Nano-Spin Sciences", Karatsu, Japan 2015. 2, Oral presentation

3. T. Nomura, G. Uematsu, and T. Kimura, Detection of spin-dependent Peltier effect using lateral spin valve, 20th International Conference on Magnetism (ICM2015), Barcelona, SPAIN. 2015. 7, Poster presentation

4. T. Nomura, S. Hu, G. Uematsu, and T. Kimura, Indirect detection of magnetization direction using thermal spin injection, 9th International Symposium on Metallic Multilayers (MML 2016), Uppsala, SWEDEN 2016. 6, Poster presentation

5. T. Nomura, G. Uematsu, N. Asam, and T. Kimura, Indirect evaluation of magnetization direction using thermal spin injection, International School on Spintronics and Spin-Orbitronics, 2016. 12, Poster presentation

6. T. Nomura, G. Uematsu, N. Asam, and T. Kimura, Indirect evaluation of magnetization direction using thermal spin injection, Korea-Japan Spin-Orbit Workshop, 2016. 12, Poster presentation

7. T. Nomura, T. Ariki, G. Uematsu, and T. Kimura, Optimization of Co/Fe ratio for efficient thermal spin injection in CoFeAl alloy, SPINTECH IX (International School and Conference), Fukuoka, Japan 2017. 6, Poster presentation

7.4 Domestic Conference Presentation (JPN)

1. T. Nomura, G. Uematsu, S. Hu, K. Ohnishi, T. Kimura, Indirect detection of spin signal using thermal spin injection, Annual meeting of the Physical Society of Japan in 2014, Chubu University, September 7-10 (2014) Oral presentation.

2. T. Nomura, G. Uematsu, M. Hidegara, T. Kimura, Detection of spin-dependent Peltier effect using lateral spin valve, Spring meeting of the Physical Society of Japan in 2015, Waseda University, March 21-24 (2015) Oral presentation.

3. T. Nomura, G. Uematsu, S. Hu, T. Kimura, Efficient thermal spin injection using CoFe-based alloy, The japan institute of Metals and Materials in 2015, Kyushu University, September 16-18 (2015) Oral presentation.

4. T. Nomura, S. Hu, G. Uematsu, T. Ogawa, T. Kimura, Spin absorption into ferromagnetic nano dot using novel lateral spin valve structure, Spring meeting of the Physical Society of Japan in 2016, Tohoku Gakuin University, March 19-22 (2016) Oral presentation.

5. T. Nomura, S. Hu, T. Kimura, Indirect detection of magnetization direction using thermal spin injection. Nano-spin conversion A01 group meeting., Kyushu University, 2016. 4., Poster presentation.

6. T. Nomura, T. Ariki, G. Uematsu, T. Kimura, Thermal transport and efficient thermal spin injection in CoFeAl film.,The 40th Conference of Magnetics in Japan, Kanazawa University, September 5-8 (2016) Oral presentation.

7. T. Nomura, G. Uematsu, S. Hu, K. Ohnishi, T. Kimura, Spin and heat transports in nanopillar-based lateral spin valve., Annual meeting of the Physical Society of Japan in 2016, Kanazawa University, 2016. 9. Poster presentation.

8. T. Nomura, T. Ariki, K. Ohnishi, T. Kimura, Temperature dependence of spin relaxation in ferromagnetic/nonmagnetic bilayer channel. Nano Spin Conversion Summer Workshop., Osaka University, 2017. 9. Poster presentation.

9. T. Nomura, T. Ariki, T. Kimura, Temperature dependence of spin relaxation in ferromagnetic/nonmagnetic bilayer channel., Technical Committee on Magnetic Recording (MR), Kashiwa, 2017. 10. Oral presentation.